Numerical and Experimental Study of Multiport Diffusers with Non-Uniform Port Orientation

by

Seyedahmadreza Saeidihosseini

Thesis submitted to the University of Ottawa
in partial fulfillment of the requirements for the
Doctorate in Philosophy degree in Civil Engineering

Department of Civil Engineering
Faculty of Engineering
University of Ottawa

Abstract

Dense wastewater discharges into marine environments can severely impact water bodies. This study addresses the disposal of hypersaline brines from desalination plants through multiport diffusers into seas and oceans. Accurate prediction of the mixing of discharges with the receiving water bodies is crucial for the optimal design of outfall systems. Designers can enhance mixing and increase dilution by modifying outfall properties. However, the interaction of discharges from multiport diffusers poses a significant challenge, impairing the mixing process. The main aim of this study is to improve multiport diffuser designs by limiting the negative effects of jet interaction on mixing.

This research applies a three-dimensional numerical model, the Launder, Reece, and Rodi (LRR) turbulence model, to evaluate the predictive capabilities of the Reynolds Stress Models (RSM) for multiple dense jets and to explore the mixing characteristics and merging process of multiple jets. To validate the model, its predictions are compared with available experimental data. The LRR model showed good agreement with the experimental measurements, and the model outperformed the standard and re-normalization group (RNG) $k{-}\varepsilon$ turbulence models, making it a promising tool for studying the mixing behavior of multiport diffusers.

This study proposes multiport diffusers with non-uniform port orientation as a means for mitigating the negative effect of jet mering on the mixing process and increasing dilution. Using the validated numerical model and the laser-induced fluorescence (LIF) technique, the effect of non-uniform port orientation on the mixing process is explored. The numerical results indicated that the orientation of adjacent jets significantly affected the behavior of individual jets. An individual jet exhibited a longer trajectory and higher dilution when its neighboring jets were disposed of with a different angle, compared to that of uniform discharges. Laboratory experiments on uniform and non-uniform diffusers, with varying port angles in the range of highest reported dilution rates for single discharges (40º-70º), are reported, and the major flow properties and merging processes are compared. Investigations revealed that non-uniform diffusers achieved overall higher mean dilutions due to different mixing behavior in the interaction zones. Non-uniform port orientation provided more space between the jets to expand before interacting with their neighbors, resulting in higher dilutions.

This study challenges the application of formulae obtained from single discharge experiments for multiport diffuser designs and emphasizes the importance of considering source characteristics specific to multiport diffusers, such as angle difference, for efficient desalination outfall. The new data and analysis provided in this study can benefit the design of desalination discharge systems with considerable potential cost savings, especially for tunneled outfalls, due to shorter diffusers with non-uniform port orientations and environmental risk reductions.

Acknowledgements

I would like to thank my supervisor, Dr. Abdolmajid Mohammadian, whose guidance and support have been instrumental in the completion of this doctoral thesis. Mohammadian's expertise and encouragement have inspired me to delve into the complexities of my research with passion and determination. I wish to extend my thanks to Dr. Simone Ferrari, Dr. Philip JW Roberts, and Mostafa Taherian for their valuable contributions in this thesis.

I am profoundly thankful to my parents, Mehri and Masoud, for their boundless love, encouragement, and sacrifices throughout my academic journey. They consistently believed in my capabilities, providing ongoing motivation. I am grateful for the values and resilience they instilled in me.

To my wife, Shabnam, I owe immeasurable thanks. Her patience, understanding, and unyielding support during the challenges of pursuing a PhD have been my anchor. Her belief in my dreams and the sacrifices she made have been indispensable to my success.

Table of Contents

1 Introduction and Objectives 1
1.1 Introduction 1
1.2 Research Background and Significance 3
1.2.1 Mixing Zone 3
1.2.2 Diffuser Design 5
1.2.3 Outfall Discharge Modeling 8
1.3 Research Objectives, Novelty, and Contributions 11
1.4 Thesis Outline 12
1.5 List of Publications (form the thesis) 13
2 Overview of Outfall Discharge Modeling with a Focus on Turbulence Modeling Approaches 17
2.1 Environmental Regulations 17
2.2 Outfall Discharge Principles and Classification 18
2.3 Turbulence Modeling 20
2.3.1 Reynolds-Averaged Navier-Stokes (RANS) 20
2.3.2 Large Eddy Simulation (LES) 24
2.3.3 Comparison of Turbulence Modeling Approaches 26
2.4 Outfall Discharge Analysis 28
2.4.1 Single Discharges 28
2.4.2 Multiport Discharges 35
2.5 Concluding Remarks 41
3 Numerical Study on the Effect of Port Orientation on Multiple Inclined Dense Jets 45
3.1 Introduction 45
3.2 Methodology 51
3.2.1 Analysis 51
3.2.2 Governing Equations 53
3.2.3 Flow and Mesh Configurations 55
3.2.4 Model Setup and Numerical Algorithms 58
3.3 Results and Discussion 62
3.3.1 Model Validation 62
3.3.2 Effect of Non-Uniform Port Orientation on Jet Merging Process 65

3.4 Conclusions 70
4 Mixing Behavior of Multiport Diffusers with Non-Uniform Port Orientation 77
4.1 Introduction 78
4.2 Analysis 83
4.3 Experimental Procedure 86
4.4 Results 89
4.4.1 General Flow Behaviour 89
4.4.2 Major Flow Parameters 91
4.4.3 Merging Process 96
4.5 Conclusions 99
5 Summary, Concluding Remarks, and Recommendations 104
5.1 Summary and Concluding Remarks 104
5.2 Recommendations for Future Studies 107
Appendix A: Large Eddy Simulation of Multiple Inclined Brine Discharges 109
A.1 Introduction 110
A.2 Methodology 112
A.2.1 Multiple Jets Analysis 112
A.2.2 Governing Equations 112
A.2.3 Computational Setup 113
A.3 Results and Discussion 115
A.4 Conclusions 117
Appendix B: Test setup and equipment employed in this research 120

List of Figures

Figure 1-1 Brine entering the Mediterranean, 300 metres off the coast of Israel. (Image: Hagai Nativ / Alamy; Adopted from chinadialogueocean.net) 2

Figure 1-2 Typical configuration of a desalination plant outfall system. 2

Figure 1-3 Approximate time and length scales of different mixing phases of outfall discharges (P. J. Roberts et al., 2010). 5

Figure 1-4 (a) Rosette-type riser employed in the Boston outfall (P. J. Roberts et al., 2010); (b) A conventional multiport produced by Tideflex (adopted from measurit.com). 7

Figure 1-5 Concentration fields of (a) a 60º jet on a multiport diffuser with closely spaced ports and (b) a single 60º jet; F=24 for both jets (Abessi & Roberts, 2014). 7

Figure 1-6 Outfall discharge modeling approaches. 9

Figure 2-1 Schematic of different types of outfall discharges. 20

Figure 2-2 An instantaneous variable and its mean and fluctuating components. 21

Figure 2-3 Spatial filtering in the LES approach. 25

Figure 2-4 Comparison of the filtered velocity and the actual velocity. 26

Figure 2-5 Definition sketch for typical inclined jet parameters. 29

Figure 2-6 Schematic top-view of (a) eight-port rosette (b) one-sided and (c) two-sided diffusers. 36

Figure 3-1 Schematic (a) plan and (b) side views of multiple inclined dense jets. 52

Figure 3-2 (a) Computational domain and mesh setup; (b) detailed grids near the nozzles. 57

Figure 3-3 Flowchart of the PIMPLE algorithm; * and ** correspond to predicted and corrected fields, respectively. 59

Figure 3-4 Time-series graphs for the velocity magnitude along the trajectory of the central jet in case C2 at (a) x/(D.Fd) = 0.4, (b) x/(D.Fd) = 0.75, and (c) x/(D.Fd) = 1.2. 60

Figure 3-5 Experimental measurements (Abessi & Roberts, 2014) and numerical results of the normalized terminal rise height. 63

Figure 3-6 Experimental measurements (Abessi & Roberts, 2014) and numerical results of the normalized impact point distance. 64

Figure 3-7 Experimental measurements (Abessi & Roberts, 2014) and numerical results of the normalized impact dilution. 65

Figure 3-8 Visualization of (a) uniform (case C2) and (b) non-uniform (case S1) inclined dense jets, using a velocity isosurface (U = 0.015 m/s). 66
Figure 3-9 Concentration fields at different cross sections of uniform (case C2) and non-uniform (case S1) multiple inclined dense jets; (a) Section 1 (x/(D.Fd) = 0.25); (b) Section 2 (x/(D.Fd) = 1.5); (c) Section 2 (x/(D.Fd) = 2.5). 67
Figure 3-10 Concentration contours at the central plane for (a) case C2 and (b) case S1. 68
Figure 3-11 (a) Trajectory and (b) concentration of the central jet of cases C2 and S1. 69
Figure 3-12 Concentration at x/(D.Fd) = 3.4 and the elevation of nozzle tip on the centerline planes of (a) central and (b) adjacent jets. 70
Figure 4-1 Schematic (a) side- and (b) overhead-view of multiple inclined negatively buoyant jets (INBJs). 83
Figure 4-2 Side-view of multiport diffusers with (a) uniform and (b) non-uniform port orientation; demonstrating main angle (θ) and angle difference (φ). 86
Figure 4-3 (a) Schematic depiction and (b) photograph of the laser-induced fluorescence (LIF) experimental setup. 87
Figure 4-4 Photographs of the (a) uniform diffuser type III and (b) non-uniform diffuser type IIII 88
Figure 4-5 Lateral concentration profiles for the uniform diffuser Type I (a-d) and non-uniform diffuser Type II (e-h) at different cross-sections, F=29.6. 90
Figure 4-6 Snapshot of concentration fields for the (a) uniform diffuser Type I and (b) non-uniform diffuser Type II, F=29.6, x/dF=0.61. 91
Figure 4-7 Return or impact point distance versus port spacing for various diffuser configurations. 94
Figure 4-8 Terminal rise height versus port spacing for various diffuser configurations. 94
Figure 4-9 Return or impact point dilution versus port spacing for various diffuser configurations. 95
Figure 4-10 Cross-sectional concentration profiles along the lines between the central jets and their neighbouring jets for the (a) uniform diffuser Type I and (b) non-uniform diffuser Type II, F=23.5. 97
Figure 4-11 Variance of concentration ($\sigma 2/CMax2$) profiles over the lines presented in Figure 9 for the (a) uniform diffuser Type I and (b) non-uniform diffuser Type II, F=23.5. 98

Figure 4-12 The distance between the jets' centerline versus distance to diffusers for the (a) uniform diffuser Type I and (b) non-uniform diffuser Type II, F=23.5. 99

List of Tables

Table 1-1 Mixing zone terminology (reproduced from (P. J. Roberts et al., 2010)). 4
Table 2-1 International brine discharge regulations (T. Missimer et al., 2015) (Abessi, 2018)... 18
Table 2-2 Comparison between different applicable turbulence modeling approaches for outfall discharge modeling. 28
Table 2-3 Prominent numerical studies using the RANS modeling approaches for the simulation of single jets and their remarks. 31
Table 2-4 Prominent numerical studies using the LES modeling approach for the simulation of single jets and their remarks. 34
Table 2-5 Prominent numerical studies on the simulation of multiple jets and their remarks. 38
Table 3-1 Characteristics of numerical cases.. 56
Table 3-2 Simulation characteristics of the previous (Yan & Mohammadian, 2019) and present study.. 61
Table 4-1 Experimental conditions for uniform and non-uniform diffusers. 88
Table 4-2 Summary of experiments and flow parameters. 92

List of Abbreviations

3D	Three-Dimensional
AI	Artificial Intelligence
AIZ	Allocated Impact Zone
ARC	Advanced Research Computing
CFD	Computational Fluid Dynamics
CCD	Charge-Coupled Device
DES	Detached Eddy Simulation
DNS	Direct Numerical Simulation
DPSS	Diode-Pumped Solid-State
EPA	Environmental Protection Agency
EU	European Union
EVM	Eddy Viscosity Model
INBJ	Inclined Negative Buoyant Jet
LES	Large Eddy Simulation
LIF	Laser-Induced Fluorescence
LMZ	Legal Mixing Zone
LRR	Launder, Reece, and Rodi
MAPE	Mean Absolute Percentage Error
MGGP	Multigene Genetic Programming
NPDES	National Pollutant Discharge Elimination System
OpenFOAM	Open Field Operation and Manipulation
PBiCG	Preconditioned Bio Conjugate Gradient
PCG	Preconditioned Conjugate Gradient
RANS	Reynolds-Averaged Navier-Stokes
RNG	Re-Normalization Group
RSM	Reynolds Stress Model
SGGP	Single-Gene Genetic Programming
SGS	Subgrid-Scale
SST	Shear Stress Transport
TDZ	Toxic Dilution Zone

USEPA	United States Environmental Protection Agency
WFD	Water Framework Directive
ZID	Zone of Initial Dilution

List of Symbols

θ	Discharge Initial Angle [^{o}]
φ	Angle Difference Between Adjacent Ports [^{o}]
$\emptyset(t)$	Instantaneous Variable [depends on the variable]
$\overline{\emptyset}$	Mean Component of An Instantaneous Variable [depends on the variable]
$\emptyset'(t)$	Fluctuating Component of An Instantaneous Variable [depends on the variable]
ϕ_{ij}	Pressure-Strain Parameter []
α	Volume Fraction []
Δ	LES Filter Size []
ρ	Local Density [kg/m^3]
ρ_0	Effluent Density [kg/m^3]
ρ_a	Ambient Density [kg/m^3]
ε_{ij}	Turbulence Dissipation Rate Parameter [m^2/s^3]
ν_t	Turbulent Eddy Viscosity [m^2/s]
μ	Dynamic Viscosity [$N.s/m^2$]
μ_t	Turbulent Viscosity [$N.s/m^2$]
τ_{ij}	Stress Tensor []
Ω_{ij}	Transport Term by Rotation []
Π_{ij}	Transport Term by Turbulent Pressure-Strain Interactions []
δ_{ij}	Kronecker Delta []
d or d_0	Nozzle Diameter [m]
s	Port Spacing [m]
U_0 or U	Jet Velocity [m/s]

F_r	Froude Number []
F_d or F_0	Jet Densimetric Froude Number []
Q	Volume Flux [m/s]
M	Kinematic Momentum Flux [N/m^2]
B	Buoyancy Flux [N/(m^2.s)]
q_0	Volume Flux Per Unit Length [1/s]
m_0	Kinematic Momentum Flux Per Unit Length [N/m^3]
b_0	Buoyancy Flux Per Unit Length [N/(m.s)]
g	Gravitational Acceleration [m/s^2]
g_0'	Reduced Gravitational Acceleration [m/s^2]
l_Q and l_M	Jet Length Scales [m]
S_i	Impact Point Dilution []
S_r	Return Point Dilution []
S_c	Dilution Corresponds to Maximum Centerline Height []
S_n	Near Field Dilution []
x_i	Impact Point Location [m]
x_r	Return Point Location [m]
x_c	Horizontal Distance Corresponds to Maximum Centerline Height [m]
x_n	Near Field Location [m]
y_t	Terminal Rise Height [m]
y_c	Maximum Centerline Height [m]
y_l	Thickness Of Spreading Layer [m]
C_0	Initial Concentration [mg/L]
C_i	Impact Point Concentration [mg/L]
C	Local Concentration [mg/L]
t	Time [s]
h	Fluid Column Height [m]
D_{ab}	Molecular Diffusivity [m^2/s]
S_C	Turbulent Schmidt Number [m^2/s]
$\overline{u_i'u_j'}$	Reynolds Stress [m^2/s^2]
D_{ij}^T	Turbulent Diffusion Parameter []

D_{ij}^{ν}	Viscous Diffusion Parameter []
P_{ij}	Production Rate Parameter []
R_{ij}	Reynolds Stress [m^2/s^2]
$\bar{u}_i$	Filtered Velocity Field [m/s]
$\bar{p}$	Filtered Pressure Field [$kg/(m.s^2)$]

1 Introduction and Objectives

1.1 Introduction

The demand for freshwater is increasing due to industrialization and rapid population growth (Kucera, 2019), resulting in a more prevalent freshwater scarcity around the world (Ridoutt & Pfister, 2010). Although seawater desalination has been introduced as a sustainable solution for this issue during the past decades, hypersaline brines produced as waste by-products of desalination facilities can be a source of environmental issues if not properly disposed into the environment. Brine effluent is typically returned to the source ocean environment, altering the salinity, temperature, and contaminant levels in the surrounding environment, see Figure 1-1. Adverse impacts on the marine environment may arise, particularly substantial effluent discharges that coincide with sensitive ecosystems (Lattemann & Höpner, 2008). Although many organisms can adjust to slight changes in their environment, persistent exposure to unfamiliar conditions can result in lethality (Lattemann & Höpner, 2008) (Cooley & Heberger, 2013). To mitigate the environmental effects of brine effluents, some pre-disposal and disposal techniques should be considered. Effluents can be pre-diluted with other waste streams to reduce their salinity, and outfalls can incorporate cooling towers to mitigate the temperature before entering the water body. The treatment and substitution of hazardous substances can also minimize the adverse effects of chemicals on the environment (Lattemann & Höpner, 2008).

As an efficient disposal method, brine effluents are transported with long submarine pipelines to locations far from the shoreline, eliminating shoreline impacts, and then discharged as high-velocity turbulent jets through diffusers into seas and oceans, providing rapid mixing with ambient water, therefore protecting the marine environment, see Figure 1-2. These effluents are typically discharged at an upward angle to the horizontal and are negatively buoyant; therefore, they are referred to as inclined negative buoyant jets (INBJs). INBJs, which have a density higher than that of ambient water, first move upward, then turn downward, and finally impact the seabed. The dispersion of brine over the seabed can adversely affect benthic communities, such as seagrass beds, due to the high salinity and chemical residues (Lattemann & Höpner, 2008). Understanding the hydrodynamics of desalination discharges is crucial for minimizing the adverse environmental effects of desalination plants. Accurate prediction of the mixing of discharges with surrounding water bodies enables outfall designers to provide efficient designs for outfall systems.

Figure 1-1 Brine entering the Mediterranean, 300 metres off the coast of Israel. (Image: Hagai Nativ / Alamy; Adopted from chinadialogueocean.net)

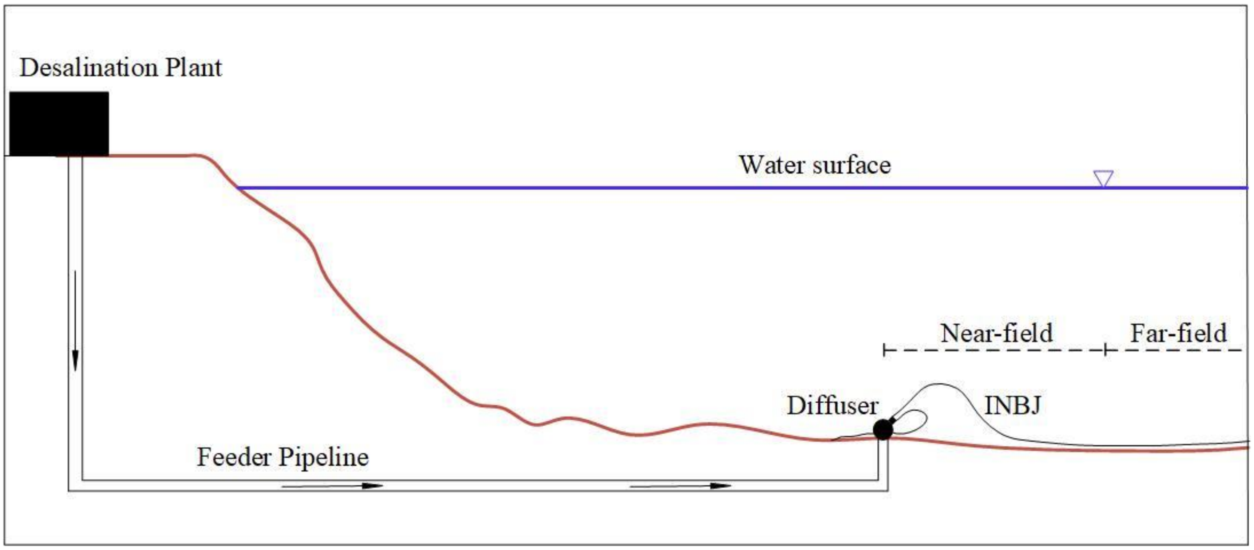

Figure 1-2 Typical configuration of a desalination plant outfall system.

The mixing process is affected by the marine environment and the discharge characteristics. The former encompasses elements such as receiving water stratification, topography of the seabed, waves, and currents—variables primarily beyond the control of designers. Conversely, the latter encompasses factors such as port geometry, jet momentum and buoyancy fluxes, and diffuser configuration, which can be modified by designers to enhance dilution. The mixing properties of discharges are closely related to diffuser characteristics (H Lai et al., 2015) (Yan & Mohammadian, 2019), highlighting the importance of studying diffusers with different configurations.

1.2 Research Background and Significance

This section briefly explains the key concepts and terminology crucial for the present study. It also addresses existing gaps in the literature and outlines the significance of this thesis.

1.2.1 Mixing Zone

The core of understanding the environmental effects associated with ocean outfalls and their regulatory framework lies in the concept of a mixing zone. The mixing zone represents an area of non-compliance and limited water use in the vicinity of the diffuser (P. J. Roberts et al., 2010). Therefore, it is necessary to satisfy the water quality criteria at the edge of the mixing zone. In this region, the concentration of most contaminants rapidly decreases to safe levels due to rapid and energetic mixing. The entrainment of substantial amounts of ocean water reduces the concentration of contaminants by more than 99% within this zone (P. J. Roberts et al., 2010). For brine discharges, the salinity increment or the absolute salinity at a specific distance from the outfalls is used as a basis to define regulations. Detailed international brine discharge regulations are presented in Chapter 2. Unfortunately, there is no universal definition of mixing zones yet, and the terminology associated with mixing processes includes different terms, as presented in Table 1-1. The mixing zone is a regulatory concept and may not necessarily align with actual physical mixing processes (P. J. Roberts et al., 2010) (Palomar & Losada, 2011). It could entirely enclose the near field and extend a certain distance into the far field, or it might not even fully encompass the near field.

Mixing generally includes three major phases: near field, far field, and long-term flushing. The near-field region is in the vicinity of outfall diffusers and is characterized by initial mixing. In this area, the initial momentum and buoyancy of the high-velocity discharges provide rapid mixing, resulting in high dilution rates. The location where the self-induced turbulence collapses under the effect of induced density stratification is defined as the end of the near field (P. J. W. Roberts et al., 1997). Far-field mixing occurs beyond the near field, where the initial mixing is complete. In this region, the effluent moves on the seabed as a density current and is affected by ocean currents and turbulence. Long-term flushing refers to the long-term buildup of contaminants and occurs over long timescales.

Table 1-1 Mixing zone terminology (reproduced from (P. J. Roberts et al., 2010)).

Term	Definition and Comments
Mixing zone / Allocated impact zone (AIZ)	- A limited area where rapid mixing takes place and where numeric water quality criteria can be exceeded but acutely toxic conditions must be prevented. - Specified dilution factors and water quality requirements must be met at the edge of the mixing zone.
Regulatory mixing zone / Legal mixing zone (LMZ)	- As defined by the appropriate regulatory authority - Can be a length, an area, or a volume of the water body
Near field / Hydrodynamic mixing zone	- Region where mixing is caused by turbulence and other processes generated by the discharge itself. - Near field processes are intimately linked to the discharge parameters and are under the control of the designer.
Far field	- Region where mixing is due to ambient oceanic turbulence - Far field processes are not under control of the designer
Toxic dilution zone (TDZ)	- A more restrictive mixing zone within the usual mixing zone
Initial dilution	- A general term for the rapid dilution that occurs near the diffuser
Zone of initial dilution (ZID)	- A region extending over the water column and extending up to one water depth around the diffuser. - A regulatory mixing zone, as defined in the U.S. EPA's 301(h) regulations (USEPA, 1994)

The length and time scales involved in the different phases are substantially diverse, making it impossible to simulate them using a single comprehensive model (see Figure 1-3). These scales progressively expand as the effluent moves farther away from the diffuser (Brooks, 1984). As shown, the far field is not located immediately after the near field, and there is a gradual transition between them. However, for simulations, it is more convenient to consider a sudden transition.

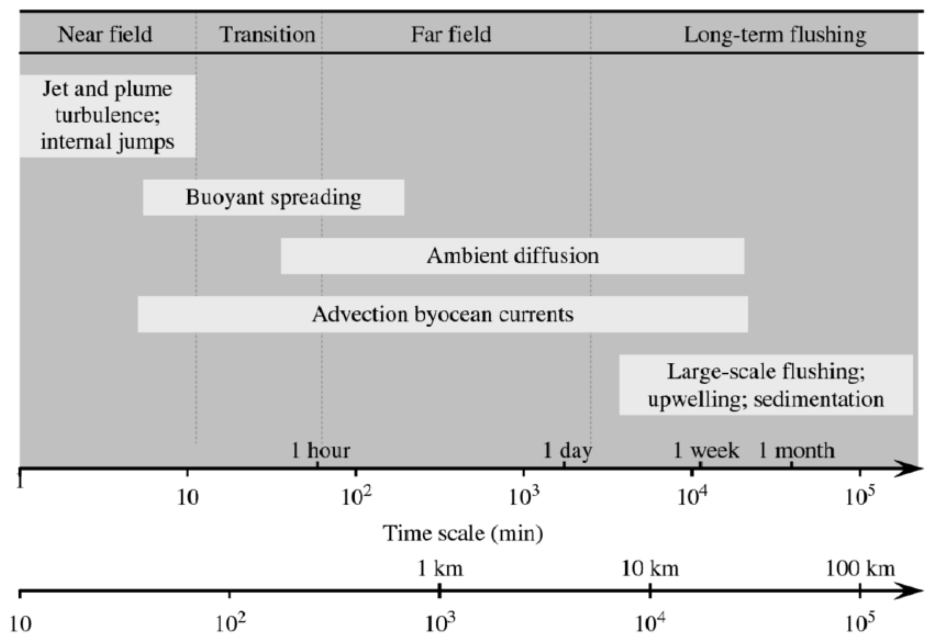

Figure 1-3 Approximate time and length scales of different mixing phases of outfall discharges (P. J. Roberts et al., 2010).

1.2.2 Diffuser Design

Diffusers are applied at the end of an outfall system to enhance the mixing of brine with the surrounding water and thus reducing environmental risks. The application of diffusers in outfall systems has shown a significant impact on effluent dispersion. For example, one study evaluated the effects of installing a 60° single-port diffuser at the Nuevo Canal de Cartagena desalination plant pipeline on the dispersion of brine (Loya-Fernández et al., 2018) and showed that the dilution rate of samples taken 1 km from the outfall increased by almost 17 times after the diffuser installation.

Desalination diffusers are typically designed as single-port discharges for low flow rates. For single discharges, the port angle to the horizontal direction is an important design feature affecting the mixing process. Ports with high angles to the horizontal direction typically cannot result in high dilution rates. The vertical discharges (90°) fall back on themselves (Fischer et al., 1979) (P. J. W. Roberts et al., 1997) (Missimer et al., 2015), and the nozzles with angles > 80° experience significant re-entrainment resulting from the interaction of the ascending and descending components of the jets (Ferrari & Querzoli, 2010), impairing the mixing of brine with the ambient water. Very shallow-angled nozzles cannot provide long trajectories, and only provide a limited surface for entrainment, resulting in low dilution rates. It is widely accepted that 60º jets result in the highest dilution rates (Kikkert et al., 2007) (Zeitoun et al., 1970) (Zeitoun et al., 1972); however, almost the same rates have been reported in some studies in the range of 45º to 75º (Jirka, 2008) (Oliver et al., 2013) (Papakonstantis et al., 2011) (Abessi & Roberts, 2015).

Diffusers are designed as multiport discharges at high flow rates. The design of a multiport diffuser requires more factors to be considered because the individual jets on a multiport diffuser do not mix with the ambient water separately and may be affected by their neighboring discharges. The nozzles on a multiport diffuser can be arranged in either rosette patterns or evenly spaced configurations. The rosette-type diffusers include some risers each having 2-8 ports, typically discharged horizontally (Lai & Lee, 2012). A conventional multiport diffuser consists of evenly spaced ports oriented at the same angle to the horizontal. The focus of this thesis is on conventional diffusers, and they are called uniform diffusers in the present study. As an example, Figure 1-4 (a) illustrates a rosette-type riser with eight ports out of the 55 risers employed for the Boston outfall, and Figure 1-4 (b) depicts a conventional multiport diffuser.

The mixing behaviors of single and multiple jets differ because of the interaction of the discharges on a multiport diffuser. Single jets entrain the surrounding water without any interaction. A primary concern regarding multiport diffusers is the spacing between ports. If they are too close, jet merging limits the entrainment of ambient water and causes the jets to have a reduced terminal rise height and bend inwards. This shortened trajectory diminishes the available surface for entrainment, resulting in a reduction in dilution (Abessi & Roberts, 2014). As an example, different behaviors of single and multiple jets are evident in Figure 1-5, where the two jets are discharged with the same velocity, but the jet on a multiport diffuser with closely spaced ports (Figure 1-5(a)) experiences a shorter trajectory and depicts higher concentrations compared to the single discharge (Figure 1-5(b)).

(a) (b)

Figure 1-4 (a) Rosette-type riser employed in the Boston outfall (P. J. Roberts et al., 2010); (b) A conventional multiport produced by Tideflex (adopted from measurit.com).

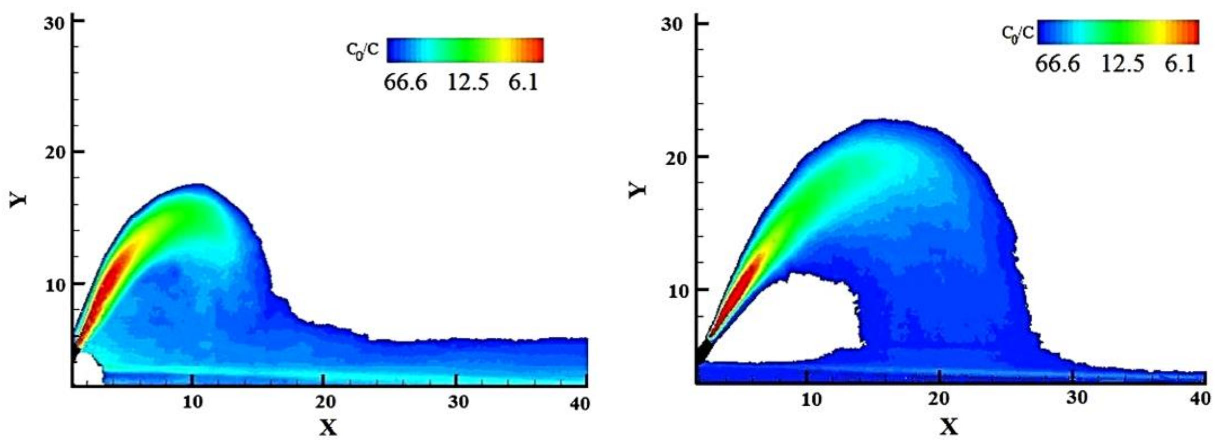

(a) (b)

Figure 1-5 Concentration fields of (a) a 60° jet on a multiport diffuser with closely spaced ports and (b) a single 60° jet; F=24 for both jets (Abessi & Roberts, 2014).

Abessi and Roberts investigated the extent of this reduction in mixing efficiency by exploring the variation in impact dilution with port spacing for multiple 60° jets. They showed that when the ports on a multiport diffuser were closely spaced, there was a high interaction between discharges, and the impact dilution was approximately one-quarter of that for single discharges. Despite this huge reduction in dilution due to jet merging, most designs of multiport diffusers were based on investigations of single jets before 2014 (M. Baum, 2019). They also recommended maintaining a normalized port spacing (s/dF) of approximately two between the ports to minimize jet interaction and therefore avoid a reduction in dilution, where s is the port spacing, d is the port diameter, and F is the Froude number. However, more space between ports can impose high costs on desalination outfall projects because of the longer diffuser pipes. These costs may vary from a few thousand to more than US$30,000/m (Roberts et al., 2010).

1.2.3 Outfall Discharge Modeling

Designers can apply different scenarios using reliable modeling tools to provide the most efficient designs while maintaining regulatory demands. Outfall discharges can be simulated using length-scale, integral, and computational fluid dynamics (CFD) models (Figure 1-6). Length-scale models are semi-empirical approaches obtained based on numerous field or experimental data. These models can provide simplified formulas that represent the general behavior of the flow field. CORMIX and NRFIELD are examples of simulation tools working based on these models.

Integral entrainment models are widely employed by designers to assess jet mixing behavior and are the basis for commercial mixing tools such as JetLag (Joseph W Lee et al., 1990) (Lee et al., 2003), CoreJet (Jirka, 2004), and UM3 (Frick, 2004). These models assume the jet velocity profiles to be Gaussian or top-hat and axisymmetric without radial changes, resulting in simplified governing momentum and mass conservation equations. The application of these commercial tools for the study of inclined dense jets has shown many discrepancies in the prediction of terminal rise height and more than 50% under-prediction of dilution (Palomar et al., 2012). Furthermore, they are unable to resolve the re-entrainment and Coanda effect (M. J. Baum & Gibbes, 2020) (Taherian & Mohammadian, 2021). The negative impact of these limitations on the predictions can be more pronounced when employing these models for multiple INBJs, where re-entrainment and the Coanda effect play a significant role in the mixing behavior (Abessi & Roberts, 2014) (P. J. W. Roberts, 2015), compared to single INBJs.

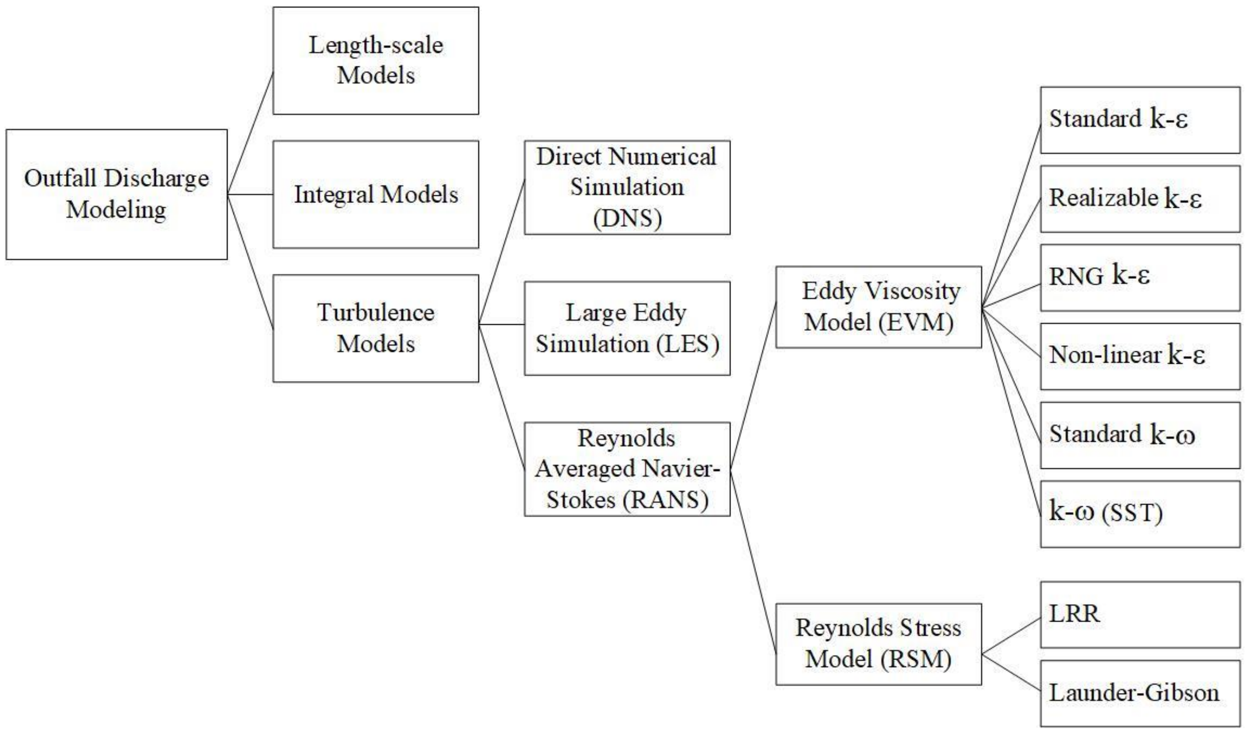

Figure 1-6 Outfall discharge modeling approaches.

CFD modeling includes fewer simplifying assumptions than integral models and is currently a promising tool for the simulation of effluent discharges. Abaqus/CFD and ANSYS Fluent are commercial tools, and OPEN Field Operation and Manipulation (OPENFOAM) is an open-source software used for CFD analysis. CFD tools are used to solve the Navier–Stokes fluid flow governing equations. The Navier–Stokes equations describe fluid flow using a set of partial differential equations (PDEs), including continuity and momentum equations. The physical concept behind the continuity equation is that mass is conserved. It can be expressed as

$$\frac{\partial u}{\partial x}+\frac{\partial v}{\partial y}+\frac{\partial w}{\partial z}=0 \qquad (1\text{-}1)$$

where u, v, and w are the mean velocity components in the x-, y-, and z-directions, respectively. The momentum equations are defined as follows:

$$\frac{Du}{Dt}=-\frac{1}{\rho}\frac{\partial p}{\partial x}+\frac{\partial}{\partial x}\left(\nu_{eff}\left(\frac{\partial u}{\partial x}\right)\right)+\frac{\partial}{\partial y}\left(\nu_{eff}\left(\frac{\partial u}{\partial y}\right)\right)+\frac{\partial}{\partial z}\left(\nu_{eff}\left(\frac{\partial u}{\partial z}\right)\right) \qquad (1\text{-}2)$$

$$\frac{Dv}{Dt} = -\frac{1}{\rho}\frac{\partial p}{\partial y} + \frac{\partial}{\partial x}\left(\nu_{eff}\left(\frac{\partial v}{\partial x}\right)\right) + \frac{\partial}{\partial y}\left(\nu_{eff}\left(\frac{\partial v}{\partial y}\right)\right) + \frac{\partial}{\partial z}\left(\nu_{eff}\left(\frac{\partial v}{\partial z}\right)\right) - g\frac{\rho - \rho_0}{\rho} \quad (1\text{-}3)$$

$$\frac{Dw}{Dt} = -\frac{1}{\rho}\frac{\partial p}{\partial z} + \frac{\partial}{\partial x}\left(\nu_{eff}\left(\frac{\partial w}{\partial x}\right)\right) + \frac{\partial}{\partial y}\left(\nu_{eff}\left(\frac{\partial w}{\partial y}\right)\right) + \frac{\partial}{\partial z}\left(\nu_{eff}\left(\frac{\partial w}{\partial z}\right)\right) \quad (1\text{-}4)$$

where t is the time, ν_{eff} is the effective kinematic viscosity ($\nu_{eff} = \nu + \nu_t$; ν_t is the turbulent kinematic viscosity), and p is the fluid pressure.

Turbulence modeling in CFD analysis includes the effect of turbulence in the simulation of outfall discharges (M. J. Baum & Gibbes, 2020). These models are very practical for discharge modeling because brine effluents are usually discharged as high-velocity jets and are highly turbulent. These models mainly include Reynolds-averaged Navier–Stokes (RANS), large eddy simulation (LES), and direct numerical simulation (DNS), which are explained in detail in Chapter 2. These methods have been widely validated against the mixing behavior of single jets in prior research (Oliver et al., 2008) (Huai et al., 2010) (Ardalan & Vafaei, 2019) (Kheirkhah Gildeh et al., 2014) (Kheirkhah Gildeh et al., 2015) (Kheirkhah Gildeh et al., 2016) (Zhang et al., 2016) (Zhang et al., 2017) (Ardalan & Vafaei, 2019) (Jiang et al., 2019) (Tofighian et al., 2022). However, their application in multiport diffusers has received less attention. The application of LES and DNS for the simulation of multiple jets requires a very high computational cost. The reason behind this is that the LES directly resolves large eddies and only models small eddies, and DNS computes all turbulent flow problems. In contrast, the RANS technique focuses on the impact of turbulence on the mean flow field properties and models all eddies, requiring less computational cost compared to the other two models. In this method, the Navier-Stokes equations are time-averaged before being numerically solved, resulting in the emergence of an unknown term called Reynolds stress tensor. Different RANS turbulence models have been introduced to estimate this term, including the eddy viscosity model (EVM) and Reynolds stress model (RSM). The former assumes that Reynolds stresses are proportional to the mean deformation rates. Conversely, the latter employs Reynolds stress transport equations to obtain the Reynolds stress tensor directly.

Although some studies have evaluated the performance of RSMs for single INBJs, previous studies on multiple INBJs have mainly employed EVMs. A recent study (Yan & Mohammadian, 2019) showed that the standard and re-normalization group (RNG) k-ε turbulence models predicted the terminal rise height and impact point dilution with errors lower than 15%. The standard and (RNG) k–ε models could provide predictions of the impact distance of less than 18.6% and 13.3%, respectively. Another study (M. J. Baum & Gibbes, 2020) validated the performance of the k- ω (SST) model for the prediction of the Gold Coast Desalination Plant offshore inclined multiport brine diffuser under different ambient velocity conditions.

1.3 Research Objectives, Novelty, and Contributions

The overall objective of this study was to improve the design of desalination discharge systems, which can be divided into the following sub-objectives:

- Developing a three-dimensional numerical model to accurately predict the mixing behavior of multiple discharges with ambient water.
- Improving understanding of the merging process of multiple discharges.
- Modifying the design of multiport diffusers to improve their mixing performance and therefore reduce environmental risks.

The novel elements of this study can be outlined as:

- This study three-dimensionally simulated multiple INBJs employing the Launder, Reece, and Rodi (LRR) turbulence model as a new approach in this context to close the Navier-Stokes equations. The numerical studies available in the literature have mainly investigated the prediction capabilities of EVMs for multiple INBJs. As the LRR is an RSM, unlike the EVMs, it directly solves the transport equations for the Reynolds stresses and considers different values for viscosity in each direction; thus, the prediction capability of this model for multiple jets was evaluated. The choice of the turbulence model is very important in predicting the flow behavior (Kheirkhah Gildeh et al., 2015); therefore, the examination of new turbulence models can add to the knowledge of choosing the best model for this application.
- This study experimentally and numerically investigates the merging process of multiple dense jets. It explored the expansion and interaction of jets on a multiport diffuser at different distances from the diffuser in detail. Although there are limited studies on the merging process of positively buoyant jets, to the best of the author's knowledge, there has

been no systematic study on the evolution of discharges and jet merging with distance from the diffuser for multiple dense jets. The merging of INBJs differs from that of positively buoyant jets as INBJ experiences both rising and falling stages while merging with adjacent jets. Studying the merging process clarifies how jet merging limits entrainment and mitigates dilution in multiport discharge. Furthermore, the merging process of multiport diffusers with non-uniform port orientations was studied for the first time.

- This paper proposes a novel concept for the modification of multiport desalination outfalls. It investigated the mixing behavior of multiport diffusers with non-uniform port orientation and introduced the angle difference as an effective factor in the mixing of multiple discharges. The flow fields resulting from multiport diffusers with uniform and non-uniform diffusers were experimentally, using the laser-induced fluorescence (LIF) technique and numerically compared. Previous studies have shown the effect of port orientation on the mixing behavior of single jets and that of port spacing on that of multiple jets. The ports on multiport diffusers are mainly discharged at the same angle of 60^o to the horizontal, and there have been no systematic studies on the influence of port orientation on multiple jets.
- To the best of our knowledge, this research provides the first computational fluid dynamics (CFD) simulation of multiple INBJs with non-uniform port orientations.

1.4 Thesis Outline

This thesis is organized as a sequence of technical papers and is divided into five chapters. Following the current chapter (Chapter 1), an overview of outfall discharge modeling with a focus on turbulence modeling approaches is presented in Chapter 2. In particular, this chapter explains the environmental regulations, outfall discharge analysis, turbulence modeling approaches, and pros and cons of each turbulence model. In addition, prominent numerical studies on the simulation of single and multiple jets and their conclusions are presented in different tables. This chapter was published as part of a book chapter in Advances in Fluid Mechanics, Modelling, and Simulations (Springer).

A numerical study of the effect of port orientation on multiple inclined dense jets is presented in Chapter 3. An introduction and extensive literature review on outfall discharge modeling are described at the beginning of this chapter, followed by the methodology including analysis, governing equations, flow and mesh configurations, and model setup and numerical algorithm. Multiport diffusers with 60º inclined jets were three-dimensionally modeled using the LRR model, and the predictions for the terminal rise height, impact point distance, and impact point dilution were compared against the available experimental data in the literature for validation, as presented in the first part of the results section. The validated model was further employed for the simulation of multiport diffusers with non-uniform diffusers, incorporating 60º and 45º ports, and for comparison. The second part of the results section is devoted to a comparison of the mixing process of uniform and non-uniform diffusers. This chapter has been published in the Journal of Marine Science and Engineering (MDPI).

The mixing behavior of multiport diffusers with non-uniform port orientations is presented in Chapter 4. This chapter first describes how jet mering impairs the mixing process of multiport diffusers and provides different examples showing the extent of this negative effect. Subsequently, the LIF experimental setup and designed uniform and non-uniform multiport diffusers are presented. In the results section, the general flow behavior and major flow parameters of the uniform and non-uniform diffusers are compared, and the reasons for their different behaviors are explained using the merging processes. This chapter was published in the Desalination (Elsevier).

Finally, Chapter 5 presents conclusions from different chapters and recommendations for further studies.

1.5 List of Publications (form the thesis)

- Taherian, M., Saeidi Hosseini, S. A. R., & Mohammadian, A. (2022). Overview of outfall discharge modeling with a focus on turbulence modeling approaches. In Advances in Fluid Mechanics: Modelling and Simulations (pp. 139-177). Singapore: Springer Nature Singapore.
  https://link.springer.com/chapter/10.1007/978-981-19-1438-6_4
- Saeidi Hosseini, S. A. R., Mohammadian, A., Roberts, P. J., & Abessi, O. (2022). Numerical Study on the Effect of Port Orientation on Multiple Inclined Dense Jets. Journal of Marine Science and Engineering, 10(5): 590.
  https://www.mdpi.com/2077-1312/10/5/590

- Hosseini, S. A. R. S., Taherian, M., Mohammadian, A., Ferrari, S., Roberts, P. J. (2023). Mixing behavior of multiport diffusers with nonuniform port orientations. Desalination, 116962.
  https://www.sciencedirect.com/science/article/abs/pii/S0011916423005945

References

Abessi, O., & Roberts, P. J. W. (2014). Multiport Diffusers for Dense Discharges. Journal of Hydraulic Engineering, 140(8), 04014032. https://doi.org/10.1061/(ASCE)HY.1943-7900.0000882

Abessi, O., & Roberts, P. J. W. (2015). Effect of nozzle orientation on dense jets in stagnant environments. Journal of Hydraulic Engineering, 141(8), 06015009. https://doi.org/10.1061/(ASCE)HY.1943-7900.0001032

Ardalan, H., & Vafaei, F. (2019). CFD and Experimental Study of 45° Inclined Thermal-Saline Reversible Buoyant Jets in Stationary Ambient. Environmental Processes, 6(1), 219–239. https://doi.org/10.1007/s40710-019-00356-z

Baum, M. (2019). Dense jet behaviour in dynamic receiving environments, Ph.D. thesis, University of Queensland Brisbane.

Baum, M. J., & Gibbes, B. (2020). Field-Scale Numerical Modeling of a Dense Multiport Diffuser Outfall in Crossflow. Journal of Hydraulic Engineering, 146(1), 05019006. https://doi.org/10.1061/(asce)hy.1943-7900.0001635

Bleninger, T. (2006). Coupled 3D hydrodynamic models for submarine outfalls: Environmental hydraulic design and control of multiport diffusers, Doctoral Dissertation, Karlsruhe, Zugl.

Brooks, N. H. (1984). Dispersal of wastewater in the ocean-a cascade of processes at increasing scales. In Water for Resource Development: Proceedings of the Conference (pp. 1–7).

Cooley, H., & Heberger, M. (2013). Key issues for seawater desalination in California: Energy and greenhouse gas emissions.

Ferrari, S., & Querzoli, G. (2010). Mixing and re-entrainment in a negatively buoyant jet. Journal of Hydraulic Research, 48(5), 632–640. https://doi.org/10.1080/00221686.2010.512778

Fischer, H.B., List, E.J., Koh, R.C.Y., Imberger, J., Brooks, N.H. (1979) Mixing in Inland and Coastal Waters; Academic Press: Amsterdam, The Netherlands.

Frick, W. E. (2004). Visual Plumes mixing zone modeling software. Environmental Modelling & Software, 19(7–8), 645–654.

Huai, W.-X., Li, Z.-W., Qian, Z., Zeng, Y.-H., Han, J., Peng, W.-Q. (2010). Numerical simulation of horizontal buoyant wall jet. Journal of Hydrodynamics, 22(1), 58–65. https://doi.org/10.1016/S1001-6058(09)60028-7

Jiang, M., Law, A. W. K., & Lai, A. C. H. (2019). Turbulence characteristics of 45° inclined dense jets. Environmental Fluid Mechanics, 19(1), 27–54. https://doi.org/10.1007/s10652-018-9614-8

Jirka, G. H. (2004). Integral Model for Turbulent Buoyant Jets in Unbounded Stratified Flows. Part I: Single Round Jet. Environmental Fluid Mechanics, 4(1), 1–56. https://doi.org/10.1023/A:1025583110842

Jirka, G. H. (2008). Improved discharge configurations for brine effluents from desalination plants. Journal of Hydraulic Engineering, 134(1), 116–120. https://doi.org/10.1061/(ASCE)0733-9429(2008)134:1(116)

Joseph W Lee, B. H., Member, A., & Cheung, V. (1990). Generalized Lagrangian Model for Buoyant Jets in Current. Journal of Environmental Engineering, 116(6), 1085–1106. https://doi.org/10.1061/(ASCE)0733-9372(1990)116:6(1085)

Kheirkhah Gildeh, H., Mohammadian, A., Nistor, I., & Qiblawey, H. (2014). Numerical Modeling of Turbulent Buoyant Wall Jets in Stationary Ambient Water. Journal of Hydraulic Engineering, 140(6), 04014012. https://doi.org/10.1061/(asce)hy.1943-7900.0000871

Kheirkhah Gildeh, H., Mohammadian, A., Nistor, I., & Qiblawey, H. (2015). Numerical modeling of 30∘ and 45∘ inclined dense turbulent jets in stationary ambient. Environmental Fluid Mechanics, 15(3), 537–562. https://doi.org/10.1007/s10652-014-9372-1

Kheirkhah Gildeh, H., Mohammadian, A., Nistor, I., Qiblawey, H., & Yan, X. (2016). CFD modeling and analysis of the behavior of 30° and 45° inclined dense jets - New numerical insights. Journal of Applied Water Engineering and Research, 4(2), 112–127. https://doi.org/10.1080/23249676.2015.1090351

Kikkert, G. A., Davidson, M. J., & Nokes, R. I. (2007). Inclined Negatively Buoyant Discharges. Journal of Hydraulic Engineering, 133(5), 545–554. https://doi.org/10.1061/(ASCE)0733-9429(2007)133:5(545)

Kucera, J. (2019). Desalination: water from water, 2nd edition, John Wiley & Sons.

Lai, A. C. H., & Lee, J. H. W. (2012). Dynamic interaction of multiple buoyant jets. Journal of Fluid Mechanics, 708, 539–575. https://doi.org/10.1017/jfm.2012.332

Lai, A. C. H., Zhao, B., Wing-Keung Law, A., Eric Adams, E., H Lai, A. C., Zhao, B., W-K Law, A., & Adams, E. E. (2015). A numerical and analytical study of the effect of aspect ratio on the behavior of a round thermal. Springer, 15, 85–108. https://doi.org/10.1007/s10652-014-9362-3

Lattemann, S., & Höpner, T. (2008). Environmental impact and impact assessment of seawater desalination. Desalination, 220(1–3), 1–15. https://doi.org/10.1016/j.desal.2007.03.009

Lee, J.H.W.; Chu, V.H. (2003) Turbulent Jets and Plumes: A Lagrangian Approach; Springer Science & Business Media: Berlin/Heidelberg, Germany, 1.

Loya-Fernández, Á., Ferrero-Vicente, L. M., Marco-Méndez, C., Martínez-García, E., Zubcoff Vallejo, J. J., & Sánchez-Lizaso, J. L. (2018). Quantifying the efficiency of a mono-port diffuser in the dispersion of brine discharges. Desalination, 431(October 2017), 27–34. https://doi.org/10.1016/j.desal.2017.11.014

Missimer, T. M., Jones, B., & Maliva, R. G. (2015). Intakes and Outfalls for Seawater Reverse-Osmosis Desalination Facilities: Innovations and Environmental Impacts. Springer, New York, NY, USA.

Oliver, C. J., Davidson, M. J., & Nokes, R. I. (2008). k-ε Predictions of the initial mixing of desalination discharges. Environmental Fluid Mechanics, 8(5–6), 617–625. https://doi.org/10.1007/s10652-008-9108-1

Oliver, C. J., Davidson, M. J., & Nokes, R. I. (2013). Behavior of dense discharges beyond the return point. Journal of Hydraulic Engineering, 139(12), 1304–1308. https://doi.org/10.1061/(ASCE)HY.1943-7900.0000781

Palomar, P., Lara, J., & Losada, I. (2012). Near field brine discharge modeling part 2: Validation of commercial tools. Desalination, 290, 28–42.

Palomar, P., & Losada, I. J. (2011). Desalination, trends and technologies. (M. Schorr, Ed.).

Papakonstantis, I. G., Christodoulou, G. C., & Papanicolaou, P. N. (2011). Inclined negatively buoyant jets 2: Concentration measurements. Journal of Hydraulic Research, 49(1), 13–22. https://doi.org/10.1080/00221686.2010.542617

Ridoutt, B. G., & Pfister, S. (2010). A revised approach to water footprinting to make transparent the impacts of consumption and production on global freshwater scarcity. Global Environmental Change, 20(1), 113–120.

Roberts, P. J., Salas, H. J., Reiff, F. M., Libhaber, M., Labbe, A., & Thomson, J. C. (2010). Marine wastewater outfalls and treatment systems. IWA publishing.

Roberts, P. J. W. (2015). Near field flow dynamics of concentrate discharges and diffuser design. Environmental Science and Engineering (Subseries: Environmental Science), 149, 369–396. https://doi.org/10.1007/978-3-319-13203-7_17

Roberts, P. J. W., Ferrier, A., & Daviero, G. (1997). Mixing in inclined dense jets. Journal of Hydraulic Engineering, 123(8), 693–699. https://doi.org/10.1061/(ASCE)0733-9429(1997)123:8(693)

Taherian, M., & Mohammadian, A. (2021). Buoyant jets in cross-flows: review, developments, and applications. Journal of Marine Science and Engineering, 9(1), 61.

Tofighian, H., Aghajanpour, A., & Abessi, O. (2022). Simulation of inclined dense jets in stagnant environments: an LES and experimental study. Environmental Fluid Mechanics, 22(5), 1161–1185.

Yan, X., & Mohammadian, A. (2019). Numerical modeling of multiple inclined dense jets discharged from moderately spaced ports. Water (Switzerland), 11(10), 14–16. https://doi.org/10.3390/w11102077

Zeitoun, M. A., McHilhenny, W. F., & Reid, R. O. (1970). Conceptual Designs of Outfall Systems for Desalination Plants. In Offshore Technology Conference; OnePetro: Washington, DC, USA.

Zeitoun, M. A., Reid, R. O., McHilhenny, W. F., & Mitchell, T. M. (1972). Model Studies of Outfall Systems for Desalination Plants. Part III. Numerical Simulation and Design Considerations; Dow Chemical Co.: Freeport, TX, USA.

Zhang, S., Jiang, B., Law, A. W. K., & Zhao, B. (2016). Large eddy simulations of 45° inclined dense jets. Environmental Fluid Mechanics, 16(1), 101–121. https://doi.org/10.1007/s10652-015-9415-2

Zhang, S., Law, A. W. K., & Jiang, M. (2017). Large eddy simulations of 45° and 60° inclined dense jets with bottom impact. Journal of Hydro-Environment Research, 15, 54–66. https://doi.org/10.1016/j.jher.2017.02.001

2 Overview of Outfall Discharge Modeling with a Focus on Turbulence Modeling Approaches[1]

Abstract

A comprehensive understanding of outfall discharge behavior can significantly benefit the optimal design of outfall systems while ensuring compliance with regulatory requirements. Advances in computational resources and techniques over the past two decades have paved the way for the introduction of numerical modeling as a promising approach for simulating outfall discharges and gathering comprehensive data for the entire outfall region. Thus, there is a growing need to explore numerical methods for modeling jet and plume-type flows in greater detail. Among the various numerical techniques available, the computational fluid dynamics (CFD) method stands out, as it can provide highly detailed insights into the flow patterns of outfall discharge systems without relying on some of the simplified assumptions found in length-scale and jet integral approaches.
This chapter aims to offer an overview of the current state-of-the-art in outfall discharge modeling and a summary of the research endeavors undertaken in this field. Additionally, it explores different aspects concerning turbulence modeling approaches within the CFD technique, showcasing the applicability of both Reynolds-averaged Navier-Stokes (RANS) and large eddy simulation (LES) in the modeling of outfall discharges.

Keywords: environmental impacts; outfall discharge modeling; flow behavior; CFD technique; turbulence modeling approaches.

2.1 Environmental Regulations

The consideration of environmental standards and regulations, such as US Environmental Protection Agency (EPA) (EPA, 1994) and EU Water Framework Directive (WFD) (Chave, 2001), is vital during the design, implementation, and monitoring of outfall systems, irrespective of the type of discharge. The reason behind this is that without such regulations it is impossible to check if one discharge system is properly designed and capable of efficiently providing the required

[1] This chapter has been published as a part of a book chapter as: Taherian, M., Saeidi Hosseini, S. A. R., & Mohammadian, A. (2022). Overview of outfall discharge modeling with a focus on turbulence modeling approaches. In Advances in Fluid Mechanics: Modelling and Simulations (pp. 139-177). Singapore: Springer Nature Singapore.

mixing at various distances. The requirements for wastewater and thermal discharges are being quite well developed. For instance, discharges into rivers, lakes, and coastal waters of the US are regulated via the National Pollutant Discharge Elimination System (NPDES) (T. Missimer et al., 2015). Some regulations for brine discharges and their compliance points are indicated in Table 2-1. The international regulations are usually defined based on either the salinity increment or the absolute salinity at a specific distance from outfalls.

Table 2-1 International brine discharge regulations (T. Missimer et al., 2015) (Abessi, 2018).

Region/Authority	Salinity increment limit (ppt)	Absolute salinity limit (ppt)	Compliance point (relative to discharge) (m)
Sydney, Australia	≤ 1	-	50-75
Gold Coast, Australia	≤ 2	-	120
Oman	≤ 2	-	300
US EPA	≤ 4	-	-
Okinawa, Japan	≤ 1	-	Mixing zone boundary
Huntington Beach, CA	-	≤ 40	304.8
Carlsbad, CA	-	≤ 40	304.8

2.2 Outfall Discharge Principles and Classification

The Froude number is an important non-dimensional parameter in fluid dynamics and is mainly related to the influence of gravity on fluid motion. It can be defined as:

$$F_r = \frac{u}{\sqrt{gl}} \tag{2-1}$$

where u is the characteristic flow velocity, g is the acceleration of the external field, and l is the characteristic length depending on the geometry of the flow channel.

However, when it comes to buoyant jets, the densimetric Froude number (F_0) is more common, which can be expressed as follows:

$$F_0 = \frac{U_0}{\sqrt{g'l}} \tag{2-2}$$

$$g' = \frac{\Delta\rho}{\rho_0} g \tag{2-3}$$

where g' is the modified gravitational buoyancy acceleration and $\Delta\rho$ is the density difference between the jet flow and the ambient fluid.

To design an ocean outfall system, it is essential to adopt the most efficient discharge form to reach rapid and efficient mixing. The classification of buoyant jets can vary depending on the different standards. Buoyant jets can be classified based on the discharge location, the jet density relative to the ambient water, or the discharge direction.

Regarding the discharge location, wastewaters may be discharged either as surface or submerged jets. Surface discharges do not achieve efficient mixing and rapidly change to density currents moving at the bottom of the surrounding water. However, the dilution rates for submerged jets are much higher compared to surface discharges since the surrounding fluid entrains into the jet in all directions. Previous studies confirm the idea that efficient mixing of the highly concentrated brine effluent can be reached by submerged discharge in an upwards direction as a high velocity turbulent jet (P. J. W. Roberts et al., 1997) (Kheirkhah Gildeh et al., 2015b) (Loya-Fernández et al., 2018).

Considering the jet density compared to the surrounding water density, jets can be categorized into two main groups: positively and negatively buoyant jets, as shown in Figure 2-1. A positively buoyant jet has a density less than the ambient fluid density ($\rho_0 < \rho_a$) so that both momentum and buoyancy affect the flow dynamics. Thermal discharges from power plants into colder ambient water and sewage discharges into denser ocean water can be the most applicable examples of positively buoyant jets. The effluent rises because of buoyancy forces until it reaches the water surface, and then spreads horizontally as plumes. However, the effluent may not reach the water surface in a stratified ambient. In stratified receiving water, the effluent rises to a level where its density is the same as the ambient water, then spreads horizontally. In contrast, a negatively buoyant jet has a density higher than the ambient water ($\rho_0 > \rho_a$); as a result, its trajectory is completely different. Since the jet density is higher than the receiving water, the negative buoyancy causes the dense jet to reach a terminal rise height and then fall back to the lower boundary. Once the dense jet impacts the seabed, it spreads as a density current.

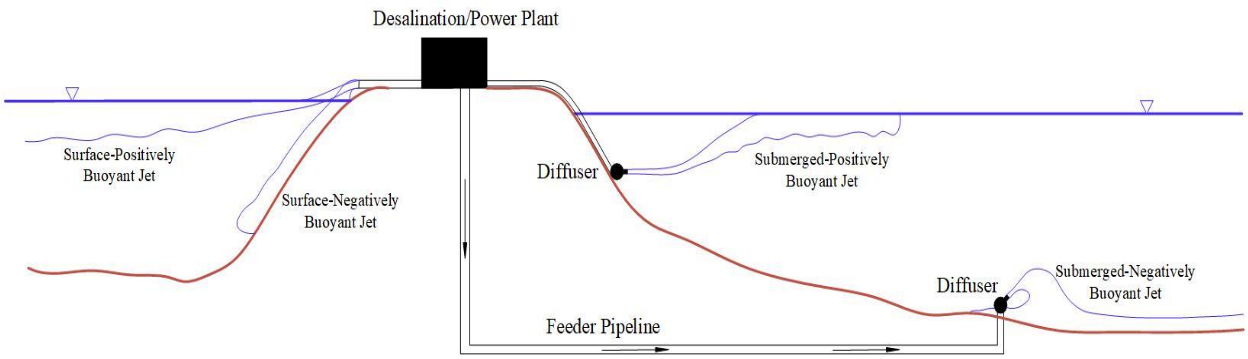

Figure 2-1 Schematic of different types of outfall discharges.

A buoyant jet can also be discharged horizontally (horizontal jet) or upwards, either vertically (vertical jet) or at some angle to the horizontal (inclined jet). The vertical dense jet in stagnant water tends to fall back on the source. This feature disturbs the dilution process and causes lower dilution, which may not be desirable in outfall discharge design (Fischer et al., 1979a) (P. J. W. Roberts et al., 1997) (T. Missimer et al., 2015). In contrast, inclined jets can clear the effluent from the jet discharge site because of their horizontal component of momentum (Pincince & List, 1973).

2.3 Turbulence Modeling

Turbulence modeling involves a large number of scale motions that need to be resolved or modeled. The three methods of Reynolds-averaged Navier-Stokes (RANS), large eddy simulation (LES), and direct numerical simulation (DNS) are the main numerical methods used to model turbulent flows. The application of DNS for prediction of mixing behavior of outfall discharges is limited since it requires very high computational cost, although it can resolve all the turbulent flow problems. In this section, the two most practical modeling approaches of RANS and LES in outfall discharge modeling are described.

2.3.1 Reynolds-Averaged Navier-Stokes (RANS)

The focus of the RANS method is on the effects of turbulence on the mean flow field properties. In this approach, Navier-Stokes equations are usually time averaged prior to being numerically solved. More precisely, any instantaneous flow variable is decomposed into mean and fluctuating components. Afterward, they are replaced in the original equations, then the obtained equations are time averaged (Versteeg & Malalasekera, 2007) (Moukalled et al., 2016). Figure 2-2 represents fluctuating ($\emptyset'(t)$) and mean ($\overline{\emptyset}$) components of an instantaneous variable ($\emptyset(t)$). Each instantaneous variable ($\emptyset(t)$) can be demonstrated as in Equation (2-4):

$$\emptyset(t) = \overline{\emptyset} + \emptyset'(t) \tag{2-4}$$

For instance, the instantaneous values of velocity (u) and pressure (p) can be decomposed as fluctuating components of u' and p', and mean values as $\bar{u}$ and $\bar{p}$:

$$u_i = \bar{u}_i + u_i' \tag{2-5}$$

$$p = \bar{p} + p' \tag{2-6}$$

The spread of the fluctuation component about the mean is usually represented by the variance $\overline{(\emptyset')^2}$:

$$\overline{(\emptyset')^2} = \frac{1}{\Delta t}\int_0^{\Delta t} (\emptyset')^2 dt \tag{2-7}$$

The velocity variances $\overline{(u_1')^2}$, $\overline{(u_2')^2}$, and $\overline{(u_3')^2}$ are employed to define the turbulent kinetic energy per mass (k) as Equation (2-8), where u_1', u_2' and u_3' are the fluctuations of the velocity components.

$$k = 0 \cdot 5\left(\overline{(u_1')^2} + \overline{(u_2')^2} + \overline{(u_3')^2}\right) \tag{2-8}$$

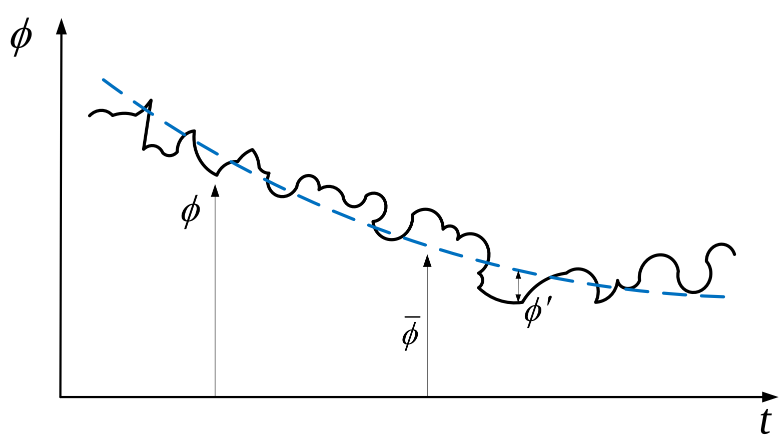

Figure 2-2 An instantaneous variable and its mean and fluctuating components.

Time averaging of Navier-Stokes equations leads to so-called RANS equations, which can be expressed as follows:

$$\frac{\partial \bar{u}_i}{\partial x_i} = 0 \tag{2-9}$$

$$\rho \frac{\partial \bar{u}_i}{\partial t} + \rho \bar{u}_j \frac{\partial \bar{u}_i}{\partial x_j} = -\frac{\partial p}{\partial x_i} + \frac{\partial}{\partial x_i}\left[\mu\left(\frac{\partial \bar{u}_i}{\partial x_j} + \frac{\partial \bar{u}_j}{\partial x_i}\right) - \rho \overline{u'}_i \overline{u'}_j\right] + \rho g \tag{2-10}$$

where μ is the dynamic viscosity of the fluid.

The process of time averaging results in the introduction of six extra unknowns of the Reynolds stress tensor ($-\rho \overline{u}'_i \overline{u}'_j$). These unknown terms must be estimated to be able to close the system of equations; otherwise, the closure problem emerges. Therefore, various turbulence models are developed to perform the estimations, which introduce additional transport equations in most cases. Turbulence models can be categorized based on the number of these extra transport equations into:

- Algebraic models (zero additional equation)
  In these models, eddy viscosity is computed based on an algebraic equation.
- Spalart-Allmaras models (one additional equation)
  In these models, one turbulent quantity is obtained based on a transport equation, and another turbulent quantity is acquired based on an algebraic expression.
- $k - \varepsilon$ and $k - \omega$ models (two additional equations)
  These models are more complicated and apply two transport equations, which describe transport of two scalars. For instance, in the case of the $k - \varepsilon$ model, one transport equation is applied to describe transport of the turbulent kinetic energy and one for its dissipation.
- Reynold stress models (seven additional equations)
  These models consider six transport equations for the Reynolds tensor and one equation for the length scale of the turbulence.

From another point of view, the RANS turbulence models can be classified into Eddy viscosity model and Reynolds stress model (RSM), as discussed below.

2.3.1.1 Eddy Viscosity Model

This model has been proposed based on the Boussinesq assumption, which declares that Reynolds stresses are proportional to mean rates of deformation:

$$-\rho\overline{u'_i u'_j} = \tau_{ij} = \mu_t\left(\frac{\partial \bar{u}_i}{\partial x_j} + \frac{\partial \bar{u}_j}{\partial x_i}\right) - \frac{2}{3}\rho k \delta_{ij} \tag{2-11}$$

where μ_t is the eddy viscosity and δ_{ij} is the Kronecker delta:

$$\begin{aligned} \delta_{ij} &= 1 \; if \; i = j \\ \delta_{ij} &= 0 \; if \; i \neq j \end{aligned} \tag{2-12}$$

The Kronecker delta causes the correct answers for the normal Reynold stresses, where $i = j$. $k - \omega$, shear stress transport (SST) $k - \omega$, standard $k - \varepsilon$, re-normalization group (RNG) $k - \varepsilon$, and realizable $k - \varepsilon$ can be the best examples of the turbulence models based on the eddy viscosity model.

2.3.1.2 Reynolds Stress Model (RSM)

This model applies the Reynolds stress transport equations to obtain the Reynolds stress tensor. Accordingly, the direct effects of the Reynolds stress field can be achieved. This leads RSM to perform better compared to the Eddy viscosity model under the conditions where the flow fields are sophisticated (Versteeg & Malalasekera, 2007).

The Reynolds stress (R_{ij}) and the transport equation of R_{ij} are presented as Equations (2-13) and (2-14), respectively:

$$R_{ij} = -\frac{\tau_{ij}}{\rho} = \bar{u}_i\bar{u}_j - \overline{u_i u_j} \tag{2-13}$$

$$\frac{\partial R_{ij}}{\partial t} + u_j\frac{\partial R_{ij}}{\partial x_j} = P_{ij} + D_{ij} - \varepsilon_{ij} + \Pi_{ij} + \Omega_{ij} \tag{2-14}$$

where $\frac{\partial R_{ij}}{\partial t}$ is the rate of change of R_{ij}, $u_j\frac{\partial R_{ij}}{\partial x_j}$ is the transport term by convection, P_{ij} is the production rate of R_{ij}, D_{ij} is the transport term by diffusion, ε_{ij} is the dissipation rate of R_{ij}, Π_{ij} is the transport term by turbulent pressure-strain interactions, and Ω_{ij} is the transport term by rotation. In RSM, three terms: convection, production, and rotation maintain their exact forms, and the terms of diffusion, dissipation rate, and pressure-strain interactions need to be modeled; see (Launder et al., 1975) and (Rodi, 1984) for the required models.

2.3.2 Large Eddy Simulation (LES)

The LES approach was first proposed by Smagorinsky (Smagorinsky, 1963). LES is a method in which the different behavior of large and small eddies is considered. The large eddies are almost anisotropic, and their behavior is affected by external forces, the geometry of the domain, and boundary conditions, while the small eddies are almost isotropic and homogeneous (Versteeg & Malalasekera, 2007) (Zhiyin, 2015). Furthermore, the large eddies are the reason for most of the momentum transfer and incorporate most of the turbulence energy (Zhiyin, 2015). Unlike the RANS models in which all eddies are modeled, in the LES approach, the unsteady nature of the large eddies is directly computed, and just small eddies are modeled using turbulence models.

LES employs the following steps to simulate the behavior of flows. The procedure of the LES approach is demonstrated in Figure 2-3. At first, a spatial filter function and a filter size are determined to distinguish between the large and small eddies. Afterward, the filter is applied to the flow equations; the large eddies are resolved, and the small eddies are eliminated. At the end, the small eddies are modeled using sub-grid scale (SGS) models. It is worth noting that the accuracy of LES strictly depends on the adopted SGS model (Mohammadian et al., 2020). The small eddies can be accurately modeled since they are independent of boundary conditions and the flow type (Moukalled et al., 2016).

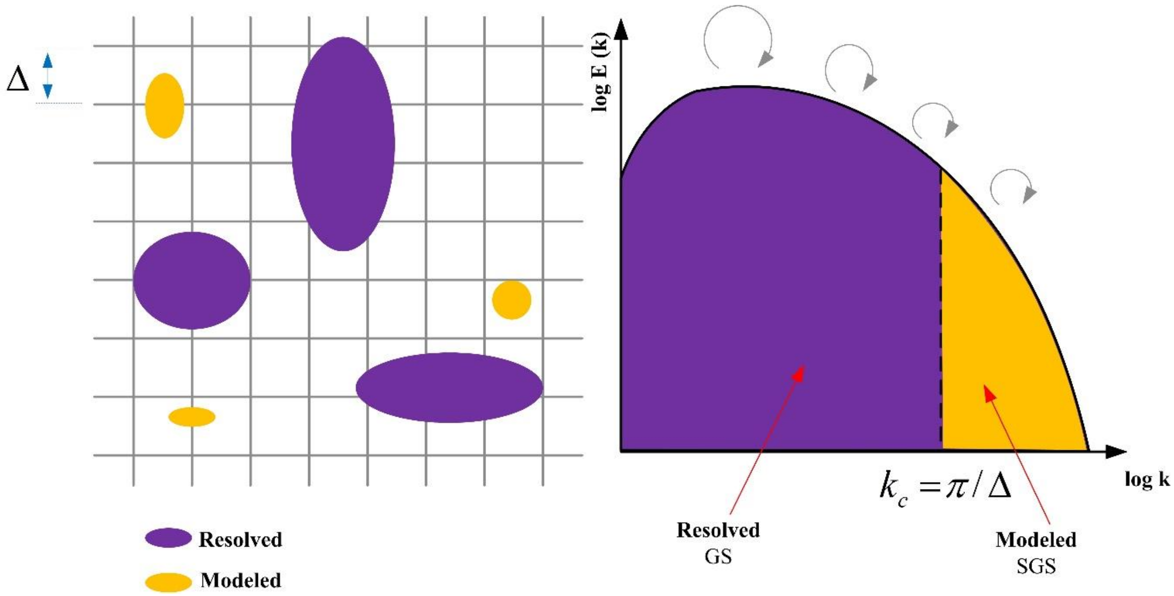

Figure 2-3 Spatial filtering in the LES approach.

The filtering operation in this method is defined as follows:

$$\bar{\varphi}(x.t) = \iiint_{-\infty}^{\infty} G(x.x'.\Delta)\varphi(x'.t)dx_1'dx_2'dx_3' \quad (2\text{-}15)$$

where $G(x.x'.\Delta)$ is the filtered function, Δ is the filter size, and $\varphi(x'.t)$ is the original function. Box filter, Gaussian filter, and spectral cutoff are the most common filtering functions in LES. The filter size (Δ) should not be smaller than the cell size. The truncation error can be almost eliminated when the filter size is larger than the cell size (Lund, 1997). It is usually considered to be the cube root of the cell volume (Versteeg & Malalasekera, 2007):

$$\Delta = \sqrt[3]{\Delta x \Delta y \Delta z} \quad (2\text{-}16)$$

where Δx, Δy, and Δz are the grid cell sizes in x, y, and z directions. The filtered Navier-Stokes equations including continuity and momentum equations can be presented for an incompressible fluid as Equations (2-17) and (2-18), respectively.

$$\frac{\partial(\bar{u}_i)}{\partial x_i} = 0 \quad (2\text{-}17)$$

$$\frac{\partial(\bar{u}_i)}{\partial t} + \frac{\partial(\bar{u}_i\bar{u}_j)}{\partial x_j} = -\frac{1}{\rho}\frac{\partial \bar{p}}{\partial x_i} + \nu\frac{\partial^2 \bar{u}_i}{\partial x_j \partial x_j} - \frac{\partial \tau_{ij}}{\partial x_j} \quad (2\text{-}18)$$

where $\bar{u}_i$ is the filtered velocity, $\bar{p}$ is the filtered pressure field, and τ_{ij} indicates the SGS stresses. The difference between the filtered velocity and the actual velocity is indicated in Figure 2-4. The SGS stress can be defined as follows:

$$\tau_{ij} = \overline{u_i u_j} - \bar{u}_i \bar{u}_j \tag{2-19}$$

The SGS stresses in LES are somewhat like the Reynolds stresses in RANS, but they are created as a result of spatial filtering operation, not time averaging. Furthermore, like the Reynold stresses in RANS, they need to be modeled. They can be modeled either via standard or dynamic Smagorinsky methods.

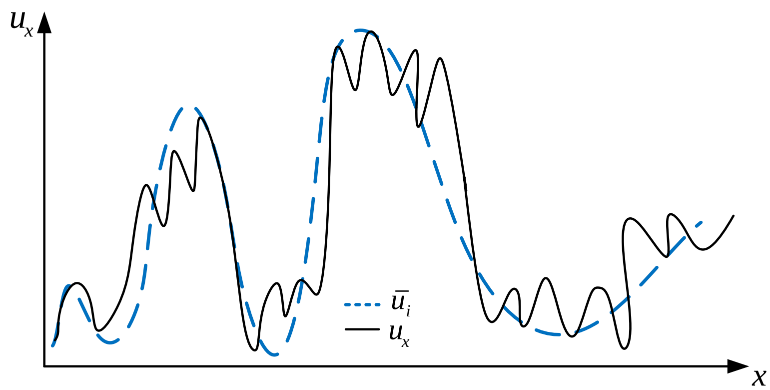

Figure 2-4 Comparison of the filtered velocity and the actual velocity.

2.3.3 Comparison of Turbulence Modeling Approaches

The relative advantages and disadvantages of applicable turbulence modeling approaches for the prediction of mixing behavior of outfall systems can be explained by considering their conceptual differences.

RANS has some advantages over LES in simulating outfall discharges. The main relative advantages have to do with the computational cost and the validation. Time averaging and modeling all eddies allow RANS to have reasonable computational cost, which makes it quite favorable for industrial and full-scale simulations. When an engineer's focus is on the steady-state flow, simulation of detailed instantaneous flow is a waste of time and money. The computation of unsteady flow equations in LES leads it to require a much larger computational expense compared to RANS. In addition to the fact that high computational time is undesirable for industrial applications, it may also lead to the unreliability of simulation results. The high computing times required for LES prevent performing multiple grid-dependency tests and sensitivity analysis in industrial studies, which may result in unreliable predictions (Gant, 2010). Furthermore, the performance of RANS is validated by many studies, while there are fewer LES models, resulting in a lack of validation compared to the RANS method; therefore, the risk of applying LES models for field scale diffusers can be somewhat high. More precisely, to the authors' knowledge, there is no validated LES model for the simulation of multiport diffusers, even at the research stage. The limited studies on single port diffusers have mentioned the weakness of SGS models in dealing with low turbulence intensity (Zhang et al., 2015), the reproduction of the wall interaction processes (Zhang et al., 2017), and the convective mixing due to the buoyancy-induced instability (Zhang et al., 2016). In addition, a need for considering stratified effects in SGS models has been noted (M. Jiang et al., 2019). Due to the mentioned advantages, RANS has been the most widely used approach in industrial applications for turbulent flow simulations in recent decades (Moukalled et al., 2016).

On the other hand, LES has some unique features that distinguish it from RANS. The main superiority of LES over RANS is its accuracy and the detailed information that it can provide. Directly computing and capturing the large eddies which incorporate most of the turbulence energy has made LES a more accurate approach compared to RANS, in which all eddies are modeled. The dimensions of this difference may be even more highlighted for field-scale simulations. The accuracy of RANS has always been a concern in turbulent flow problems due to time averaging (Mohammadian et al., 2020). Furthermore, unlike RANS, LES is capable of providing statistics of the resolved fluctuations. With the recent advances in computational resources, more attention is given to these models, and the application of LES for industrial problems is becoming more promising (Moukalled et al., 2016) (Mohammadian et al., 2020).

It should be noted that taking advantage of hybrid approaches such as detached eddy simulation (DES) has shown great potential in the simulation of turbulent flows, although it has not been adopted to simulate outfall discharges yet. For comparison, Table 2-2 lists the differences between different turbulence modeling approaches.

Table 2-2 Comparison between different applicable turbulence modeling approaches for outfall discharge modeling.

Turbulence Models	**Advantage**	**Limitations**	**Applications**
DNS	1. Resolves NS equations with no turbulence approximation 2. Resolves all temporal and spatial turbulence scales	1. Extreme computational cost 2. Very fine meshes required to capture all the spatial scales	Simple flow or low Reynolds number flow/ less applicable to engineering problems
RANS	Most computationally inexpensive and easy to implement	Cannot be accurate within the entire flow field	Most suitable for steady flow
LES	1. High accuracy, as it directly computes large scale eddies 2. Much cheaper than DNS computationally due to modeling of only small scales	1. High computational cost 2. Small-scale turbulence theory still needs development for complex geometries	Unsteady flow with vortex and recirculation
DES	Combines the benefits of both RANS and LES	1. Difficult to couple RANS-LES interface 2. Unaffordable for large computational domains	Massively separated flow

2.4 Outfall Discharge Analysis

2.4.1 Single Discharges

The primary flow parameters for a single brine jet in stagnant ambient fluid are illustrated in Figure 2-5. At first, due to the initial vertical momentum flux produced by the diffuser, the jet moves upwards. The buoyancy forces continuously decrease this momentum flux until it almost vanishes at the point where the jet reaches its maximum. Subsequently, the jet turns downwards and falls back to the sea bottom and develops as a gravity current.

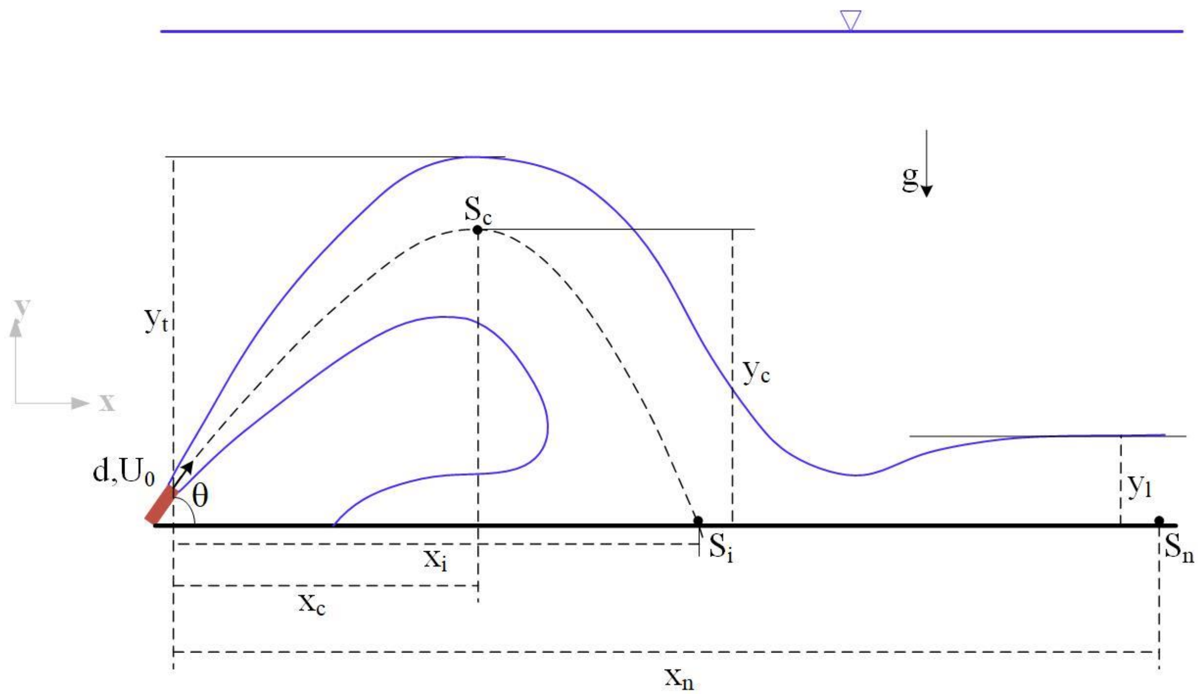

Figure 2-5 Definition sketch for typical inclined jet parameters.

Typically, jet-densimetric Froude number F_0, discharge volume flux Q_0, discharge momentum flux M_0, and discharge buoyancy flux B_0 determine the primary flow characteristics of jet. These variables in the dimensional analysis are defined as follows:

$$Q_0 = \frac{\pi d_0^2}{4} U_0 \, , M_0 = \frac{\pi d_0^2}{4} U_0^2 = U_0 Q_0, B_0 = \mathrm{g}\frac{\rho_0 - \rho_a}{\rho_a} Q_0 = \mathrm{g}_0' Q_0 \tag{2-20}$$

where g_0' is the reduced gravitational buoyancy acceleration at the source. Furthermore, the flow characteristics mainly depend on some length scales derived from the volume, momentum, and buoyancy fluxes. These length scales are as below (P. J. W. Roberts & Toms, 1988):

$$l_M = \frac{M_0^{3/4}}{B_0^{1/2}} \;\; and \;\; l_Q = \frac{Q_0}{M_0^{1/2}} \tag{2-21}$$

l_Q quantifies the distance over which the volume flux of the entrained ambient fluid becomes approximately equal to the initial volume flux. Therefore, for distances from the nozzle much larger than l_Q, the initial volume flux will not dynamically be of significance. l_M is a measure of the distance over which the buoyancy generates momentum approximately equal to the initial momentum. At distances from the nozzle much greater than l_M, the effect of initial momentum flux becomes negligible, and the buoyant jet has essentially become a plume (Wright, 1984) (P. J. W. Roberts et al., 1997) (Doneker & Jirka, 2007). It should be mentioned that since the direction of momentum and buoyancy are different in negatively buoyant jets, the initial momentum flux will always be an important parameter (P. J. W. Roberts et al., 1997).

If the flow is fully turbulent or F>20, Q is not dynamically significant (Abessi & Roberts, 2014). Therefore, any dependent variable for a jet with a specific angle, for example the terminal rise height y_t, is a function of M_0 and B_0 only:

$$y_t = f(M_0, B_0) \tag{2-22}$$

The maximum rise height can be expressed in terms of l_M as:

$$\frac{y_t}{l_M} = K \tag{2-23}$$

where K is a constant. Equation (2-23) for a round jet can be rewritten as

$$\frac{y_t}{d_0 F_0} = c_1 \tag{2-24}$$

where c_1 is a constant. Applying the same procedure, the other geometric jet parameters including the maximum centerline height y_c and its relevant horizontal location x_c, the thickness of the spreading layer y_l, the impact point location x_i, and the length of the near field x_n can be similarly obtained, as Equation (2-25). Moreover, the minimum dilution at the horizontal location x_c (S_c), the impact dilution S_i, and the ultimate dilution S_n are found to be constant as follows:

$$\frac{y_c}{d_0 F_0}, \frac{y_l}{d_0 F_0}, \frac{x_c}{d_0 F_0}, \frac{x_i}{d_0 F_0}, \frac{x_n}{d_0 F_0} = c_2, c_3, c_4, c_5, c_6 \qquad \frac{S_c}{F_0}, \frac{S_i}{F_0}, \frac{S_n}{F_0} = c_7, c_8, c_9 \tag{2-25}$$

These constants (c_1 to c_9) are estimated by experiments and specify the trajectory of the jet and dilution rate at different points for the jet.

A summary of some prominent numerical studies using the RANS approaches to simulate single jets is presented in Table 2-3. These studies confirm the predictive capability of these models in simulating the mixing behavior of single jets. Among different RANS models, the realizable $k -$

ε and LRR models can be considered as the most reliable models for single jets and can be utilized when designing outfall systems. Furthermore, Table 2-4 presents a summary of numerical studies using the LES models for the simulation of single jets.

Table 2-3 Prominent numerical studies using the RANS modeling approaches for the simulation of single jets and their remarks.

Ref.	**Applied models**	**Jet type**	**Outcome/Remarks**
(Plum et al., 2008)	Standard $k-\varepsilon$, realizable $k-\varepsilon$, standard $k-\omega$, and RSM	60° inclined dense jet	• The realizable $k-\varepsilon$ model provided the most accurate predictions of the mixing in the negatively buoyant plume and the spreading bed layer. • The RSM models required unacceptable processing time for the level of accuracy required for the problem.
(Oliver et al., 2008)	Standard $k-\varepsilon$ and calibrated $k-\varepsilon$	Inclined dense jet	• A $k-\varepsilon$ model based on the calibration of the turbulent Schmidt number was proposed. • $k-\varepsilon$ models led to more accurate predictions of the behavior of inclined dense jets compared to integral models and analytical solutions. • Both models underestimated the flow spread and the centerline dilution at the maximum height. • There was no improvement in the quality of the predictions of bulk flow parameters at the centerline maximum height when using $k-\varepsilon$ models compared to analytical solutions.
(El-Amin et al., 2010)	Standard $k-\varepsilon$, realizable $k-\varepsilon$, RNG $k-\varepsilon$, and standard $k-\omega$	Heated and unheated confined vertical jets	• The realizable $k-\varepsilon$ model provided the most accurate predictions of the jet characteristics. • The heated jet was a lazy plume. • The maximum velocity was theoretically predicted.
(Huai et al., 2010)	Realizable $k-\varepsilon$	Horizontal wall jet	• The realizable $k-\varepsilon$ model could successfully predict velocity distribution and temperature dilutions. • Velocity profile had a Gaussian form after the distance of $5d_0$ from the nozzle.

			• The distributions of velocity and temperature dilutions indicated a similarity along the axial direction at centerline in the near-field.
(Kheirkhah Gildeh et al., 2014b)	Standard $k-\varepsilon$, realizable $k-\varepsilon$, RNG $k-\varepsilon$, $k-\omega$ SST, LRR, and Launder-Gibson	Thermal and saline wall jet	• The LRR and realizable $k-\varepsilon$ models led to the most accurate solutions for saline and thermal wall jets. • Stream-wise and span-wise profiles for velocity and temperature were self-similar after an initial distance from the nozzle. • The stream-wise temperature profiles had a general Gaussian pattern at various distances from the nozzle. • Bed slope shortened the cling length. • The bed roughness effect on the temperature field was less than on the velocity field.
(Gildeh et al., 2014)	Realizable $k-\varepsilon$ and LRR	60º, 80º, and 85º inclined dense jets	• Brine discharges could be accurately modeled using the realizable $k-\varepsilon$ and LRR models. • The terminal rise height was underestimated by about 5% using both models. • The terminal rise height for 80° jets was higher than 85° jets. • The LRR model captured secondary flows and buoyancy-induced forces since it considers the effects of the stress anisotropy.
(Kheirkhah Gildeh et al., 2015b)	Realizable $k-\varepsilon$, RNG $k-\varepsilon$, nonlinear $k-\varepsilon$, LRR, and Launder-Gibson	30º and 45º inclined dense jet	• The LRR and realizable $k-\varepsilon$ models resulted in more accurate solutions compared to the other models. • The nonlinear $k-\varepsilon$ model led to the least accurate results. • The dilution was slightly underestimated by all models. • Port inclination did not have a significant effect on the dilution at the return point. • The cross-sectional velocity and concentration profiles of the outer half of the jet had an axisymmetric Gaussian pattern.

(Kheirkhah Gildeh et al., 2016b)	Realizable $k-\varepsilon$ and LRR	30º and 45º inclined dense jet	• The LRR model led to a slightly better prediction of the jet geometry and dilution characteristics since it could capture secondary flows and buoyancy-induced forces. • After the potential core region ($x/d_0 > 3$), the maximum velocity at the jet centerline decreased almost linearly. • Considering the density-induced term in the turbulence model caused the inner part of the jet to spread more widely.
(Ardalan & Vafaei, 2019)	Realizable $k-\varepsilon$	45º thermal-saline jet	• Thermal-saline discharges could be accurately modeled by the realizable $k-\varepsilon$ model. • The accuracy of the predictions decreased from the jet-like regions toward the plume-like region • The outer side boundary of the flow was predicted less accurately compared to the inner side boundary. • The salinity and temperature dilution ratios in thermal-saline jets were 93% and 89% for the return point and the centerline peak, respectively. • The combination of saline and thermal effluent could be a proper approach to optimize the mixing of effluent.
(Yan, Mohammadian, et al., 2020)	RNG $k-\varepsilon$	45º inclined plane jet	• The accuracy of the RNG $k-\varepsilon$ model in simulating inclined jets in linearly stratified fluids was evaluated. • The prediction errors for the terminal rise height, the depth of the under-flow, and the spreading layer thickness were about 4%, 9%, and 9%, respectively. • A new length scale that characterizes the effects of ambient stratification was proposed.

Table 2-4 Prominent numerical studies using the LES modeling approach for the simulation of single jets and their remarks.

Ref.	Jet type	Outcome/Remarks
(R. Q. Wang et al., 2011)	Vertical downward jet	• Buoyancy flux had a positive effect on the penetration rate. • The penetrative distances driven by the initial buoyancy and momentum fluxes were independent. • The total penetration distance can be treated as a linear combination of the penetrative mechanisms driven by the initial buoyancy and momentum fluxes.
(Zhang et al., 2015)	Wall jet	• LES model, compared to standard $k-\varepsilon$ and $k-\omega$ models, led to more accurate results of both the kinematic and scalar mixing characteristics. • Standard $k-\varepsilon$ and $k-\omega$ models were unable to predict the strong anisotropic spreading of the wall jet near the boundary. • The weakness of the Smagorinsky SGS model in dealing with low turbulence intensity in regions far from the centerline led to faster reduction of spanwise turbulence intensity in those regions.
(Ghaisas et al., 2015)	Horizontal jet	• The velocity decay rate was dependent on the Richardson number. • The Richardson number had a significant positive effect on the vertical deflection. • The anisotropy increased when increasing the Richardson number. • The co-flow affected the jet trajectory and the radial half-widths, but not the turbulent energetics. • The Reynolds number, Re, had no effect on the total radial spread, the jet trajectory, and the turbulent fluctuations. • The ratio of scalar and velocity spreads was non-constant. • Coherent vortex rings were formed on the upper side of the jet, while intermittent coherent vortices and small-scale structures were produced on the lower part.
(Zhang et al., 2016)	45^{o} inclined jet	• The LES model was able to predict the geometric characteristics with a slight over-prediction of 10% and the return point dilution with an under-prediction of 20%. • The LES approach outperformed the integral models. • The jet spread widths were reasonably predicted in regions close to the nozzle, but not beyond the centerline peak.

		• Both the Smagorinsky and dynamic Smagorinsky SGS models were not fully able to capture the convective turbulence under the influence of buoyancy.
(Zhang et al., 2017)	45º and 60º inclined jets	• The LES model was able to simulate reasonably well the geometric characteristics. • The return point dilution was underestimated by 20%. • The LES model was able to reproduce the localized concentration build-up at the impact point.
(M. Jiang et al., 2019)	45º inclined jet	• The LES model could reasonably reproduce the time-averaged first order mixing characteristics. • Turbulence kinetic energy spectrum decreased with the log slope of − 5/3 at the frequency from 2 to 20 Hz near and beyond the centerline peak. • SGS models needed to be improved in such a way that incorporate the stratification effects.
(Tofighian et al., 2022)	15º, 30º, 45º, 60º, and 75º inclined jets	• The model was able to reasonably predict the geometrical and mixing features; however, the flow features were still underestimated by up to 25%. • The model was able to reproduce the local concentration build-up near the impact point.

2.4.2 Multiport Discharges

Multiport diffusers are typically employed for the disposal of high volumes of effluents produced by large plants. The ports on a multiport diffuser can be clustered in rosettes or distributed evenly at the same angle to the horizontal. The rosette-type diffusers consist of risers each having 2-8 ports, typically discharged horizontally (A. C. H. Lai & Lee, 2012). Figure 2-6(a) shows a schematic top view of an 8-port rosette riser. A conventional multiport diffuser can be discharged from either one side or two sides, as shown in Figure 2-6(b) and (c). In both cases, the right-hand side of Equation (2-25) is no longer constant, and the flow properties are affected by the nondimensional parameter of port spacing ($\frac{s}{d_0F_0}$) (Abessi & Roberts, 2014) (T. Missimer et al., 2015). See Equation (2-26) for the geometrical properties and Equation (2-27) for the dilution properties.

$$\frac{y_t}{d_0F_0} = f\left(\frac{s}{d_0F_0}\right); \frac{x_i}{d_0F_0} = f\left(\frac{s}{d_0F_0}\right); \frac{x_n}{d_0F_0} = f\left(\frac{s}{d_0F_0}\right) \quad (2\text{-}26)$$

$$\frac{S_i}{F_0} = f\left(\frac{s}{d_0 F_0}\right); \frac{S_n}{F_0} = f\left(\frac{s}{d_0 F_0}\right) \quad (2\text{-}27)$$

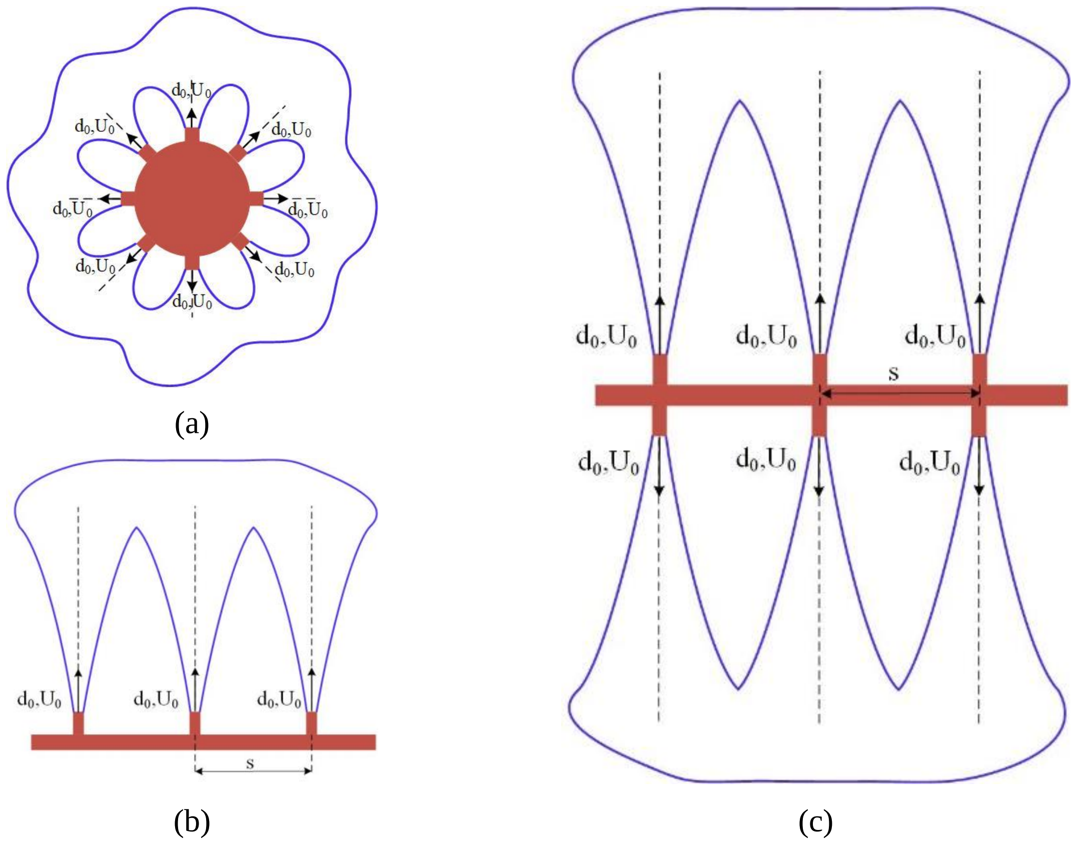

Figure 2-6 Schematic top-view of (a) eight-port rosette (b) one-sided and (c) two-sided diffusers.

When the nozzles are located very far from each other ($\frac{s}{d_0 F_0} \gg 1$), the jets do not interact, and each jet behaves separately. Therefore, the equations presented for single jets can be applied to predict their geometrical and mixing characteristics, as shown in Equations (2-24) and (2-25). Conversely, when the ports are placed very close to each other ($\frac{s}{d_0 F_0} \ll 1$), it can be considered that they are discharged from a line source, introducing the jet parameters per unit length. The discharge volume, momentum, and buoyancy fluxes per unit length can be expressed as q_0, m_0, and b_0, respectively.

$$q_0 = \frac{Q_T}{L}; m_0 = U_0 q_0; \; b_0 = g'_0 q_0 \quad (2\text{-}28)$$

where Q_T is the total discharge from the diffuser, and L is the diffuser length. For a line source, any dependent variable, such as y_t, is a function of the momentum and buoyancy fluxes per unit length, as shown in Equation (2-29).

$$y_t = f(m_0, b_0) \tag{2-29}$$

Following a dimensional analysis Equation (2-29) becomes:

$$\frac{y_t {b_0}^{2/3}}{m_0} = Constant \tag{2-30}$$

Using the definition of the Froude number and considering $b_0 = B_0/s$ and $m_0 = M_0/s$ for a long diffuser, Equation (2-30) becomes as follows after some manipulation (Abessi & Roberts, 2014) (T. Missimer et al., 2015):

$$\frac{y_t}{d_0 F_0} = c_{10}(\frac{s}{d_0 F_0})^{-1/3} \tag{2-31}$$

Similarly, other geometrical parameters can be expressed as

$$\frac{y_c}{d_0 F_0} = c_{11}\left(\frac{s}{d_0 F_0}\right)^{-\frac{1}{3}};\ \frac{y_l}{d_0 F_0} = c_{12}\left(\frac{s}{d_0 F_0}\right)^{-\frac{1}{3}} \tag{2-32}$$

$$\frac{x_c}{d_0 F_0} = c_{13}\left(\frac{s}{d_0 F_0}\right)^{-\frac{1}{3}};\ \frac{x_i}{d_0 F_0} = c_{14}\left(\frac{s}{d_0 F_0}\right)^{-\frac{1}{3}};\ \frac{x_n}{d_0 F_0} = c_{15}\left(\frac{s}{d_0 F_0}\right)^{-\frac{1}{3}} \tag{2-33}$$

And dilution properties as

$$\frac{x_c}{d_0 F_0} = c_{16}\left(\frac{s}{d_0 F_0}\right)^{-\frac{1}{3}};\ \frac{x_i}{d_0 F_0} = c_{17}\left(\frac{s}{d_0 F_0}\right)^{-\frac{1}{3}};\ \frac{x_n}{d_0 F_0} = c_{18}\left(\frac{s}{d_0 F_0}\right)^{-\frac{1}{3}} \tag{2-34}$$

where c_{10}-c_{18} are experimental constants.

Some of the prominent studies on the modeling of multiport jets are presented in Table 2-5. The prediction capabilities of the RANS models for rosette buoyant, multiple inclined, and multiple vertical jets have been indicated in recent studies. These studies show that multiple jets can be simulated using the RANS models with reasonable error. Regarding the previous studies focusing on the different turbulence closures, the RNG $k - \varepsilon$ model led to more accurate results compared to the other RANS models for various multiple jet types. Thus, this model can be applied as a reliable model to predict the mixing behavior of multiport diffusers. Although the effect of port spacing on the mixing behavior of multiple jets has been well studied, the effect of port inclination on the mixing process has not been well recognized. Furthermore, to the authors' knowledge, multiple jets have not yet been simulated using the LES models. The reason may be the high computational cost and complexity when it comes to the simulation of the complex geometry of multiport discharges.

Table 2-5 Prominent numerical studies on the simulation of multiple jets and their remarks.

Ref.	**Method**	**Applied models**	**Multiple jet type**	**Outcome/Remarks**
(Anderson & Spall, 2001)	Numerical	Differential Reynolds stress (RSM) and standard $k-\varepsilon$	Dual, parallel planar jets	• A numerical model
(H. J. Wang & Davidson, 2003a)	Theoretical	-	Uni-directional multiple jets	• A theoretical model • Individual jets asymmetrically spread during jet merging. • Models that employed the summation of velocity and tracer distributions underestimated centerline dilutions.
(P. C. Yannopoulos & Noutsopoulos, 2006)	Entrainment restriction	-	Uni-directional multiple jets	• A theoretical model • The merging effect became significant on the centerline velocities and concentrations after about double the distance where the nearby optical jet boundaries intersected.
(Tang et al., 2008)	Numerical	Eddy viscosity	Multiple inclined jets	• A numerical model • Unlike empirical mixing zone models, the complex interplay of the ambient flow and thermal jets and jets interactions could be properly resolved via the CFD model.
(A. C. H. Lai & Lee, 2012)	Semi-analytical	-	Rosette buoyant jets	• A Semi-analytical model • Jet interactions significantly affected mixing behavior.

				• Dynamic interactions between the jet groups were negatively affected by ambient cross-flow.
(Yan et al., 2019)	Numerical	Standard $k-\varepsilon$ and RNG $k-\varepsilon$	Rosette buoyant jets with upward and downward 30°, 45°, and 60° inclined ports	• A numerical model • The port inclination affected mixing behavior. • The RNG $k-\varepsilon$ outperformed the standard $k-\varepsilon$. • Jets became less diluted in the cases with greater angles. • The better performance of the RNG $k-\varepsilon$ was due to the consideration of the influence of the Reynolds number on the effective turbulence transport, incorporating a new term in the ε, and determination of the inverse effective Prandtl numbers.
(Yan & Mohammadian, 2019)	Numerical	Standard $k-\varepsilon$ and RNG $k-\varepsilon$	Multiple 60° inclined jets	• A numerical model • The port spacing significantly impacted mixing behavior. • The RNG $k-\varepsilon$ model outperformed the standard $k-\varepsilon$. • Both the standard and RNG $k-\varepsilon$ models could provide results of terminal rise height and impact dilution with errors smaller than 15%.
(Yan & Mohammadian, 2020a)	Artificial intelligence (AI)	Single-gene genetic programming (SGGP) and multigene genetic programming (MGGP)	Multiple 60° inclined jets	• AI-based models • The MGGP models outperformed the SGGP models and the existing regression-based empirical models.
(Yan & Mohamma	AI	MGGP	Multiple vertical jets	• AI-based models

dian, 2020b)				• The non-dimensional vertical displacement of the merging point and concentration where the jets were well mixed became more sensitive to port spacing than to the Froude number. • The non-dimensional centerline concentration was more sensitive to the Froude number than to port spacing. • There was no clear trend regarding the sensitivity of the non-dimensional vertical displacement of the merging point versus the Froude number.
(M. J. Baum & Gibbes, 2020)	Numerical	$k-\omega$ (SST)	Multiple 60º inclined jets	• A numerical model • Cross-flow conditions significantly affected mixing behavior. • Quasi-quiescent conditions produced the largest areal extent across the salinity spectrum. • Cross-flow decreased the salinity footprint. • Impact distances and dilutions were about 10% lower for the logarithmic cross-flow regime compared to the equivalent uniform velocity regime.
(Yan et al., 2020)	Numerical	Standard $k-\varepsilon$, RNG $k-\varepsilon$, standard $k-\omega$, and $k-\omega$ (SST)	Multiple vertical jets	• A numerical model • The port spacing significantly influenced the mixing behavior. • The RNG $k-\varepsilon$ outperformed other RANS models. • The port spacing positively affected the characteristic jet width in the streamwise direction. • The jets with larger port spacing merged at locations farther from the nozzle.

	• A new formula for centerline concentration profiles considering the effect of port spacing was proposed.

2.5 Concluding Remarks

Outfall systems have been introduced as a solution for the adverse environmental impacts on marine life resulting from the disposal of effluents in oceans and seas. Outfall discharges protect marine habitats by providing rapid mixing, which leads to a drop in salinity and thermal levels. Modeling of outfall discharge empowers engineers to predict the mixing behavior of discharges and design proper discharges that meet water quality standards at the point of compliance. This chapter provided a comprehensive description of the basic concepts involved in outfall discharge modeling and a critical review on the current state-of-the-art in this field.

Thanks to the advancements in computational resources over the past two decades, the application of CFD modeling in the prediction of jet-mixing behavior has been dramatically increased. It was shown that numerical modeling is a promising tool for simulating both outfall single and multiple discharges, and it can be predicted that, in the near future, CFD modeling will be widely applied in engineering designs to decrease experimental and field costs. Considering the pros and cons of different turbulence modeling approaches, the LES approach provides more accurate results compared to the RANS approach, although it requires higher computational cost. Therefore, as computational resources improve, more attention should be given to the application of the LES for outfall discharge simulation, compared to the RANS. Regarding different turbulence closures adopted in the RANS approach, realizable $k-\varepsilon$ and RNG $k-\varepsilon$ models have shown better performance in the simulation of single and multiple jets, respectively. These comparisons would provide valuable insight into the efficient modeling of outfalls for engineering applications. Finally, by the identification of knowledge gaps and research directions, this study can be addressed as a reference for future researchers conducting numerical assessments on the outfall discharges.

References

Abessi, O. (2018). Brine Disposal and Management—Planning, Design, and Implementation. In Sustainable Desalination Handbook: Plant Selection, Design and Implementation (pp. 259–303). Elsevier Inc.

Abessi, O., & Roberts, P. J. W. (2014). Multiport Diffusers for Dense Discharges. Journal of Hydraulic Engineering, 140(8), 04014032. https://doi.org/10.1061/(ASCE)HY.1943-7900.0000882

Anderson, E. A., & Spall, R. E. (2001). Experimental and numerical investigation of two-dimensional parallel jets. Journal of Fluids Engineering, Transactions of the ASME, 123(2), 401–406. https://doi.org/10.1115/1.1363701

Ardalan, H., & Vafaei, F. (2019). CFD and Experimental Study of 45° Inclined Thermal-Saline Reversible Buoyant Jets in Stationary Ambient. Environmental Processes, 6(1), 219–239. https://doi.org/10.1007/s40710-019-00356-z

Baum, M. J., & Gibbes, B. (2020). Field-Scale Numerical Modeling of a Dense Multiport Diffuser Outfall in Crossflow. Journal of Hydraulic Engineering, 146(1), 05019006. https://doi.org/10.1061/(asce)hy.1943-7900.0001635

Chave, P. (2001). The EU water framework directive. IWA Publishing.

Doneker, R. L., & Jirka, G. H. (2007). Cormix User Manual 6.0E: A Hydrodynamic Mixing Zone Model and Decision Support System for Pollutant Discharges into Surface Waters. U.S. Environmental Protection Agency, Washington DC.

El-Amin, M. F., Sun, S., Heidemann, W., & Müller-Steinhagen, H. (2010). Analysis of a turbulent buoyant confined jet modeled using realizable k-ε model. Heat and Mass Transfer/Waerme- Und Stoffuebertragung, 46(8–9), 943–960. https://doi.org/10.1007/s00231-010-0625-3

EPA, U. (1994). Water Quality Standards Handbook (2nd ed.).

Fischer, H.B., List, E.J., Koh, R.C.Y., Imberger, J., Brooks, N.H. (1979) Mixing in Inland and Coastal Waters; Academic Press: Amsterdam, The Netherlands.

Gant, S. (2010). Reliability Issues of LES-Related Approaches in an Industrial Context. Flow Turbulence Combust, 84, 325–335. https://doi.org/10.1007/s10494-009-9237-8

Ghaisas, N. S., Shetty, D. A., & Frankel, S. H. (2015). Large eddy simulation of turbulent horizontal buoyant jets. Journal of Turbulence, 16(8), 772–808. https://doi.org/10.1080/14685248.2015.1008007

Gildeh, H. K., Mohammadian, A., Nistor, I., & Qiblawey, H. (2014). Numerical Modelling of Brine Discharges Using OpenFOAM. Proceedings of the International Conference on New Trends in Transport Phenomena, 51.

Huai, W.-X., Li, Z.-W., Qian, Z., Zeng, Y.-H., Han, J., Peng, W.-Q. (2010). Numerical simulation of horizontal buoyant wall jet. Journal of Hydrodynamics, 22(1), 58–65. https://doi.org/10.1016/S1001-6058(09)60028-7

Jiang, M., Law, A. W. K., & Lai, A. C. H. (2019). Turbulence characteristics of 45° inclined dense jets. Environmental Fluid Mechanics, 19(1), 27–54. https://doi.org/10.1007/s10652-018-9614-8

Kheirkhah Gildeh, H., Mohammadian, A., Nistor, I., & Qiblawey, H. (2014). Numerical modeling of turbulent buoyant wall jets in stationary ambient water. Journal of Hydraulic Engineering, 140(6). https://doi.org/10.1061/(ASCE)HY.1943-7900.0000871

Kheirkhah Gildeh, H., Mohammadian, A., Nistor, I., & Qiblawey, H. (2015). Numerical modeling of 30∘ and 45∘ inclined dense turbulent jets in stationary ambient. Environmental Fluid Mechanics, 15(3), 537–562. https://doi.org/10.1007/s10652-014-9372-1

Kheirkhah Gildeh, H., Mohammadian, A., Nistor, I., Qiblawey, H., & Yan, X. (2016). CFD modeling and analysis of the behavior of 30° and 45° inclined dense jets - New numerical insights. Journal of Applied Water Engineering and Research, 4(2), 112–127. https://doi.org/10.1080/23249676.2015.1090351

Lai, A. C. H., & Lee, J. H. W. (2012). Dynamic interaction of multiple buoyant jets. Journal of Fluid Mechanics, 708, 539–575. https://doi.org/10.1017/jfm.2012.332

Launder, B., Reece, G., & Rodi, W. (1975). Progress in the development of a Reynolds-stress turbulence closure. Journal of Fluid Mechanics, 68(3), 537–566. https://doi.org/10.1017/S0022112075001814

Loya-Fernández, Á., Ferrero-Vicente, L. M., Marco-Méndez, C., Martínez-García, E., Zubcoff Vallejo, J. J., & Sánchez-Lizaso, J. L. (2018). Quantifying the efficiency of a mono-port diffuser in the dispersion of brine discharges. Desalination, 431(October 2017), 27–34. https://doi.org/10.1016/j.desal.2017.11.014

Lund, T. (1997). On the use of discrete filters for large eddy simulation. Annual Res. Briefs, 83–95.

Missimer, T. M., Jones, B., & Maliva, R. G. (2015). Intakes and Outfalls for Seawater Reverse-Osmosis Desalination Facilities: Innovations and Environmental Impacts. Springer, New York, NY, USA.

Mohammadian, A., Gildeh, H. K., & Nistor, I. (2020). CFD modeling of effluent discharges: A review of past numerical studies. Water (Switzerland), 12(3), 856. https://doi.org/10.3390/w12030856

Moukalled, F., Mangani, L., & Darwish, M. (2016). Fluid Mechanics and Its Applications the Finite Volume Method in Computational Fluid Dynamics. Springer.

Oliver, C. J., Davidson, M. J., & Nokes, R. I. (2008). k-ε Predictions of the initial mixing of desalination discharges. Environmental Fluid Mechanics, 8(5–6), 617–625. https://doi.org/10.1007/s10652-008-9108-1

Pincince, A. B., & List, E. J. (1973). Disposal of brine into an estuary. Water Pollution Control Federation, 45(11), 2335–2344.

Plum B, Webb T, Young J (2008) Modelling of Desalination Plant Outfalls. Sch. Aerospace, Civ. Mech. Eng., p. 24.

Roberts, P. J. W., Ferrier, A., & Daviero, G. (1997). Mixing in inclined dense jets. Journal of Hydraulic Engineering, 123(8), 693–699. https://doi.org/10.1061/(ASCE)0733-9429(1997)123:8(693)

Roberts, P. J. W., & Toms, G. (1988). Ocean outfall system for dense and buoyant effluents. Journal of Environmental Engineering, 114(5), 1175–1191.

Rodi, W.: Turbulence models and their applications in hydraulics-a state-of-the-art review. Delft, The Netherlands.

Smagorinsky, J. (1963). General circulation experiments with the primitive equations: I. The basic experiment. Monthly Weather Review, 91(3), 99–164. https://doi.org/10.1175/1520-0493(1963)091<0099:GCEWTP>2.3.CO;2

Tang, H. S., Paik, J., Sotiropoulos, F., & Khangaonkar, T. (2008). Three-Dimensional Numerical Modeling of Initial Mixing of Thermal Discharges at Real-Life Configurations. Journal of Hydraulic Engineering, 134(9), 1210–1224. https://doi.org/10.1061/(asce)0733-9429(2008)134:9(1210)

Tofighian, H., Aghajanpour, A., & Abessi, O. (2022). Simulation of inclined dense jets in stagnant environments: an LES and experimental study. Environmental Fluid Mechanics, 22(5), 1161–1185.

Versteeg, H. K., & Malalasekera, W. (2007). An introduction to computational fluid dynamics: the finite volume method (2nd ed.). Pearson education.

Wang, H. J., & Davidson, M. J. (2003). Jet Interaction in a Still Ambient Fluid. Journal of Hydraulic Engineering, 129(5), 349–357. https://doi.org/10.1061/(asce)0733-9429(2003)129:5(349)

Wang, R. Q., Law, A. W. K., Adams, E. E., & Fringer, O. B. (2011). Large-eddy simulation of starting buoyant jets. Environmental Fluid Mechanics, 11(6), 591–609. https://doi.org/10.1007/s10652-010-9201-0

Wright, S. J. (1984). Buoyant jets in density-stratified crossflow. Journal of Hydraulic Engineering, 110, 643–656.

Yan, X., Ghodoosipour, B., & Mohammadian, A. (2020). Three-Dimensional Numerical Study of Multiple Vertical Buoyant Jets in Stationary Ambient Water. Journal of Hydraulic Engineering, 146(7), 04020049. https://doi.org/10.1061/(asce)hy.1943-7900.0001768

Yan, X., & Mohammadian, A. (2019). Numerical modeling of multiple inclined dense jets discharged from moderately spaced ports. Water (Switzerland), 11(10), 14–16. https://doi.org/10.3390/w11102077

Yan, X., & Mohammadian, A. (2020a). Evolutionary Modeling of Inclined Dense Jets Discharged from Multiport Diffusers. Journal of Coastal Research, 36(2), 362–371. https://doi.org/10.2112/JCOASTRES-D-19-00057.1

Yan, X., & Mohammadian, A. (2020b). Evolutionary prediction of multiple vertical buoyant jets in stationary ambient water. Desalination and Water Treatment, 178, 41–52. https://doi.org/10.5004/dwt.2020.24938

Yan, X., Mohammadian, A., & Chen, X. (2019). Three-dimensional numerical simulations of Buoyant Jets discharged from a Rosette-type multiport diffuser. Journal of Marine Science and Engineering, 7(11), 1–15. https://doi.org/10.3390/jmse7110409

Yan, X., Mohammadian, A., & Chen, X. (2020). Numerical modeling of inclined plane jets in a linearly stratified environment. Alexandria Engineering Journal, 59(3), 1857–1867. https://doi.org/10.1016/j.aej.2020.05.023

Yannopoulos, P. C., & Noutsopoulos, G. C. (2006). Interaction of vertical round turbulent buoyant jets - Part I: Entrainment restriction approach. Journal of Hydraulic Research, 44(2), 218–232. https://doi.org/10.1080/00221686.2006.9521677

Zhang, S., Jiang, B., Law, A. W. K., & Zhao, B. (2016). Large eddy simulations of 45° inclined dense jets. Environmental Fluid Mechanics, 16(1), 101–121. https://doi.org/10.1007/s10652-015-9415-2

Zhang, S., Law, A. W. K., & Jiang, M. (2017). Large eddy simulations of 45° and 60° inclined dense jets with bottom impact. Journal of Hydro-Environment Research, 15, 54–66. https://doi.org/10.1016/j.jher.2017.02.001

Zhang, S., Law, A. W. K., & Zhao, B. (2015). Large eddy simulations of turbulent circular wall jets. International Journal of Heat and Mass Transfer, 80, 72–84. https://doi.org/10.1016/j.ijheatmasstransfer.2014.08.082

Zhiyin, Y. (2015). Large-eddy simulation: Past, present and the future. Chinese Journal of Aeronautics, 28(1), 11–24. https://doi.org/10.1016/j.cja.2014.12.007

3 Numerical Study on the Effect of Port Orientation on Multiple Inclined Dense Jets[2]

Abstract

Wastewaters are commonly discharged into the seas and oceans through multiport diffusers. Accurate prediction of the complex interactions of multiport diffusers with the receiving water bodies is significant for the optimal design of outfall systems and has yet to be fully illuminated. In the current study, the mixing and dilution characteristics of multiple inclined dense jets are studied using a three-dimensional numerical simulation. The Launder, Reece, and Rodi (LRR) turbulence model is employed to perform the simulations, and the predictions are compared against available experimental data. The results indicate that the LRR turbulence model is a promising tool for the study of inclined dense jets discharged from multiport diffusers, and it can provide more accurate predictions of the mixing behavior than standard and re-normalization group (RNG) k-ε turbulence models. The model is further employed to evaluate and compare the dispersion capabilities of multiport diffusers with uniform and non-uniform jet orientation to the horizontal, as a novel idea. The comparisons demonstrate the middle discharge may have a longer trajectory (7% and 5% increase in terminal rise height and impact point distance, respectively) and therefore a higher dilution rate (14% increase in impact dilution) when its adjacent jets are disposed with a different angle, compared to that of uniform discharges. The outcomes may be favorable for outfall systems applications involving dilution.

Keywords: numerical simulations; multiple discharges; inclined dense jets; mixing and dilution; discharge inclination

3.1 Introduction

Brine wastewaters from desalination plants are commonly discharged into the seas and oceans through diffusers. These effluents, which have a density higher than the surrounding water, sink to the sea-bottom and can increase salinity near the diffuser, which can result in adverse effects on

[2] This chapter has been published as: Saeidi Hosseini, S. A. R., Mohammadian, A., Roberts, P. J., & Abessi, O. (2022). Numerical Study on the Effect of Port Orientation on Multiple Inclined Dense Jets. Journal of Marine Science and Engineering, 10(5), 590.

the local natural environment if not properly discharged (Einav & Lokiec, 2003). The mixing characteristics of the wastewater discharges are closely related to the properties of the outfall diffusers (A. C. H. Lai et al., 2015) (Yan & Mohammadian, 2019). Thus, it is essential to predict the mixing behavior of the jets from different kinds of diffusers to enable an economically efficient design while complying with regulatory demands.

Discharges may be positively, neutral, or negatively buoyant. Positively buoyant jets have a density lower than the ambient water density and rise due to a positive buoyancy until they reach the water surface and then spread horizontally as a plume; the horizontal and vertical multiple discharges are typically positively buoyant or neutral. Negatively buoyant jets have a density higher than the surrounding water, and they are affected by a negative buoyancy which hinders the flow moving upward and leads the jets to move back to the sea bottom; the inclined jets are mainly negatively buoyant. Thus, the trajectory and therefore mixing behavior of inclined jets may differ from the horizontal and vertical discharges, which highlights the importance of the separate study of inclined jets. On the other hand, the diffusers may be either single- or multi-port. Single-port discharges can freely mix with the receiving water without any interactions. However, multiport diffusers are frequently applied around the world, e.g., Melbourne, Perth, Sydney, and Boston, to enable high dilutions with high effluent flow rates (S. Lyu et al., 2013) (H. J. Wang & Davidson, 2003b). The mixing process of multiport discharges differs from single-port jets, and its study is much more complicated because of the complex mechanisms resulting from jet interactions and the Coanda effect. Although the mixing behavior of single inclined dense jets has been widely studied for many years, the dilution properties of multiple jets have received less attention.

The investigations on multiple buoyant jets were quite often experimental or analytical. Some prior experimental studies on multiple buoyant jets have focused on multiple horizontal (Knystautas, 1964) (Liseth, 1973) (Seo & Yeo, 2002) (H. J. Wang & Davidson, 2003b) (Tian et al., 2004) (Tian & Roberts, 2011) (P. J. W. Roberts et al., 2011) and some others on vertical (P. C. Yannopoulos & Noutsopoulos, 2006) (S. Lyu et al., 2013) discharges. Some studies analytically investigated multiple buoyant jets and estimated the distance over which the interacting 3D buoyant jets behave as a plane jet (Koh & Fan, 1970) (Liseth, 1973). Knystautas theoretically predicted the velocity field of multiple turbulent jets using the superposition technique based on the Reichardt hypothesis (Knystautas, 1964). Knystautas' model was further improved to predict the concentration field based on an extension of the Reichardt hypothesis to the lateral transport of pollutants (Hodgson et al., 1999). Wang and Davidson (H. J. Wang & Davidson, 2003b) argued that the models presented by Knystautas (Knystautas, 1964) and Hodgson et al. (Hodgson et al., 1999) did not capture the possible change in spreading rate due to jet merging and extended their models by considering the changes in the spreading rates and concentration to velocity length scale ratio between the axisymmetric and 2D flow limits. Yannopoulos and Noutsopoulos analyzed interacting vertical buoyant jets in stagnant ambient conditions and developed analytical expressions concerning the concentration and velocity distributions based on the entrainment restriction approach (P. C. Yannopoulos & Noutsopoulos, 2006) and superposition method (P. Yannopoulos et al., 2006). Lai and Lee (A. C. H. Lai & Lee, 2012) proposed a general semi-analytical model for the dynamic interaction of multiple buoyant jets, and showed that merging point, jet trajectories, as well as the centerline concentration and velocity of the buoyant jet group were perfectly matched with the measurements. Furthermore, multiple inclined discharges have been mainly studied experimentally (Adams, 1972) (Marti et al., 2011) (Abessi & Roberts, 2014) (Abessi & Roberts, 2017) (Abessi & Roberts, 2018) (Shrivastava et al., 2019) (Xu et al., 2019).

Although experimental studies have significantly contributed to a better understanding of multiple jets, they are expensive and time-consuming options. Thus, supplementary methods such as integral entrainment models have always been of interest. These models are widely employed by designers to assess jet mixing behavior and are a basis for commercial mixing tools such as JetLag (Joseph W Lee et al., 1990) (Lee et al., 2003), CoreJet (Jirka, 2004), and UM3 (Frick, 2004). According to integral entrainment models, the velocity profiles of a jet is assumed to be Gaussian or top hat and axisymmetric without radial changes, resulting in simplified governing momentum and mass conservation equations (Taherian & Mohammadian, 2021a). These models are unable to resolve re-entrainment, boundary effects, and the Coanda effect (M. J. Baum & Gibbes, 2020) (Taherian & Mohammadian, 2021a). The last limitation may shed doubt on the prediction capabilities of integral entrainment models for multiple jets, where the Coanda effect reduces jet dilution and terminal rise height (Abessi & Roberts, 2014) (P. J. W. Roberts, 2015). Palomar et al. (Palomar, Lara, & Losada, 2012) evaluated the prediction capabilities of JetLag, CoreJet, and UM3 tools for inclined dense jets. They found a lot of discrepancies for the prediction of terminal rise height and showed more than 50% under-prediction for dilution. This underestimation has roots in the simplified mass and momentum equations of the integral models resulting from the simplex assumptions for the jet velocity profiles.

Thanks to the advancements in computational resources over the past two decades, the application of computational fluid dynamics (CFD) modeling in the prediction of jet-mixing behavior has dramatically increased (Taherian et al., 2022). CFD includes fewer simplifying assumptions, compared to integral entrainment models, and is currently a promising approach to simulate desalination outfalls (M. J. Baum & Gibbes, 2020). The application of CFD modeling, including the Reynolds Averaged Navier Stokes (RANS) model (Oliver et al., 2008) (Kheirkhah Gildeh et al., 2014a) (Kheirkhah Gildeh et al., 2015a) (Kheirkhah Gildeh et al., 2016a) (Huai et al., 2010) and large eddy simulation (LES) (Zhang et al., 2016) (Zhang et al., 2017) (M. Jiang et al., 2019) (Ardalan & Vafaei, 2019), has been reported for single port discharges in recent works. However, there have been only a limited number of reports covering the predictive capabilities of CFD models for multiple jets. Some studies have numerically investigated multiple buoyant jets. Xue et al. (Xue et al., 2014) indicated that the standard k-ε model could reasonably predict the mixing behavior of multiple horizontal jets in crossflow. Tang et al. (Tang et al., 2008) applied a buoyancy-corrected eddy viscosity model (EVM) to predict the primary mixing of buoyant jets from multiple ports and compared the results to the CORMIX model predictions. They showed that the CFD model could capture the changes of the plumes' depth along the trajectory, which the CORMIX model was incapable of capturing. Yan et al. (Yan et al., 2020) investigated the prediction capabilities of four different turbulence closures including the standard k-ε, re-normalization group (RNG) k-ε, k-ω, and k-ω shear stress transport (SST) for multiple vertical jets and showed that (RNG) k-ε resulted in more accurate outcomes. As the mixing behavior of multiple inclined discharges may differ from buoyant jets due to the negative buoyancy, some studies have attempted to validate the application of CFD for those jets. Yan and Mohammadian (Yan & Mohammadian, 2019) validated the performance of the standard and re-normalization group (RNG) k-ε turbulence models for the prediction of multiple inclined dense jets and showed that both models could provide predictions of the terminal rise height and the impact point dilution with errors lower than 15%. Moreover, the predictions for the impact distance based on the standard and (RNG) k-ε closures were found to be accurate with errors of 18.6% and 13.3%, respectively. A recent study (M. J. Baum & Gibbes, 2020) conducted numerical CFD simulations based on k-ω (SST) closure to investigate the Gold Coast Desalination Plant offshore inclined multiport brine diffuser while affected by different ambient velocity conditions, in the range of 0.03–0.26 m/s, and validated impact dilutions and plume trajectory against physical experimental data.

Experimental and numerical models are adopted to predict the mixing behavior of discharges, which are significantly affected by the properties of outfall diffusers (A. C. H. Lai et al., 2015) (Yan & Mohammadian, 2019). For single dense discharges, inclined jets result in a higher dilution rate than vertical discharges since vertical jets tend to fall back on themselves and it significantly impairs the dilution process (Fischer et al., 1979b) (P. J. W. Roberts et al., 1997) (T. M. Missimer et al., 2015). It is widely accepted that the 60° inclined discharges provide the longest trajectory for entrainment and therefore the highest dilution rate (Zeitoun et al., 1970) (Zeitoun et al., 1972) (Kikkert et al., 2007) (Abessi & Roberts, 2015). The effects of flow orientation on the flow field have also been investigated in other hydraulic conditions (P. J. W. Roberts et al., 1987) (Lim & Lam, 2020) (Lim & Lam, 2021). The main issue with multiple inclined dense discharges arises when the ports are not sufficiently spaced apart, and the jets are closely or moderately spaced. The dynamic interaction and the Coanda effect cause these jets to have a reduced terminal rise height and to bend inward, and thus to have a shorter trajectory compared to a single jet (Abessi & Roberts, 2014). The shortened trajectory further decreases dilution since it diminishes the available surface for entrainment. To overcome this reduction in dilution, it has been recommended to space the jets sufficiently apart in multiport diffusers (Abessi & Roberts, 2014), which lets the jets freely entrain the surrounding water without any interactions, as single jets do. The effect of port spacing on the mixing process of multiport diffusers has been the focus of some prior research. Yan et al. (Yan et al., 2020) focused on multiple vertical buoyant jets and indicated that as the port spacing was reduced, the jets' centerline dilution was lower, and the plume-like region was placed farther from the port. Moreover, they proposed a novel formula for concentration profiles that considers the influence of port spacing. Abessi and Roberts (Abessi & Roberts, 2014) conducted laboratory experiments on the influences of port spacing on multiple inclined dense jets and indicated that the port spacing can have a negative effect on the rise height and other geometrical characteristics of discharges. They highlighted the minimum port spacing that avoids dynamic interaction of jets.

Based on the above explanations, two main research gaps need to be further elaborated when focusing on the study of multiport diffusers. First evaluating the prediction capabilities of less validated modeling approaches, from the CFD simulation point of view, and secondly investigating the influence of non-uniform port orientation on the mixing behavior, from the optimal design point of view. The available numerical studies have mainly investigated the prediction capabilities of the eddy viscosity models (EVMs). The EVMs consider that the Reynolds stresses are proportional to mean rates of deformation and the stresses are obtained based on the Boussinesq assumption (Versteeg & Malalasekera, 2007). These models provide good results for simple flows and some recirculating flows (Versteeg & Malalasekera, 2007), but some drawbacks have been reported for them when employed for complex flow fields (Peyret & Krause, 2000) (Hanjalic, 2004). The main drawback of most EVMs can be the consideration of isotropic character for the eddy viscosity, which causes them to be insensitive to the orientation of the turbulence structure and its mixing and transport processes (Kheirkhah Gildeh et al., 2015a). However, stress anisotropy plays a significant role in changing in the streamline trajectory and stress-induced secondary motions (Hanjalic, 2004). The RSMs solve transport equations for the Reynolds stresses and consider different values for viscosity in each direction, which may result in more accurate predictions compared to the EVMs for the complex flow fields (Versteeg & Malalasekera, 2007). Gildeh et al. (Kheirkhah Gildeh et al., 2015a) applied five different RANS models, including the re-normalization group (RNG) k-ε, realizable k-ε, nonlinear k-ε, Launder, Reece, and Rodi (LRR), and Launder-Gibson, to predict the mixing behavior of 30° and 45° inclined dense jets. They showed that the two RSMs could provide more accurate predictions for the velocity fields compared to the other applied models. Additionally, the LRR model could better capture secondary flows. It is likely that the RSMs will begin to be more widely applied for industrial projects once a consensus has been reached about the best numerical solution strategies for their convergence problems (Versteeg & Malalasekera, 2007). Additionally, the advances in computational resources in the early future may lead these models to be more employed by industrial users. Therefore, this study simulates multiple inclined dense discharges employing the Launder, Reece, and Rodi (LRR) model as a new approach for multiple jets, and compares the model predictions of terminal rise height, impact point distance, and impact dilution to existing experimental measurements.

Furthermore, previous studies have mainly focused on the influence of port spacing on the mixing characteristics of multiport diffusers. However, the influence of non-uniform port orientation on the merging process of multiport diffusers is rarely reported. Jet merging in multiport diffusers leads the jets to have shorter trajectories and lower dilution compared to single jets. It is expected that the jet merging and the Coanda effect diminish when the jets are discharged with non-uniform orientation to the horizontal, compared to uniform discharged diffusers. A change in port orientation can be of interest in practical projects, such as brackish water discharges into water bodies emitted by osmotic power plants since it may provide an inexpensive way to enhance the mixing performance. Thus, as another contribution of this study, the effect of non-uniform port orientation on the merging process of multiple inclined dense jets is also evaluated using the validated LRR model.

The rest of this paper is devoted to the description of research methodology as well as presenting and discussing the results and conclusions. Section 3.2 describes methodology where dimensional analysis, governing equations, flow, and mesh configurations, as well as model setup and numerical algorithms are discussed. Section 3.3 presents the results where the performance of the model and the effect of non-uniform port orientation on merging process are discussed. Section 3.4 also presents the conclusion and proposed future works.

3.2 Methodology

3.2.1 Analysis

A schematic view of multiple inclined dense jets is illustrated in Figure 3-1. The jets are discharged into the receiving water bodies at an initial angle θ to the horizontal with jet velocity U_0 and jet diameter D. Upon discharging, the jets move upward due to the initial vertical momentum flux. The negative buoyancy and jet entrainment continuously decrease this momentum flux until it almost vanishes at the point where the jets reach their maximum height, the terminal rise height y_t. Subsequently, the jets turn downward and impinge the seabed at the location of impact point, x_i. The dilution at the impact point S_i can be defined as $S_i = (\rho_0 - \rho_a)/(\rho - \rho_a)$, where ρ_0 is effluent density, ρ_a is ambient density, and ρ represents local density.

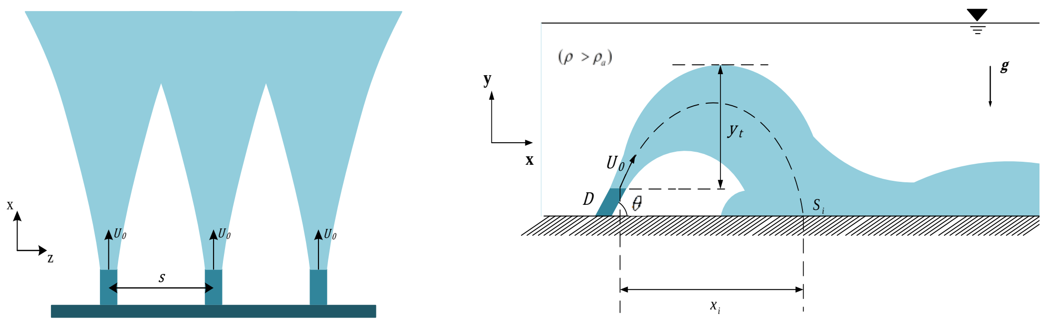

Figure 3-1 Schematic (a) plan and (b) side views of multiple inclined dense jets.

The mixing properties of the inclined dense jets are mainly characterized by discharge volume flux Q, kinematic momentum flux M, and buoyancy flux B, which can be defined by the following equations, respectively (Fischer et al., 1979b) (Abessi et al., 2012) (C. C. K. Lai & Lee, 2012):

$$Q = \frac{\pi D^2}{4} U_0; \quad M = U_0 Q = \frac{\pi D^2}{4} U_0^2; \quad B = g_0' Q \qquad (3\text{-}1)$$

where g_0' is reduced gravitational acceleration and expressed as $g_0' = g(\rho_0 - \rho_a)/\rho_a$; where g is gravitational acceleration. In the case of dense discharges $\rho_0 > \rho_a$.

The most important length-scale of the flow is the momentum length scale, L_M, which refers to the distance beyond which the buoyancy produces momentum approximately equal to the initial momentum and is defined as (P. J. W. Roberts & Toms, 1988) (P. J. W. Roberts et al., 1997)

$$L_M = \frac{M^{3/4}}{B^{1/2}} \qquad (3\text{-}2)$$

which is commonly expressed as DF_d where F_d is the jet densimetric Froude number, which measures the ratio of inertia to buoyancy and can be defined as

$$F_d = \frac{U_0}{\sqrt{g_0' D}} \qquad (3\text{-}3)$$

The effect of port spacing in dimensional analysis is expressed by the non-dimensional parameter s/DF_d where s is the port spacing. If the ports are widely spaced, $s/DF_d > {\sim}2$, the jets behave as single jets and freely mix with the ambient water. If a single jet is fully turbulent and F_d is higher than approximately 20, the dynamic effect of Q becomes insignificant. Therefore, the dependent variables of y_t, x_i, and S_i are functions of M and B only. Following a dimensional analysis and experimental measurements (P. J. W. Roberts et al., 1997)

$$\frac{y_t}{DF_d} = 2.2; \quad \frac{x_i}{DF_d} = 2.4; \quad \frac{S_i}{F_d} = 1.6 \tag{3-4}$$

For the case that the jets are not widely spaced, $s/DF_d < \sim 2$, the right-hand sides of Equation (3-4) are not constant anymore. The geometrical characteristics and impact dilution are functions of s/DF_d, as follows:

$$\frac{y_t}{DF_d} = f\left(\frac{s}{DF_d}\right); \quad \frac{x_i}{DF_d} = f\left(\frac{s}{DF_d}\right); \quad \frac{S_i}{F_d} = f\left(\frac{s}{DF_d}\right) \tag{3-5}$$

Following the experiments conducted by Abessi and Roberts (Abessi & Roberts, 2014), the normalized terminal rise height and impact distance for one- and two-sided multiport discharges can be obtained by the empirical equations:

$$\frac{y_t}{DF_d} = 1.9\left(\frac{s}{DF_d}\right)^{\frac{1}{2}}; \quad \frac{x_i}{DF_d} = 2.0\left(\frac{s}{DF_d}\right)^{\frac{1}{2}} \tag{3-6}$$

The impact dilution for one-sided multiport diffusers can be achieved by

$$\frac{S_i}{F_d} = 0.9\left(\frac{s}{DF_d}\right) \tag{3-7}$$

while for two-sided discharges it is about 20% lower.

3.2.2 Governing Equations

The mass and momentum conservation equations for an incompressible multiphase flow are as follows (Loeben et al., 2016) (Killingstad, 2018):

$$\nabla \cdot U = 0 \tag{3-8}$$

$$\frac{\partial \rho U}{\partial t} + \nabla \cdot (\rho U U) = -\nabla \cdot \left(P_{rgh}\right) - gh\nabla\rho + \nabla \cdot (\rho T) \tag{3-9}$$

where

$$\rho = \alpha_1\rho_1 + \alpha_2\rho_2 = \alpha_1\rho_1 + (1-\alpha_1)\rho_2 \tag{3-10}$$

$$T = -\frac{2}{3}\bar{\mu}_{eff}\nabla \cdot UI + \bar{\mu}_{eff}\nabla U + \bar{\mu}_{eff}(\nabla U)^T \tag{3-11}$$

$$\bar{\mu}_{eff} = \alpha_1(\mu_{eff})_1 + \alpha_2(\mu_{eff})_2 \tag{3-12}$$

$$(\mu_{eff})_i = (\mu - \mu_t)_i \tag{3-13}$$

where U is velocity, t indicates time, ρ is density, P_{rgh} represents the difference between static and hydraulic pressure, g is gravitational acceleration, h denotes height of fluid column, α is volume fraction, μ and μ_t are dynamic and turbulent viscosity, respectively, script i shows either the effluent ($i = 1$) or surrounding water ($i = 2$). The diffusion equation for the volume fraction of a fluid can be written as:

$$\frac{\partial\alpha_1}{\partial t} + \nabla \cdot (U\alpha_1) = \nabla \cdot (\left(D_{ab} + \frac{\nu_t}{S_C}\right)\nabla\alpha_1) \tag{3-14}$$

where D_{ab} indicates molecular diffusivity, ν_t represents turbulent eddy viscosity, and S_C denotes turbulent Schmidt number.

In CFD modeling, the three approaches of direct numerical simulation (DNS), LES, and RANS models can be used to simulate turbulent flows. The first two require excessive computational cost for the simulation of multiple jets. The RANS models can be classified into the RSMs and EVMs. RSMs usually need more computational resources. One study applied three different EVMs and two RSMs to predict the mixing behavior of single jets and showed that the RSMs were about 20% more expensive than the other models, regarding the computational costs (Kheirkhah Gildeh et al., 2015a). However, the RSMs may be more accurate when the flow field is complex, which has roots in dealing with stress anisotropy (Versteeg & Malalasekera, 2007). The main difference between the RSMs and EVMs is that RSMs directly solve transport equations for the Reynolds stress, as presented in Equation (3-15), while the EVMs compute the stresses using the Boussinesq assumption. This difference may lead to more accurate predictions of the mixing behavior of multiple jets using an RSM compared to an EVM. In the current study, the LRR model, as an RSM, is adopted to solve the governing equations. The LRR model was developed by Launder, Reece, and Rodi in 1975 (Launder et al., 1975) and is expressed as:

$$\frac{D\overline{u_i u_j}}{\mathrm{Dt}} = \frac{\partial \overline{u_i' u_j'}}{\partial t} + \overline{u_k} \frac{\partial \overline{u_i' u_j'}}{\partial x_k} = D_{ij}^T + D_{ij}^\nu + P_{ij} + \phi_{ij} + \varepsilon_{ij} \tag{3-15}$$

where $\overline{u_i' u_j'}$ is the Reynolds stress, and D_{ij}^T, D_{ij}^ν, P_{ij}, ϕ_{ij}, and ε_{ij} represent the turbulent diffusion, viscous diffusion, production, pressure–strain, and turbulence dissipation rate parameters, respectively. The viscous and turbulent diffusion terms are calculated as:

$$D_{ij}^\nu = \nu \frac{\partial^2 \overline{u_i' u_j'}}{\partial x_k x_k} \tag{3-16}$$

$$D_{ij}^T = \frac{\partial}{\partial x_l} (C_s \frac{\varepsilon}{k} \overline{u_i u_k} \frac{\partial \overline{u_i u_j}}{\partial x_k}) \tag{3-17}$$

where C_s=0.22, and the pressure–strain term is expressed as:

$$P_{ij} = -\overline{u_i' u_k'} \frac{\partial \overline{u}_j}{\partial x_k} - \overline{u_j' u_k'} \frac{\partial \overline{u}_i}{\partial x_k} \tag{3-18}$$

The dissipation term is calculated as:

$$\varepsilon_{ij} = -2\nu \overline{\frac{\partial u_i'}{\partial x_k} \frac{\partial u_j'}{\partial x_k}} \tag{3-19}$$

$$\frac{\partial \varepsilon}{\partial t} + \overline{u_k} \frac{\partial \varepsilon}{\partial x_k} = C_{\varepsilon 1} \frac{P_k \varepsilon}{k} - C_{\varepsilon 2} \frac{\varepsilon^2}{k} + \frac{\partial}{\partial x_j} (C_\varepsilon \frac{k}{\varepsilon} \overline{u_i' u_j'} \frac{\partial \varepsilon}{\partial x_j}) \frac{S_i}{F_d} = 0.9 \left(\frac{s}{DF_d}\right) \tag{3-20}$$

where $C_{\varepsilon 1}$=1.44, $C_{\varepsilon 2}$=1.9.

3.2.3 Flow and Mesh Configurations

As the purpose of the current study was to evaluate the predictive capabilities of RSM for multiple inclined dense jets and investigate the effects of non-uniform port orientation to the horizontal on the mixing behavior, previous experiments were first simulated to validate the LRR model predictions. The experiments conducted by Abessi and Roberts (Abessi & Roberts, 2014) were selected as a basis for model validation, and the results of their measurements and LRR simulations were compared. Their measurements were appropriate for model validation since concentration fields were mapped in three dimensions by laser-induced fluorescence, and a comprehensive dataset on multiport inclined dense effluents was provided. Afterward, the validated model was utilized for further investigations on the effects of non-uniform port angle on the mixing process.

According to the experiments, the port spacing (s) was 57 mm, the jet diameter (D) was 1.93 mm, and the nozzle height above the lower wall (y_0) was 30 mm. The effluent and tank water density were 1013.8 kg/m3 and 999.8 kg/m3, respectively.

To model a long diffuser with many nozzles, three ports were considered in the computational domain as the representatives of all possible jets on a diffuser. Overall, five cases were considered for the simulations, see Table 3-1. Cases C1, C2, C3, and C4 were utilized for model validation, and were the same as the experimental measurements conducted by Abessi and Roberts (Abessi & Roberts, 2014). In these cases, s/DF_d varies between 0.47–0.85 to cover moderately spaced ports, which was the focus of this study, and all F_d values were more than 20 to assure fully turbulent flow. In the simulations, the three considered ports were discharged with an angle of 60° to the horizontal, which represents the first configuration (60°–60°–60°). In case S1, the second configuration (45°–60°–45°) is simulated where the central jet is discharged with an angle of 60° to the horizontal and the adjacent jets are discharged with an angle of 45°. Case S1, which has similar conditions to case C2 except port inclinations, and case C2 were compared to evaluate the effects of port orientation on the mixing process of multiple inclined dense discharges.

Table 3-1 Characteristics of numerical cases.

Case	Diameters (mm)	Effluent density (kg/m3)	Ambient density (kg/m3)	Velocity (m/s)	F_d	s/DF_d	θ_1-θ_2-θ_3 (°)
C1	1.93	1013.8	999.8	1.03	63.1	0.47	60-60-60
C2	1.93	1013.8	999.8	0.92	56.8	0.52	60-60-60
C3	1.93	1013.8	999.8	0.85	52	0.57	60-60-60
C4	1.93	1013.8	999.8	0.57	34.7	0.85	60-60-60
S1	1.93	1013.8	999.8	0.92	56.8	0.52	45-60-45

The three considered jets could reflect the mixing behavior of the jets in the whole system using appropriate boundary conditions. The simulations were conducted in a rectangular domain with the dimensions of 600 mm length (along x-direction), 400 mm depth (along y-direction), and 171 mm width (along z-direction); similar domains have been used in many hydraulic simulations (Calomino et al., 2018) (Lauria et al., 2020) (Tafarojnoruz & Lauria, 2020). The computational domain was surrounded by four types of planes, including wall, outlet, free surface, and symmetry planes. Furthermore, the nozzles were defined by two sections, including nozzle tube and inlet (Figure 3-2).

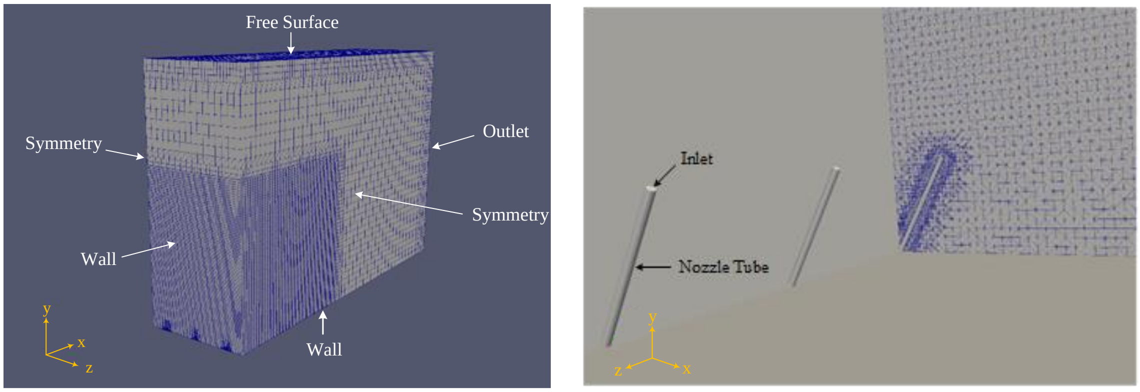

(a) (b)

Figure 3-2 (a) Computational domain and mesh setup; (b) detailed grids near the nozzles.

The accuracy and stability of numerical calculations of fluid flows are significantly affected by boundary conditions. As the wall planes and nozzle tubes are solid surfaces, a no-slip boundary condition was imposed on them to assume zero velocity at those surfaces. The boundary condition at the free surface and outlet planes was set to pressure–inlet outlet velocity. This boundary condition assigns a zero-gradient condition for flow into the domain and a velocity, based on the flux in the path-normal direction, for flow out of the domain (Palomar et al., 2012). Also, Symmetric boundary condition was imposed on the symmetry planes to assume same physical processes on the two sides of the boundary. A fixed value of velocity was assigned to the inlets, and the initial k and ε values at the inlets were estimated based on (Huai et al., 2010), $k = 0.06u^2$and $\varepsilon = 0.06u^3/D$. To simulate the system, the domain was discretized using the structured mesh shown in Figure 3-2. The mesh was modified by snappyHexMesh tool in OpenFOAM, which can divide the original grids into multiple sub-grids and snap the sub-grid boundaries onto the surfaces of interest. The employment of snappyHexMesh significantly decreased the required number of cells and therefore simulation time since there was no need to have small cells in the regions far from the area of interest. A double refinement was performed for the area in which jets move and merge, and a triple refinement was considered for the grids close to the inlets and nozzle tubes, which could perfectly determine the circular shape of the nozzles. The sensitivity of the simulation outcomes to the cell size was evaluated based on the procedures described and applied by Yan and Mohammadian (Yan et al., 2017) (Yan et al., 2019). Simulations were conducted based on four different meshes, including coarse and fine grids. The preliminary mesh structure was a relatively coarse mesh with 114,000 cells, and the difference between the predictions based on that mesh structure and experimental measurements was found to be about 10%. The finer mesh structures, Mesh 2, Mesh 3, and Mesh 4 included 311,000 cells, 385,000 cells, and 528,000 cells, respectively. The difference between the obtained results using Mesh 2 and Mesh 1 was about 10.5%. However, the difference between the predictions based on Mesh 2 and Mesh 3 was about 1.5%. The predictions of Mesh 3 and Mesh 4 were also very close, with about 2% difference between the results. Therefore, to be conservative, Mesh 4 was selected for simulations, and the final mesh structure included 528,000 cells.

3.2.4 Model Setup and Numerical Algorithms

The governing equations were numerically solved using the finite volume method. The simulations were performed using an open-source code OpenFOAM (*OpenFoam*, 2015), and the solver twoLiquidMixingFoam was employed to perform the implementation in OpenFOAM. This solver is a transient solver for multiphase fluids and has been widely applied and validated in prior research (A. C. H. Lai et al., 2015) (Li et al., 2016) (Zhang et al., 2016) (Yan & Mohammadian, 2019) (M. Jiang et al., 2019) (Yan et al., 2020). The Gauss linear scheme was adopted for the discretization of the gradient and Laplacian terms, the Euler scheme was utilized to discretize the temporal terms, and the Gauss upwind, Gauss vanleer, and Gauss linear schemes were employed to discretize the divergence terms. The adopted algorithms to solve the coupled pressure and momentum equations were PIMPLE algorithms, see Figure 3-3. The preconditioned conjugate gradient (PCG) and preconditioned bio conjugate gradient (PBiCG) methods were employed for the pressure field and the other fields, respectively.

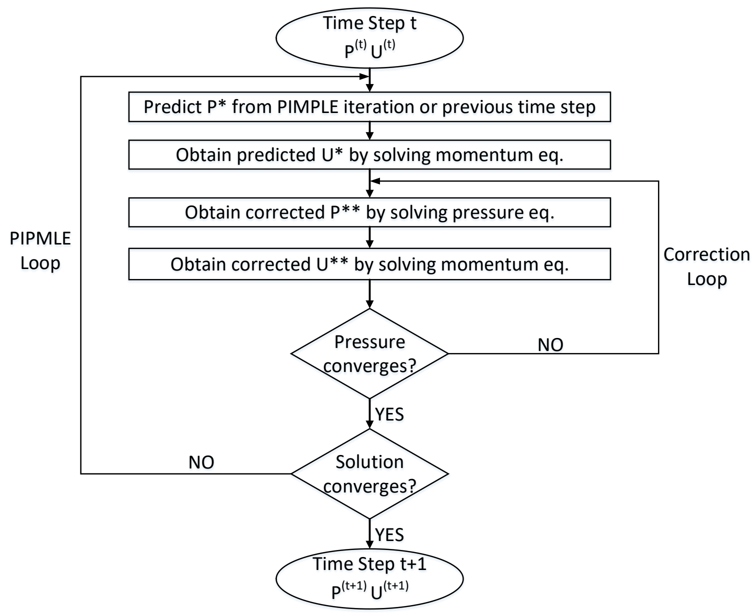

Figure 3-3 Flowchart of the PIMPLE algorithm; * and ** correspond to predicted and corrected fields, respectively.

The Courant number, C, can be defined as $C = U\Delta t/\Delta x$, where U is flow velocity, Δt represents time step, and Δx indicates cell size. The time step was adjusted during the simulations, and the maximum courant number was set to be 0.5 to provide small time steps. The simulations were run for 120 s, and the results obtained by time-averaging over the period of 70 s to 120 s to ensure fully developed flow and stable results. Figure 3-4 shows the time-series graphs for the velocity field along the trajectory of the central jet of case C2. To accelerate the simulation process, the numerical domain was decomposed into 16 regions, 4 parts in x- and 4 parts in y-directions, and then each region was processed by a processor. Afterward, the entire domain was reconstructed, and the results were extracted. All the computations were performed in the advanced research computing (ARC) systems of Compute Canada, and the real-time computing duration was ranged from 3 to 4 days.

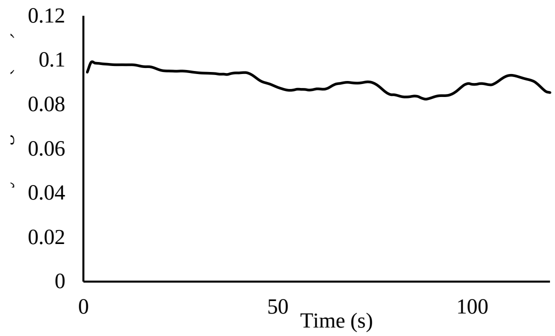

(a)

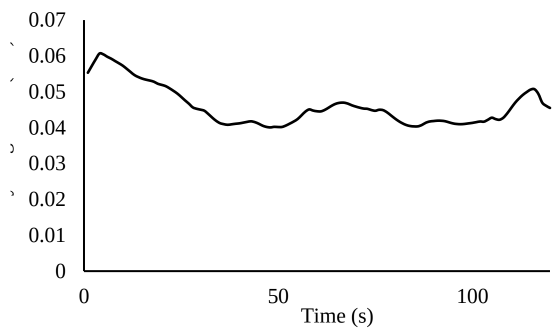

(b)

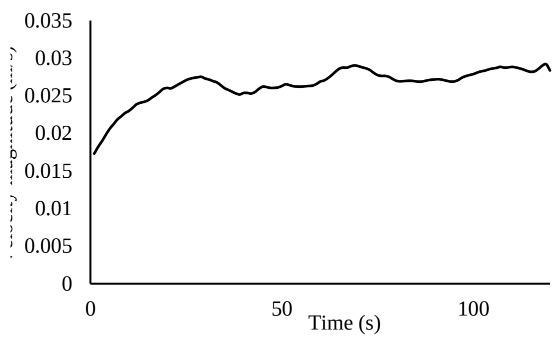

(c)

Figure 3-4 Time-series graphs for the velocity magnitude along the trajectory of the central jet in case C2 at (a) x/(D.Fd) = 0.4, (b) x/(D.Fd) = 0.75, and (c) x/(D.Fd) = 1.2.

To discuss the numerical results in the context of the literature, the accuracy of LRR predictions were compared with that of standard and (RNG) k-ε models adopted for the simulation of the same experimental work in a previous study (Yan & Mohammadian, 2019). Table 3-2 demonstrates the simulation characteristics of the previous and current study. It is worth mentioning that the numerical results obtained in both studies were mesh-independent, and adopting finer mesh does not necessarily lead to more accurate results. Therefore, the comparison of the accuracy of outcomes can provide a good insight into the performance of the turbulence models.

Table 3-2 Simulation characteristics of the previous (Yan & Mohammadian, 2019) and present study.

	(Yan & Mohammadian, 2019)	Current Study
Boundary conditions		
Bottom wall	Slip *	No-slip
Symmetry planes	Symmetric	Symmetric
Inlets	Fixed velocity inlet	Fixed velocity inlet
Atmosphere	Inlet–outlet	Pressure–inlet outlet
Outlet	Inlet–outlet	Pressure–inlet outlet
Number of cells	113,400	528,000
Software	OpenFOAM	OpenFOAM
Solver	twoLiquidMixingFoam	twoLiquidMixingFoam
Discretization schemes		
Temporal term	Euler	Euler
Gradient term	Linear	Linear
Laplacian term	Linear	Linear
Divergence term	Linear, vanLeer, and upwind	Linear, vanLeer, and upwind

* The results were the same when using slip or no-slip boundary condition for the bottom wall.

3.3 Results and Discussion

3.3.1 Model Validation

The four cases of C1, C2, C3, and C4, moderately spaced discharges, 0.47 < s/DF_d < 0.85, with different Froude numbers were numerically simulated by the LRR model, and the model predictions for the terminal rise height, impact distance, and impact dilution were compared to the measurements conducted by (Abessi & Roberts, 2014).

Terminal rise height is determined as where the vertical momentum flux almost vanishes along the jet trajectory (Kheirkhah Gildeh et al., 2015a). However, the y_t value is not defined the same in previous studies. For instance, Lai and Lee (C. C. K. Lai & Lee, 2012) defined it as where the concentration was 25% of the local maximum height concentration, C, while the integral model CorJet applied two cut-off levels, 3% and 25%, for the visual boundary (Jirka, 2004). Shao and Law (Shao et al., 2010) also adopted the cut-off level of 3%. The definition of y_t in the current simulations was considered to be the locus of 10% of the transverse maximum concentration at the location of jet maximum height, as it was defined in the experimental data (Abessi & Roberts, 2014). Figure 3-5 demonstrates the results of normalized terminal rise height, $y_t/(DF_d)$, versus port spacing values, s/DF_d, including cases C1–C4. The value of $y_t/(DF_d)$ for single jets were also included in this figure (P. J. W. Roberts et al., 1997). The numerical results of terminal rise height were in good agreement with the experimental data. The forecasting accuracy of the model was quantified using mean absolute percentage error (MAPE), the same as in the study conducted by (Yan & Mohammadian, 2019), where it was found to be 4.5%. The comparison of $y_t/(DF_d)$ values for cases C1–C4 and single ports showed that the terminal rise height of multiple inclined jets was lower than that of single discharges, which highlights the effect of jet merging. The LRR results for terminal rise height showed slight over prediction compared to the empirical equation, Equation (3-6), obtained based on the measurements for one- and two-sided multiport diffusers. However, the prediction of terminal rise height at $s/(DF_d)$ = 0.85 was matched with Equation (3-6).

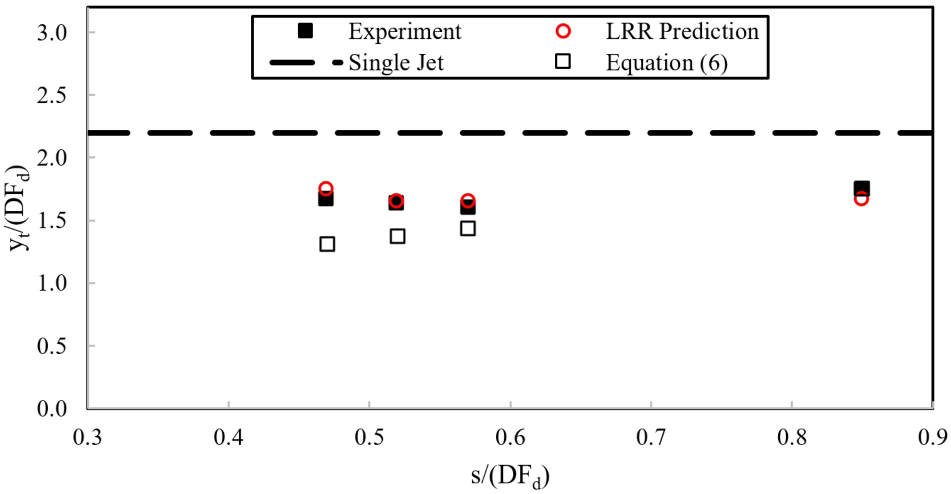

Figure 3-5 Experimental measurements (Abessi & Roberts, 2014) and numerical results of the normalized terminal rise height.

Figure 3-6 illustrates the results of normalized impact distance, $x_i/(DF_d)$, versus port spacing values. The model predictions of x_i/D demonstrated a good match with the measurements as the prediction error based on MAPE was less than 4%. The values of $x_i/(DF_d)$ increased with increasing values of port spacing, and all values were lower than the constant value presented for single discharges, $x_i/(DF_d)$ = 2.4 (P. J. W. Roberts et al., 1997). Jet merging causes multiple inclined jets to bend inward, which results in lower impact distance compared to that of single discharges. However, single jets mix with the surrounding water without any intervention. As $s/(DF_d)$ decreases, this effect is more pronounced, and the value of $x_i/(DF_d)$ decreases. The LRR predictions showed higher values for impact distance compared to the general empirical equation for one- and two-sided multiple dense jets.

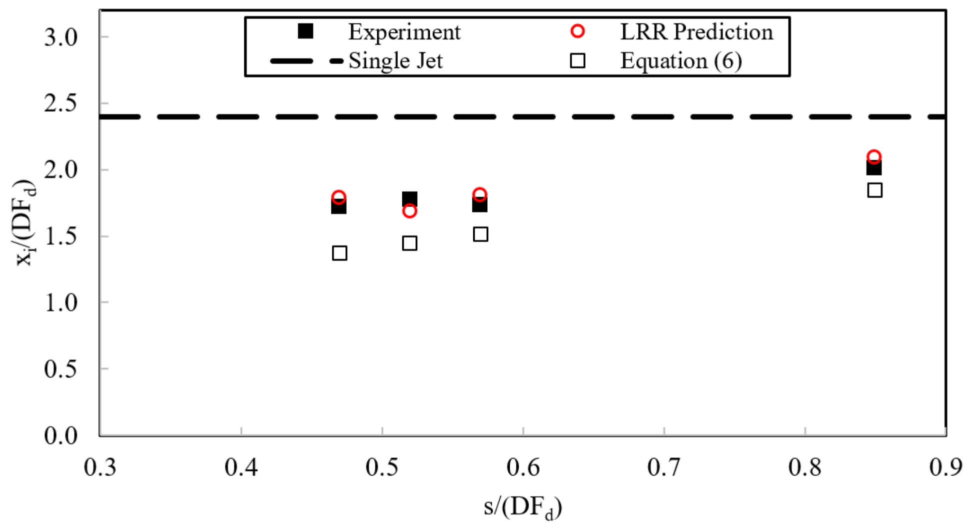

Figure 3-6 Experimental measurements (Abessi & Roberts, 2014) and numerical results of the normalized impact point distance.

Figure 3-7 indicates the results of the normalized impact dilution, S_i/F_d, against $s/(DF_d)$. The predictions were in an acceptable range of accuracy, with a MAPE value of 7%. As can be seen, $s/(DF_d)$ had a positive effect on S_i/F_d since the jet merging effect decreased for higher values of $s/(DF_d)$. Furthermore, the values of S_i/F_d were much lower for multiple discharges compared to single jets. The LRR results were in good agreement with the empirical equation presented for one-sided multiport diffusers, Equation (3-7).

Therefore, the numerical results demonstrated that LRR model, as an RSM, may be a reliable tool for the prediction of mixing behavior of multiple inclined dense jets, as it predicted the geometrical characteristics and impact dilution with mean absolute percentage errors of less than 5% and 7%, respectively. This model provided more accurate predictions compared to the EVMs employed for the simulation of same experimental work (Yan & Mohammadian, 2019), see the simulation characteristics in Table 3-2. It has been shown that RNG k-ε closure may provide results with errors within the range of 15%, and the predictions based on this model were more accurate compared to the standard k-ε closure (Yan & Mohammadian, 2019). The reason behind the higher accuracy of LRR predictions may have its roots in the main difference between RSMs and EVMs: RSMs directly solve the Reynolds stresses, while EVMs model them. In particular, EVMs consider that Reynolds stresses are proportional to mean rates of deformation (Versteeg & Malalasekera, 2007). It has also been mentioned that RSMs may perform better relative to EVMs when the flow fields are sophisticated (Versteeg & Malalasekera, 2007). Although the employment of the LRR model for the simulation of multiple jets has rarely been reported, one study focusing on 30° and 45° single inclined dense jets highlighted the outperformance of the LRR model over the RNG k-ε and nonlinear k-ε models (Kheirkhah Gildeh et al., 2015a).

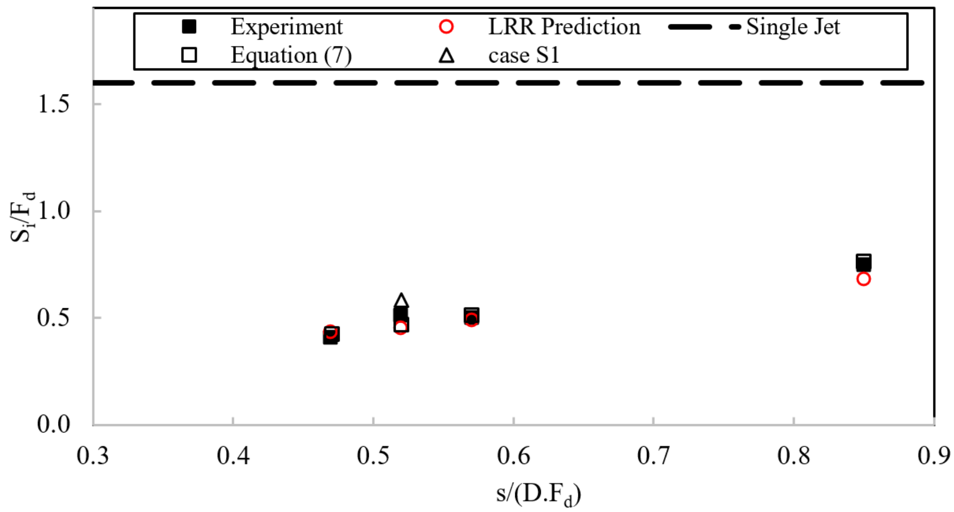

Figure 3-7 Experimental measurements (Abessi & Roberts, 2014) and numerical results of the normalized impact dilution.

3.3.2 Effect of Non-Uniform Port Orientation on Jet Merging Process

As a novel contribution to the literature, the effect of non-uniform port orientation on jet merging process was investigated by comparing cases C2 and S1. Case C2 refers to a diffuser with uniform port orientation to the horizontal, including three jets which are discharged at an angle of 60°. In case S1, the central jet is discharged with an angle of 60°, and the adjacent jets with an angle of 45°. The volume fraction, α, in the governing equations is the normalized concentration, C/C0, obtained in post-processing, where C is the local concentration and C0 is the initial concentration. Figure 3-8 demonstrates the general shape of the jets for cases C2 and S1, and the vertical slices where the data were extracted. In both cases, the jets moved upward due to the vertical component of the initial momentum, and this momentum continuously decreased due to jet entrainment and negative buoyancy until it equaled zero. Afterwards, the dense jets moved downward and subsequently impacted the bottom boundary. Unlike case C2, the central jet of the diffuser with non-uniform jet orientation to the horizontal, case S1, had higher y_t and lower x_i compared to its adjacent jets, which were discharged with an angle of 45° to the horizontal. This occurred because of the difference between the components of initial momentum of 45° and 60° inclined jets.

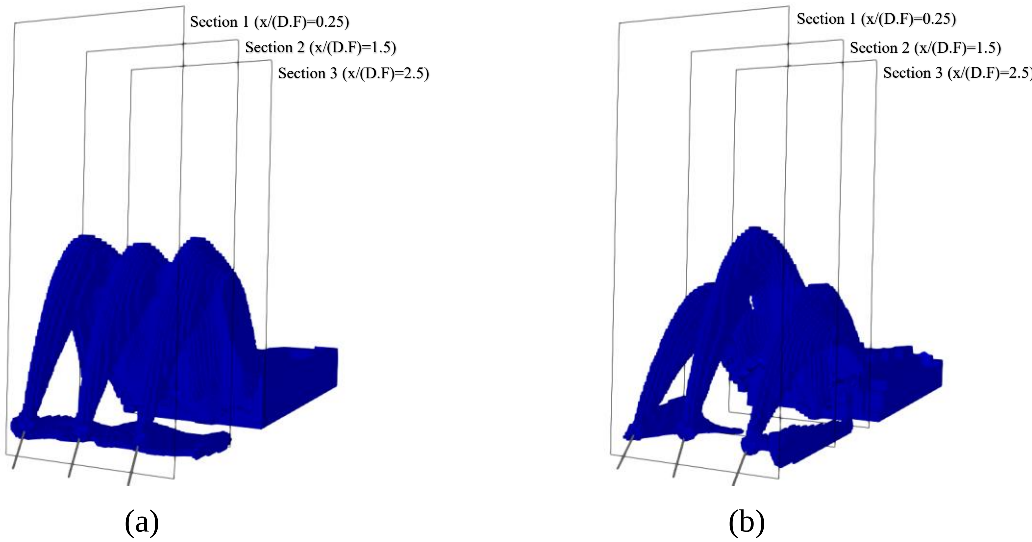

Figure 3-8 Visualization of (a) uniform (case C2) and (b) non-uniform (case S1) inclined dense jets, using a velocity isosurface (U = 0.015 m/s).

To investigate the jet merging process for the two different cases, concentration profiles at cross-sections close to and far from the nozzles were extracted, see Figure 3-9. Close to the ports, e.g., Figure 3-9(a), the jets in both cases seemed to be completely separate, like single jets, with high concentration at the jet centers, and they were not wide enough to interact with each other. Along the trajectory, the jets became more diluted due to the entrainment of the surrounding water, due to shear induced entrainment at the jets' edges. Farther away, e.g., Figure 3-9(b), the maximum concentrations were significantly decreased compared to Figure 3-9(a), and the jets were more diffused. The distance between the jet's centers in case S1 are more than that of case C2 because of the difference between the jets' elevation in case S1. Different orientations of the ports provide more space for the central jet to expand before interacting with other jets. As shown in Figure 3-9(b), at x/(D.Fd) = 1.5, the jets in case C2 were almost merged, and there was no space between them or under the central jet. This means the entrainment of fresh water into the jet was restricted in the z-direction and y-direction, from the lower edge. However, there were still some areas with almost zero concentration around the central jet in case S1. It is worth mentioning that the entrainment was restricted in both cases and, therefore, dilution was less than that of single jets. Eventually, in case C2, the individual jets were indistinguishable after the impact point of the central jet, see Figure 3-9(c). However, there was still a trace of 45° inclined dense jets in case S1.

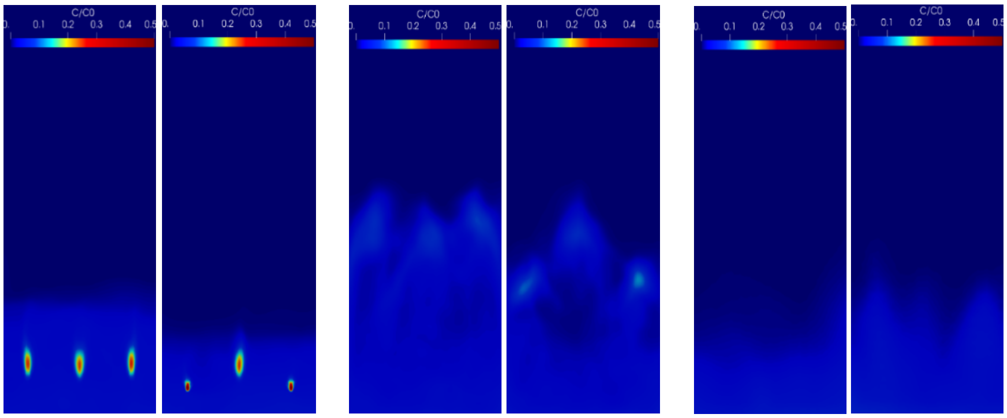

(a) (b) (c)

Figure 3-9 Concentration fields at different cross sections of uniform (case C2) and non-uniform (case S1) multiple inclined dense jets; (a) Section 1 (x/(D.Fd) = 0.25); (b) Section 2 (x/(D.Fd) = 1.5); (c) Section 2 (x/(D.Fd) = 2.5).

Jet merging may be the main source of difference between the mixing characteristics of single and multiple discharges. The Coanda interaction between the rising and descending parts of a dense jet causes the rising jet to attempt to re-entrain itself. As the jets are closely- or moderately spaced, jet merging results in a virtually impenetrable wall that prevents the entrainment of ambient water to inner surfaces and intensifies the Coanda effect. The lack of clear water on inward faces causes the jets to bend inward more sharply in search of clear water (Abessi & Roberts, 2014). Thus, multiple dense jets usually have shorter trajectories and therefore lower dilution rates compared to single jets. This difference between single and multiple jets can also be observed between the diffusers with uniform and non-uniform port orientation. Figure 3-10 indicates the contours of normalized concentration fields at the central planes for cases C2 and S1. The contours in both cases showed that the lower part of the jet was more expanded compared to the upper part. As shown in Figure 3-10, the central jet in case C2 bent inward more sharply, and there was less available clear water (C < 0.02 C0) under the central jet when the discharges were uniform, compared to that of non-uniform jets. It was found that the impact dilution for case S1 was 14% higher than that of case C2, see Figure 3-7. The availability of more clear water at the inner edge of the jet in case S1, compared to that of C2, decreased the entrainment restriction and thus caused higher dilution rates.

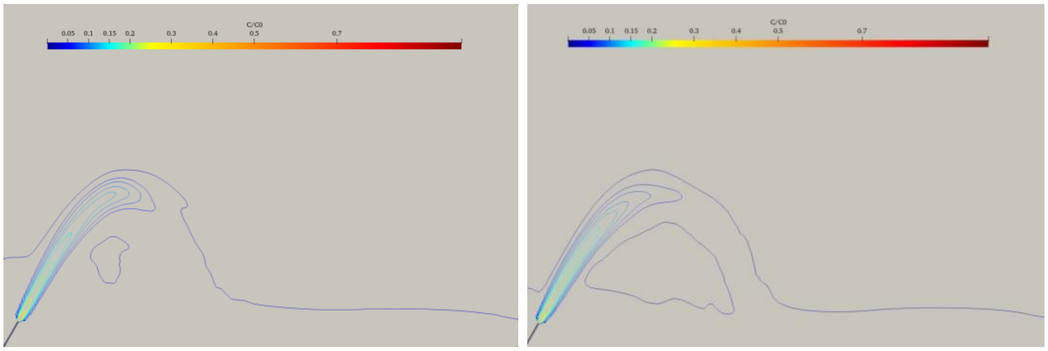

(a) (b)

Figure 3-10 Concentration contours at the central plane for (a) case C2 and (b) case S1.

A comparison of central jet trajectories more clearly highlights the effect of adjacent jets on the geometrical characteristics of central jets. As shown in Figure 3-11(a), the trajectory of the central jet in case S1 was at a lower elevation, compared to case C2, before the terminal rise height. However, it reached higher elevations after the terminal rise height and did not bend inward as sharply as the other case, demonstrating the reduced effect of jet merging and the Coanda interaction. The terminal rise height and impact point distance were found to be 7% and 5% higher for case S1 relative to case C2. A small deviation between the trajectories before the terminal rise height may be attributed to the Coanda interaction between the jets. The jets mutually attempted to entrain one another because of a pressure force, resulting from a change in the entrained flow pattern, that moves a jet to the other jet (Abessi & Roberts, 2014). This effect can be seen in a study focusing on multiple positive buoyant jets (P. J. W. Roberts et al., 1989) where the end plumes bend inwards as a result of unbalanced inward pressure force on the plumes, while the central jets move vertically because of the equally balanced forces on each side of them. Similarly, in case S1, as the adjacent jets are at a different elevation, the induced low-pressure field differs from that of case C2. As the central jet tries to entrain into the adjacent ones, which are at a lower elevation, it becomes somewhat deflected. Figure 3-11(b) illustrates how the concentration changes along the trajectory of the central jet in case S1 and case C2. As shown, before the terminal rise height, the concentration of the central jet in case C2 was lower than that for case S1. However, beyond this point, where the jets in case C2 interacted with each other and there was limited fresh water around the jets, its concentration became higher compared to case S1.

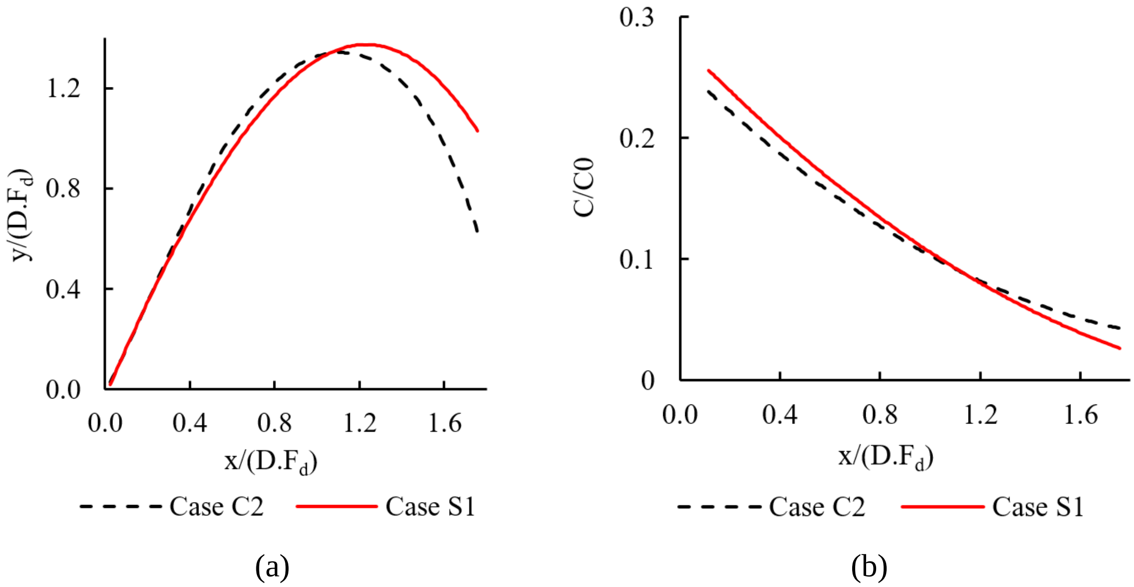

Figure 3-11 (a) Trajectory and (b) concentration of the central jet of cases C2 and S1.

To evaluate the overall effect of non-uniform port orientation, the concentration downstream of the impact point of all jets were investigated. Particularly, the concentration at x/(D.Fd) = 3.4 and the elevation of nozzle tip on the centerline planes of central and adjacent jets are shown in Figure 3-12. According to Figure 3-12, the concentration beyond the impact point on the central jet of case S1 was 3.7% lower than that on the central jet of case C2. Additionally, the concentration on the planes of adjacent jets for the non-uniform case was 8.4% lower compared to that for the uniform case. Therefore, the results show some improvements in dilution when adopting the multiport diffuser with non-uniform port orientation compared to the uniform diffuser.

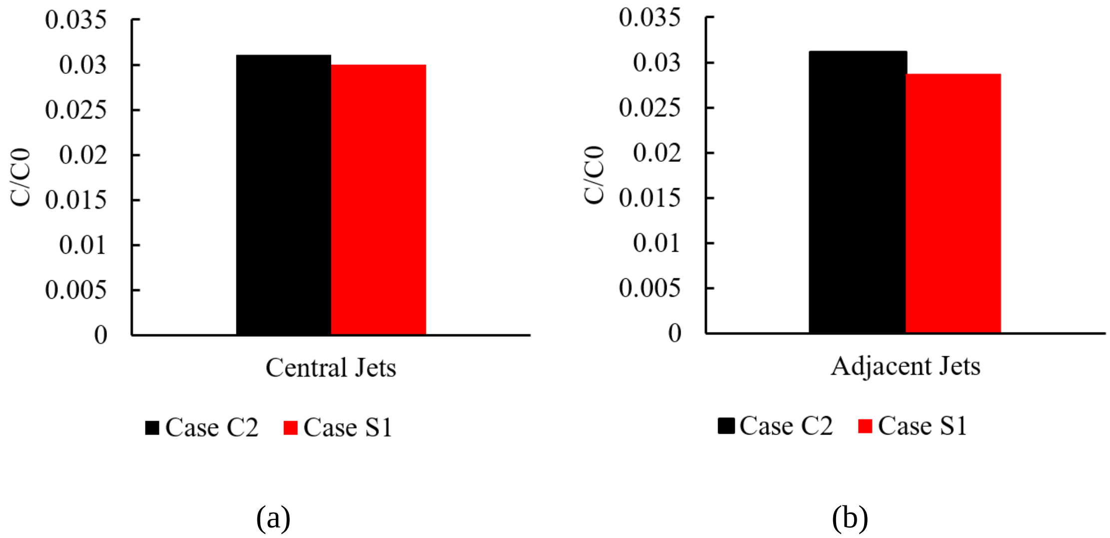

Figure 3-12 Concentration at x/(D.Fd) = 3.4 and the elevation of nozzle tip on the centerline planes of (a) central and (b) adjacent jets.

3.4 Conclusions

The first aim of the present study was to evaluate the prediction capabilities of RSMs for multiple inclined dense jets. The LRR turbulence model, as a new approach for multiple jets, was employed to perform the simulations. The predictions of geometrical characteristics and impact dilution were compared to the existing experimental measurements. Subsequently, the validated model was applied to perform further investigations on the effect of non-uniform port orientation on the merging process of multiple inclined dense jets, as a novel contribution. Particularly, diffusers with uniform, 60°–60°–60°, and non-uniform, 45°–60°–45°, port orientation were considered, and the effect of adjacent ports on the central ports was determined.

It was found that the LRR turbulence model, as an RSM, can be a reliable model for the study of the mixing behavior of multiple inclined dense jets, and can provide results of geometrical characteristics and impact dilution within the range of 5% and 7%, respectively. It also provides more accurate results compared to the EVMs including the standard and RNG k-ε turbulence models. Furthermore, the comparison of the diffuser with uniform and non-uniform port orientation showed that jet merging process is significantly affected by the port's orientation and the middle discharge may have a longer trajectory and therefore a higher dilution rate when its adjacent jets are discharged at a different angle, compared to that of uniform discharges. The terminal rise height, impact distance, and impact dilution of the central jet on a diffuser with non-uniform port inclination were found to be 7%, 5%, and 14% higher than those of the uniform case, respectively. It can be concluded that the behavior of the central jet on the diffuser with non-uniform port orientation is more like a single jet, compared to the one with uniform ports. Generally, the effects of jet merging and dynamic interactions on the central jet, including inward bending and a reduction in geometrical characteristics, are more significant when the nozzles are uniform. The evaluation of the overall effects of non-uniform port orientation showed 3.7% to 8.4% increment in dilution beyond the impact point.

This study showed how the trajectory and dilution of the middle discharge were affected by the orientation of its adjacent jets and how merging process was influenced by the orientation. The results of this study can be of interest in practical projects applying multiport diffusers to discharge brine or saline water as a by-product of osmotic power plants and municipal dense wastewaters into water bodies. A change in port orientation may provide an inexpensive way to augment dilution, compared to costly methods such as an increase in port spacing. This study highlighted the effects of non-uniform port orientation on merging process of multiple dense jets in near-field; however, the effect of non-uniform port orientation on intermediate and far fields may also be of interest. The outcomes have the potential to be considered by outfall designers. More investigations on the other parameters, such as flowing current, stratification, along with port orientation, are also recommended.

Author Contributions: Conceptualization, A.M. and S.A.R.S.H.; methodology, A.M.; software, S.A.R.S.H. and A.M.; validation, S.A.R.S.H.; formal analysis, S.A.R.S.H.; investigation, S.A.R.S.H.; resources, S.A.R.S.H.; data curation, S.A.R.S.H., A.M., P.J.W.R. and O.A.; writing—original draft preparation, S.A.R.S.H.; writing—review and editing, A.M., P.J.W.R. and O.A.; visualization, S.A.R.S.H.; supervision, A.M.; project administration, A.M.; funding acquisition, A.M. All authors have read and agreed to the published version of the manuscript.

Funding: This research was funded by Natural Sciences and Engineering Research Council of Canada (NSERC), grant number 210717. The research of S.A.R.S.H. was supported by Mitacs through the Mitacs Research Training Award.

Conflicts of Interest: The authors declare no conflict of interest.

References

Abessi, O., Roberts, P. J. W. (2017). Multiport diffusers for dense discharge in flowing ambient water. Journal of Hydraulic Engineering, 143(6), 04017003. https://doi.org/10.1061/(ASCE)HY.1943-7900.0001279

Abessi, O., & Roberts, P. J. W. (2014). Multiport Diffusers for Dense Discharges. Journal of Hydraulic Engineering, 140(8), 04014032. https://doi.org/10.1061/(ASCE)HY.1943-7900.0000882

Abessi, O., & Roberts, P. J. W. (2015). Effect of nozzle orientation on dense jets in stagnant environments. Journal of Hydraulic Engineering, 141(8), 06015009. https://doi.org/10.1061/(ASCE)HY.1943-7900.0001032

Abessi, O., & Roberts, P. J. W. (2018). Rosette Diffusers for Dense Effluents in Flowing Currents. Journal of Hydraulic Engineering, 144(1), 06017024. https://doi.org/10.1061/(ASCE)HY.1943-7900.0001403

Abessi, O., Saeedi, M., Davidson, M., Zaker, N.H. Flow Classification of Negatively Buoyant Surface Discharge in an Ambient Current. J. Coast. Res. 2012, 278, 148–155.

Adams, E.E. (1972) Submerged Multiport Diffusers in Shallow Water with Current. Ph.D. Thesis, Massachusetts Institute of Technology, Cambridge, MA, USA, 1972.

Ardalan, H., & Vafaei, F. (2019). CFD and Experimental Study of 45° Inclined Thermal-Saline Reversible Buoyant Jets in Stationary Ambient. Environmental Processes, 6(1), 219–239. https://doi.org/10.1007/s40710-019-00356-z

Baum, M. J., & Gibbes, B. (2020). Field-Scale Numerical Modeling of a Dense Multiport Diffuser Outfall in Crossflow. Journal of Hydraulic Engineering, 146(1), 05019006. https://doi.org/10.1061/(asce)hy.1943-7900.0001635

Calomino, F., Alfonsi, G., Gaudio, R., D'Ippolito, A., Lauria, A., Tafarojnoruz, A., & Artese, S. (2018). Experimental and numerical study of free-surface flows in a corrugated pipe. Water, 10(5), 638.

Einav, R., & Lokiec, F. (2003). Environmental aspects of a desalination plant in Ashkelon. Desalination, 156(1), 79–85. https://doi.org/10.1016/S0011-9164(03)00328-X

Fischer, H.B., List, E.J., Koh, R.C.Y., Imberger, J., Brooks, N.H. (1979) Mixing in Inland and Coastal Waters; Academic Press: Amsterdam, The Netherlands.

Frick, W.E. (2004) Visual Plumes mixing zone modeling software. Environ. Model. Softw., 19, 645–654.

Hanjalic, K. (2004) Closure Models for Incompressible Turbulent Flows; Lecture Notes at Von Kármán Institute: Brussels, Belgium, p. 75.

Hodgson, J.E., Moawad, A.K., Rajaratnam, N. (1999) Concentration field of multiple circular turbulent jets. J. Hydraul. Res., 37, 249–256. https://doi.org/10.1080/00221689909498309

Huai, W.-X., Li, Z.-W., Qian, Z., Zeng, Y.-H., Han, J., Peng, W.-Q. (2010). Numerical simulation of horizontal buoyant wall jet. Journal of Hydrodynamics, 22(1), 58–65. https://doi.org/10.1016/S1001-6058(09)60028-7

Jiang, M., Law, A. W. K., & Lai, A. C. H. (2019). Turbulence characteristics of 45° inclined dense jets. Environmental Fluid Mechanics, 19(1), 27–54. https://doi.org/10.1007/s10652-018-9614-8

Jirka, G. H. (2004). Integral Model for Turbulent Buoyant Jets in Unbounded Stratified Flows. Part I: Single Round Jet. Environmental Fluid Mechanics, 4(1), 1–56. https://doi.org/10.1023/A:1025583110842

Joseph W Lee, B. H., Member, A., & Cheung, V. (1990). Generalized Lagrangian Model for Buoyant Jets in Current. Journal of Environmental Engineering, 116(6), 1085–1106. https://doi.org/10.1061/(ASCE)0733-9372(1990)116:6(1085)

Kheirkhah Gildeh, H., Mohammadian, A., Nistor, I., & Qiblawey, H. (2014). Numerical Modeling of Turbulent Buoyant Wall Jets in Stationary Ambient Water. Journal of Hydraulic Engineering, 140(6), 04014012. https://doi.org/10.1061/(asce)hy.1943-7900.0000871

Kheirkhah Gildeh, H., Mohammadian, A., Nistor, I., & Qiblawey, H. (2015). Numerical modeling of 30∘ and 45∘ inclined dense turbulent jets in stationary ambient. Environmental Fluid Mechanics, 15(3), 537–562. https://doi.org/10.1007/s10652-014-9372-1

Kheirkhah Gildeh, H., Mohammadian, A., Nistor, I., Qiblawey, H., & Yan, X. (2016). CFD modeling and analysis of the behavior of 30° and 45° inclined dense jets - New numerical insights. Journal of Applied Water Engineering and Research, 4(2), 112–127. https://doi.org/10.1080/23249676.2015.1090351

Kikkert, G. A., Davidson, M. J., & Nokes, R. I. (2007). Inclined Negatively Buoyant Discharges. Journal of Hydraulic Engineering, 133(5), 545–554. https://doi.org/10.1061/(ASCE)0733-9429(2007)133:5(545)

Killingstad, P. E. (2018). A study of dead water resistance Reynolds Averaged Navier Stokes simulations of a barge moving in stratified waters. https://www.duo.uio.no/handle/10852/63458

Knystautas, R. (1964). The turbulent jet from a series of holes in line. Aeronautical Quarterly, 15(1), 1–28.

Koh, R. C. Y., & Fan, L. N. (1970). Mathematical models for the prediction of temperature distributions resulting from the discharge of heated water in large bodies of water. EPA Water Pollutant Control. Res. Ser., 16130.

Lai, A. C. H., & Lee, J. H. W. (2012). Dynamic interaction of multiple buoyant jets. Journal of Fluid Mechanics, 708, 539–575. https://doi.org/10.1017/jfm.2012.332

Lai, A. C. H., Zhao, B., Law, A. W.-K., & Adams, E. E. (2015). A numerical and analytical study of the effect of aspect ratio on the behavior of a round thermal. Springer, 15, 85–108. https://doi.org/10.1007/s10652-014-9362-3

Lai, C. C. K., & Lee, J. H. W. (2012). Mixing of inclined dense jets in stationary ambient. Journal of Hydro-Environment Research, 6(1), 9–28. https://doi.org/10.1016/j.jher.2011.08.003

Launder, B., Reece, G., & Rodi, W. (1975). Progress in the development of a Reynolds-stress turbulence closure. Journal of Fluid Mechanics, 68(3), 537–566. https://doi.org/10.1017/S0022112075001814

Lauria, A., Alfonsi, G., & Tafarojnoruz, A. (2020). Flow pressure behavior downstream of ski jumps. Fluids, 5, 168. https://www.mdpi.com/842876

Lee, J.H.W.; Chu, V.H. (2003) Turbulent Jets and Plumes: A Lagrangian Approach; Springer Science & Business Media: Berlin/Heidelberg, Germany, 1.

Li, Y., Geng, X., Wang, H., Zhuang, X., & Ouyang, J. (2016). Simulating the frontal instability of lock-exchange density currents with dissipative particle dynamics. Modern Physics Letters B, 30(17), 1–9. https://doi.org/10.1142/S0217984916502006

Lim, A. E., & Lam, Y. (2020). Numerical investigation of nanostructure orientation on electroosmotic flow. Micromachines, 11, 971. https://www.mdpi.com/874392

Lim, A. E., & Lam, Y. C. (2021). Vertical Squeezing Route Taylor Flow with Angled Microchannel Junctions. Industrial and Engineering Chemistry Research, 60(39), 14307–14317. https://doi.org/10.1021/ACS.IECR.1C02324

Liseth, P. (1973). Mixing of merging buoyant jets from a manifold in stagnant receivingwater of uniform density. Advances in Water Pollution Research, Proceedings of the Sixthinternational Conference, 921–936.

Holzmann, T. (2016) Mathematics, Numerics, Derivations and OpenFOAM®; Holzmann CFD: Loeben, Germany.

Lyu, S., Seo, I., Engineering, Y. D. K.-K. J. of C., & 2013, undefined. (2013). Experimental investigation on behavior of multiple vertical buoyant jets discharged into a stagnant ambient. Springer, 17(7), 1820–1829. https://doi.org/10.1007/s12205-013-0525-4

Marti, C. L., Antenucci, J. P., David Luketina, ;, Okely, P., Imberger, J., & Asce, M. (2011). Near-Field Dilution Characteristics of a Negatively Buoyant Hypersaline Jet Generated by a Desalination Plant. Journal of Hydraulic Engineering, 137(1), 57–65. https://doi.org/10.1061/(ASCE)HY.1943-7900.0000275

Missimer, T. M., Jones, B., & Maliva, R. G. (2015). Intakes and Outfalls for Seawater Reverse-Osmosis Desalination Facilities: Innovations and Environmental Impacts. Springer, New York, NY, USA.

Oliver, C. J., Davidson, M. J., & Nokes, R. I. (2008). k-ε Predictions of the initial mixing of desalination discharges. Environmental Fluid Mechanics, 8(5–6), 617–625. https://doi.org/10.1007/s10652-008-9108-1

OpenFoam. (2015).

Palomar, P., Lara, J., & Losada, I. (2012). Near field brine discharge modeling part 2: Validation of commercial tools. Desalination, 290, 28–42.

Palomar, P., Lara, J., Losada, I., Rodrigo, M., & Alvárez, A. (2012). Near field brine discharge modelling part 1: Analysis of commercial tools. Desalination, 290, 14–27.

Peyret, R., & Krause, E. (2000). Advanced turbulent flow computations. https://link.springer.com/content/pdf/10.1007/978-3-7091-2590-8.pdf

Roberts, P. J. W. (2015). Near field flow dynamics of concentrate discharges and diffuser design. Environmental Science and Engineering (Subseries: Environmental Science), 149, 369–396. https://doi.org/10.1007/978-3-319-13203-7_17

Roberts, P. J. W., Hunt, C. D., Mickelson, M. J., & Tian, X. (2011). Field and Model Studies of the Boston Outfall. Journal of Hydraulic Engineering, 137(11), 1415–1425. https://doi.org/10.1061/(ASCE)HY.1943-7900.0000445

Roberts, P. J. W., & Toms, G. (1987). Inclined Dense Jets in Flowing Current. Journal of Hydraulic Engineering, 113(3), 323–340. https://doi.org/10.1061/(ASCE)0733-9429(1987)113:3(323)

Roberts, P. J. W., Ferrier, A., & Daviero, G. (1997). Mixing in inclined dense jets. Journal of Hydraulic Engineering, 123(8), 693–699. https://doi.org/10.1061/(ASCE)0733-9429(1997)123:8(693)

Roberts, P. J. W., Snyder, W. H., & Baumgartner, D. J. (1989). Ocean Outfalls. III: Effect of Diffuser Design on Submerged Wastefield. Journal of Hydraulic Engineering, 115(1), 49–70. https://doi.org/10.1061/(ASCE)0733-9429(1989)115:1(49)

Roberts, P. J. W., & Toms, G. (1988). Ocean outfall system for dense and buoyant effluents. Journal of Environmental Engineering, 114(5), 1175–1191.

Seo, I. W., & Yeo, H. K. (2002). Near-field dilution of rosette type multiport wastewater diffusers. Water Engineering Research: International Journal of KWRA 3, 2, 93–111.

Shao, D., mechanics, A. L.-E. fluid, & 2010, undefined. (2010). Mixing and boundary interactions of 30 and 45 inclined dense jets. Springer, 10, 521–553. https://doi.org/10.1007/s10652-010-9171-2

Shrivastava, I., & Adams, E.E. (2019) Mixing of Tee Diffusers in Shallow Water with Crossflow: A New Look. J. Hydraul. Eng., 145, 04019006 https://doi.org/10.1061/(ASCE)HY.1943-7900.0001574

Tafarojnoruz, A., & Lauria, A. (2020). Large eddy simulation of the turbulent flow field around a submerged pile within a scour hole under current condition. Coastal Engineering Journal, 62(4), 489–503. https://doi.org/10.1080/21664250.2020.1807453

Taherian, M., & Mohammadian, A. (2021). Buoyant jets in cross-flows: review, developments, and applications. Journal of Marine Science and Engineering, 9(1), 61.

Taherian, M., Saeidi Hossein, S.A.R., Mohammadian, A. (2022) Overview of outfall discharge modeling with a focus on turbulence modeling approaches. In Advances in Fluid Mechanics: Modeling and Simulation; Springer: Singapore, ISSN 2364-6748.

Tang, H. S., Paik, J., Sotiropoulos, F., & Khangaonkar, T. (2008). Three-Dimensional Numerical Modeling of Initial Mixing of Thermal Discharges at Real-Life Configurations. Journal of Hydraulic Engineering, 134(9), 1210–1224. https://doi.org/10.1061/(asce)0733-9429(2008)134:9(1210)

Tian, X., Roberts, P.J.W., Daviero, G.J. (2004) Marine wastewater discharges from multiport diffusers. I: Unstratified stationary water. J. Hydraul. Eng., 130, 1137–1146. https://doi.org/10.1061/(ASCE)0733-9429(2004)130

Tian, X., & Roberts, P. J. W. (2011). Experiments on Marine Wastewater Diffusers with Multiport Rosettes. Journal of Hydraulic Engineering, 137(10), 1148–1159. https://doi.org/10.1061/(ASCE)HY.1943-7900.0000409

Versteeg, H.K., Malalasekera, W. (2007) An Introduction to Computational Fluid Dynamics: The Finite Volume Method, 2nd ed; Pearson Education: London, UK.

Wang, H. J., & Davidson, M. J. (2003). Jet Interaction in a Still Ambient Fluid. Journal of Hydraulic Engineering, 129(5), 349–357. https://doi.org/10.1061/(ASCE)0733-9429(2003)129:5(349)

Xu, Z., Otoo, E., Chen, Y., & Ding, H. (2019). 2D PIV Measurement of Twin Buoyant Jets in Wavy Cross-Flow Environment. Water, 11, 399. https://doi.org/10.3390/w11020399

Xue, W., Huai, W., Qian, Z., Yang, Z., & Zeng, Y. (2014). Numerical simulation of initial mixing of marine wastewater discharge from multiport diffusers. Engineering Computations (Swansea, Wales), 31(7), 1379–1400. https://doi.org/10.1108/EC-06-2013-0148/FULL/HTML

Yan, X., Asce, S. M., Mohammadian, A., & Eng, P. (2017). Numerical Modeling of Vertical Buoyant Jets Subjected to Lateral Confinement. Journal of Hydraulic Engineering, 143(7), 04017016. https://doi.org/10.1061/(ASCE)HY.1943-7900.0001307

Yan, X., Ghodoosipour, B., & Mohammadian, A. (2020). Three-Dimensional Numerical Study of Multiple Vertical Buoyant Jets in Stationary Ambient Water. Journal of Hydraulic Engineering, 146(7), 04020049. https://doi.org/10.1061/(asce)hy.1943-7900.0001768

Yan, X., & Mohammadian, A. (2019). Numerical modeling of multiple inclined dense jets discharged from moderately spaced ports. Water (Switzerland), 11(10), 14–16. https://doi.org/10.3390/w11102077

Yan, X., Mohammadian, A., & Chen, X. (2019). Three-dimensional numerical simulations of Buoyant Jets discharged from a Rosette-type multiport diffuser. Journal of Marine Science and Engineering, 7(11), 1–15. https://doi.org/10.3390/jmse7110409

Yannopoulos, P. C., & Noutsopoulos, G. C. (2006). Interaction of vertical round turbulent buoyant jets - Part I: Entrainment restriction approach. Journal of Hydraulic Research, 44(2), 218–232. https://doi.org/10.1080/00221686.2006.9521677

Yannopoulos, P.C.; Noutsopoulos, G.C. (2006) Interaction of vertical round turbulent buoyant jets—Part II: Superposition method. J. Hydraul. Res., 44, 233–248. https://doi.org/10.1080/00221686.2006.9521678

Zeitoun, M. A., McHilhenny, W. F., & Reid, R. O. (1970). Conceptual Designs of Outfall Systems for Desalination Plants. In Offshore Technology Conference; OnePetro: Washington, DC, USA.

Zeitoun, M. A., Reid, R. O., McHilhenny, W. F., & Mitchell, T. M. (1972). Model Studies of Outfall Systems for Desalination Plants. Part III. Numerical Simulation and Design Considerations; Dow Chemical Co.: Freeport, TX, USA.

Zhang, S., Jiang, B., Law, A. W. K., & Zhao, B. (2016). Large eddy simulations of 45° inclined dense jets. Environmental Fluid Mechanics, 16(1), 101–121. https://doi.org/10.1007/s10652-015-9415-2

Zhang, S., Law, A. W. K., & Jiang, M. (2017). Large eddy simulations of 45° and 60° inclined dense jets with bottom impact. Journal of Hydro-Environment Research, 15, 54–66. https://doi.org/10.1016/j.jher.2017.02.001

4 Mixing Behavior of Multiport Diffusers with Non-Uniform Port Orientation[3]

Highlights

- An experimental program was developed to study the mixing behavior of multiport diffusers with non-uniform port orientations.
- Laboratory experiments were conducted using the Laser Induced Fluorescence (LIF) method.
- A novel concept for modifying multiport desalination outfalls was proposed to enhance mixing of the brine.
- Non-uniform diffusers resulted in higher dilutions than equivalent uniform diffusers.
- The angle difference between adjacent jets on a multiport diffuser played a significant role in mixing.

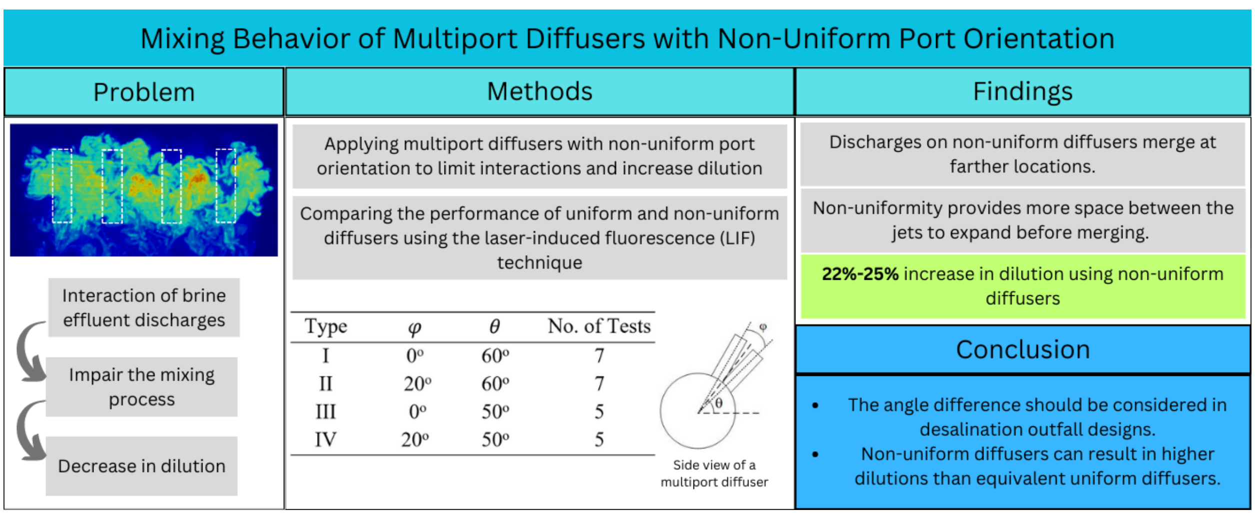

Abstract

This study addresses the disposal of hypersaline brines from desalination plants through multiport diffusers into seas and oceans. Experiments are reported on multiport diffusers with non-uniform

[3] This chapter has been published as: Hosseini, S. A. R. S., Taherian, M., Mohammadian, A., Ferrari, S., & Roberts, P. J. (2023). Mixing behavior of multiport diffusers with non-uniform port orientation. Desalination, 116962.

port orientations to limit the negative effect of jet merging on the mixing process, thus augmenting dilution. Laboratory experiments on uniform and non-uniform diffusers, with varying port angles in the range of highest reported dilution rates for dense discharges (40^{o}-70^{o}), are reported. Concentration fields were mapped using the laser-induced fluorescence (LIF) technique, and the major flow properties and merging processes were compared. Investigations revealed that the non-uniform diffusers had 22% to 25% higher dilution rates, attributed to different mixing behavior in the interaction zones. Non-uniform port orientation provided more space between the jets to expand before interacting with their neighbors, resulting in higher dilution rates. This study questions the application of formulae obtained from experiments conducted with single jets for multiport diffuser designs and proposes considering source characteristics specific to multiport diffusers, such as angle difference, for the efficient design of desalination outfalls. The new data and analysis can benefit the design of desalination discharge systems with environmental risk reductions and potential cost savings due to shorter diffusers with non-uniform jet orientations.

Keywords: Desalination; Brine disposal; Multiport diffuser; Negatively buoyant jet; Laser-induced fluorescence; Discharge inclination.

4.1 Introduction

The rapid population growth and industrialization of many developing countries have increased the demand for freshwater (Kucera, 2019). This increased demand and climate uncertainty have led freshwater stress and scarcity to become more prevalent globally (Ridoutt & Pfister, 2010). Seawater desalination has been introduced to overcome these issues (Kucera, 2019), and it has become viable as a sustainable solution over recent decades (Lattemann et al., 2010) (Caldera & Breyer, 2017). Desalination plants are supplied with seawater and produce freshwater for use and hypersaline water as a waste by-product. An efficient disposal method of hypersaline water is to eject it back into the source ocean environment (T. M. Missimer & Maliva, 2018). However, brine effluents may reduce water quality and harm marine habitats (Palomar & Losada, 2010) if not discharged properly. To provide rapid mixing of the brine with surrounding water and subsequently protect the marine environment, these effluents are discharged through submerged multiport diffusers in the form of high-velocity turbulent jets (Taherian & Mohammadian, 2021b) (Taherian et al., 2022). Brine discharges, which have a density higher than the receiving environment, are discharged at an upward angle and then turn down and impinge the sea bottom. These discharges are called inclined negatively buoyant jets (INBJs). Understanding the hydrodynamics of desalination discharges is essential to minimize adverse environmental effects resulting from desalination plants.

Discharge mixing and transport processes are affected by the characteristics of the ambient environment and discharge conditions. The former includes receiving water stratification, the topography of the seabed, waves, and currents, which cannot be manipulated by outfall designers. The latter includes port geometry, jet momentum and buoyancy fluxes, and diffuser configuration, which can be optimized by outfall designers to enhance mixing and increase dilution. As the mixing behavior of discharges is significantly affected by the properties of outfall diffusers (Bleninger, 2006) (Yan & Mohammadian, 2019) (Saeidi Hosseini et al., 2022), the focus of the present study is on the effect of port orientation on the mixing behavior of desalination discharges.

Desalination diffusers can be designed as single port discharges for small flow rates. Single jets can freely mix with the ambient water without any interactions, and the port angle to the horizontal is an important design feature affecting their mixing behavior. Inclined jets, compared to vertical discharges, result in a higher dilution rate since vertical jets tend to fall back on themselves, which significantly impairs the dilution process (Fischer et al., 1979a) (P. J. W. Roberts et al., 1997) (T. M. Missimer et al., 2015). This interaction of ascending and descending components of jets, and therefore re-entrainment, has been reported for nozzle angles greater than 80^{o} to the horizontal (Ferrari & Querzoli, 2010). Loya et al. (Loya-Fernández et al., 2018) evaluated the effects of installing a 60^{o} single-port diffuser at the Nuevo Canal de Cartagena desalination plant pipeline on the dispersion of brine. They showed that the dilution rate of samples taken 1 km from the outfall increased by almost 17 times after the diffuser installation. Although 60^{o} is commonly adopted for diffuser designs to optimize dilution, some studies have reported almost the same dilutions for port angles over the ranges of 45^{o} to 75^{o} (Papakonstantis et al., 2011), 60^{o} to 75^{o} (Jirka, 2008) (Oliver et al., 2013a) and 45^{o} to 65^{o} (Abessi & Roberts, 2015).

For large discharges, multiport diffusers are the most effective strategy (M. Baum, 2019). Although multiport brine diffusers are frequently applied worldwide, e.g., in Sydney, Perth, and Melbourne, there are fewer studies on the mixing behavior of multiport diffusers. A conventional multiport diffuser consists of evenly spaced ports oriented at the same angle to the horizontal, and the unidirectional or one-sided diffuser is the most widely employed type (S. W. Lyu, 2003). The main issue with multiple diffusers is the port spacing. If they are too close, the jets cannot freely entrain ambient water, as single jets do. Merging causes these jets to have a reduced terminal rise height and to bend inward, with a shorter trajectory compared to a single jet at the same angle (Abessi & Roberts, 2014). The shortened trajectory further decreases dilution since it diminishes the available surface for entrainment.

The effect of port spacing on the mixing process of multiple INBJs was systematically studied for the first time in 2014 (Abessi & Roberts, 2014). Before this, most designs of multiport diffusers were based on the investigations of single jets (M. Baum, 2019). Abessi and Roberts experimentally studied multiple 60^o jets discharging from one or both sides of a diffuser, using the Laser Induced Fluorescence (LIF) technique. The effect of port spacing, s, was found to depend on the non-dimensional port spacing (s/dF), where F is the Froude number and d the nozzle diameter. The influence of port spacing was investigated by varying s/dF between 0.47 and 20.63. The effect of jet merging on geometrical characteristics and dilution rates of closely and moderately spaced ports was quantitatively presented. The significant effect of port spacing on dilution was evident in their results where the impact dilution for diffusers with s/dF=0.47 was about a quarter of those with s/dF>2. They recommended maintaining s/dF>2 to avoid a reduction in dilution rate for multiport designs.

Miller et al. (B. M. Miller et al., 2006) conducted physical model tests for the multiport Perth Stage 2 diffuser and considered one and three nozzles discharging from one side at 60^o, using the conductivity probe method. The non-dimensional port spacing was varied between 0.95 and 2.9, and a reduction in impact point dilution was observed as the port spacing was reduced, for s/dF<2. Marti et al. (Marti et al., 2011) provided field observations on the Perth Stage 1 diffuser, where s/dF was about 1.3 and the ports were 60^o inclined. The observations for impact point dilution were similar to the impact point dilution presented for single jets (P. J. W. Roberts et al., 1997), noting that the field measurements were conducted in the presence of currents. A recent numerical study proposed that multiport diffusers with non-uniform port orientations could improve dilution (Saeidi Hosseini et al., 2022). Two different configurations including a diffuser with 60^o inclined ports and a diffuser with alternating 45^o and 60^o inclined ports were considered. The port spacing was the same, s/dF=0.52, for both configurations. The diffuser with non-uniform port orientation resulted in a 14% higher impact point dilution rate than the uniform diffuser.

The negative impact of jet merging on dilution has also been reported for rosette-type multiport diffusers, where the ports are clustered in rosettes each having multiple nozzles. Some studies showed that for single rosettes with four ports, jet interaction was minimal and there was little reduction in impact point dilution, dilution at the location where the flow impacts the lower boundary, compared to a single jet (B. M. Miller & Tarrade, 2010) (Abessi et al., 2017). However, the near-field dilution, dilution at the location downstream of the impact point where the ultimate turbulence collapses, was 27% lower than a single jet (Abessi et al., 2017). The jets on four-port risers had little interaction before the impact point, but four density currents that formed on the seabed finally merged, reducing the near-field dilution.

Tarrade et al. (Tarrade et al., 2009) reported about a 15% lower dilution rate for six-port risers compared to four-port risers as a result of jet interaction and competition between jets for clear water to entrain. Miller (B. Miller, 2011) indicated an approximately 50% reduction in the near-field dilution for a six-port riser relative to a single discharge. Miller and Tarrade (B. M. Miller & Tarrade, 2010) and Tarrade and Miller (Tarrade & Miller, 2010) showed that the jets for 9- and 12-port risers were so close that entrainment was mainly from above the jets. The entrainment from the gap between the jets was strictly restricted due to the Coanda effect and significant jet interactions.

While maintaining s/dF>2 has been proposed as a solution to avoid the negative effects of jet merging on dilution (Abessi & Roberts, 2014), it is essential to consider the potential high costs that could be imposed on desalination outfall projects. Discharge facilities can account for a considerable portion of the capital cost of desalination plants (B. Jiang & Law, 2013), and in some cases, they can even exceed 30% of the total costs (Seawater Desalination Costs: White Paper, 2012). Outfall costs may vary considerably depending on factors such as length, diameter, depth, construction technique and material, and local conditions (Bleninger, 2006) (P. J. Roberts et al., 2010). The average investment cost of 200 outfalls worldwide was reported to be approximately 7 million US$ each, with values ranging from 2 million to as high as 3,500 million US$ (Bleninger, 2006). Pipe supply and construction costs constitute approximately 90% of the total outfall cost, encompassing construction, design, field studies, operation and maintenance, and monitoring (P. J. Roberts et al., 2010). Chang et al. (Chang et al., 2011) investigated the database of the construction of outfall pipes in Taiwan and introduced the outfall length and diameter as the major parameters affecting outfall costs. They provided a linear construction cost function in terms of the outfall length and diameter. Maalouf et al. (Maalouf et al., 2014) expressed the outfall construction cost as a linear function of the outfall length, port diameter, and the number of ports.

Roberts et al. (P. J. Roberts et al., 2010) analyzed the relationship between outfall cost per meter and pipe diameter (in meters) using data for 145 outfalls. While the correlation between diameter and unit cost was found to be relatively weak, they proposed a preliminary estimate of the range of cost range with a linear correlation represented as C=6140D, where C is the cost in US$ (April 2009) per meter, and D is the diameter in meters. For high-density polyethylene (HDPE) outfalls with a diameter less than 1.4 meters, the costs generally fell within the range of 1,000 to 7,000 US$/m. On the other hand, outfalls greater than 2.4 meters in diameter were usually tunneled or concrete, resulting in costs ranging from 10,000 to 20,000 US$/m. For diameters exceeding 3.5 meters, costs could even surpass 30,000 US$/m (P. J. Roberts et al., 2010). The proportion of the diffuser length to the total outfall length can provide some insight into the relative cost of the diffuser section in an outfall, which exhibits significant variation across different projects. For example, the proportion was about 0.1 for the Ipanema outfall in Rio de Janeiro, Brazil, 0.25 for the Perth Seawater Desalination Plant outfall in Australia, and 0.4 for the Berazategui outfall in Buoenos Aires, Argentina. The average values for the characteristics of 200 outfalls reported by Bleninger (Bleninger, 2006) showed the average diffuser and outfall lengths were 100 m and 1300 m, respectively.

These previous studies have focused mainly on the influence of port orientation on the dilution of single jets, or the port spacing of multiple jets. The adverse effect of merging on the mixing behavior of multiple jets has also been highlighted in prior research. The motivation behind the present study is to reduce the very high cost of construction of diffusers and tunnels by minimizing port spacing and therefore outfall and diffuser length. This study explores the impact of using ports with different angles to the horizontal on a multiport diffuser. The focus is on jet merging and its consequent effect on the mixing process. As a novel approach, this study aims to determine whether this strategy positively influences dilution rates. This idea comes from the observation that different port orientations provide more space for discharges to expand before interacting with their neighboring jets. A series of systematic experiments, simulating typical ocean outfall diffusers, were carried out to determine the effect of non-uniform port orientation on the mixing behavior of multiple desalination discharges.

4.2 Analysis

A schematic view of typical multiple jets is shown in Figure 4-1. The dense effluents with density ρ_0 are discharged into the lighter receiving water ($\rho_a < \rho_0$) at an angle θ with jet velocity U_0 through round nozzles with diameter d. The initial fluxes characterising the flow behavior include the volume ($Q_0 = \pi d^2 U_0/4$), kinematic momentum ($M_0 = U_0 Q_0$), and buoyancy ($B_0 = g_0' Q_0$) fluxes. The jets experience a negative buoyancy force due to their higher densities relative to the ambient fluid and therefore turn downward where the initial vertical momentum flux almost vanishes. The overhead view shows the individual jets merging at some distance from the diffuser.

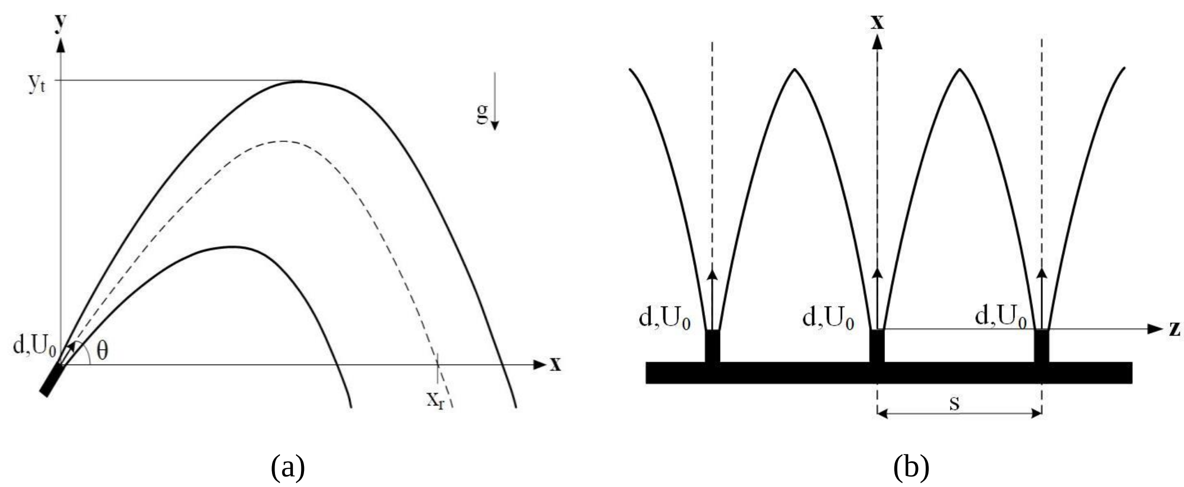

Figure 4-1 Schematic (a) side- and (b) overhead-view of multiple inclined negatively buoyant jets (INBJs).

The initial conditions affecting the flow behavior include the Froude number (F), port angle (θ), and port spacing (s). The former is a non-dimensional parameter which measures the ratio of inertia to buoyancy and is defined as:

$$F = \frac{U_0}{\sqrt{g_0' d}} \tag{4-1}$$

where g'_0 is the initial reduced gravitational acceleration. This term relates the initial density to the ambient density and is expressed as $g'_0 = g(\rho_0 - \rho_a)/\rho_a$, where g is the gravitational acceleration.

The flow geometry can be mainly characterized by defining the return point distance (x_r) and terminal rise height (y_t). The former determines the horizontal distance between the nozzle tip and the return point, where the flow returns to the nozzle tip level; the latter characterizes the vertical distance between the nozzle tip and the maximum height of the flow. In accordance with previous studies (Kikkert et al., 2007) (Oliver et al., 2013b) (Ramakanth et al., 2022), the boundaries of the jets are defined as the lines with a concentration of $e^{-1}C_{Max}$ along a cross-section of the flow, where C_{Max} is the local centerline tracer concentration. Dilution (S) at any location is defined as the ratio of initial tracer concentration (C_0) to the concentration at that location (C); thus, dilution at the return point is expressed as $S_r = C_0/C_r$.

The effect of port spacing in dimensional analysis is expressed by the non-dimensional parameter (s/dF).

$s/dF > \sim 2$

For the case that the ports are widely spaced ($s/dF > \sim 2$), the jets have little interaction and behave as single jets (Abessi & Roberts, 2014). For these jets, the geometric parameters and dilution are independent of s/dF. The geometric parameters can be normalised by F and d, and dilution by F, to create coefficients that are only a function of θ, as shown below (Abessi & Roberts, 2015).

$$\frac{x_r}{\mathrm{dF}} = f_1(\theta) \quad (4\text{-}2)$$

$$\frac{y_t}{\mathrm{dF}} = f_2(\theta) \quad (4\text{-}3)$$

$$\frac{S_r}{\mathrm{F}} = f_3(\theta) \quad (4\text{-}4)$$

In the presence of a lower boundary, the impact point distance (x_i) can also be considered to characterize the flow geometry. It is the horizontal distance between the nozzle tip and the impact point where the flow impacts the lower boundary. The normalized impact point distance, terminal rise height, and impact point dilution ($S_i = C_0/C_i$) for 60° jets are constants and can be expressed as (P. J. W. Roberts et al., 1997)

$$\frac{x_i}{\mathrm{dF}} = 2.4 \quad (4\text{-}5)$$

$$\frac{y_t}{\mathrm{dF}} = 2.2 \quad (4\text{-}6)$$

$$\frac{S_i}{\mathrm{F}} = 1.6 \quad (4\text{-}7)$$

$s/dF < \sim 2$

If the ports are not widely spaced ($s/dF < \sim 2$), both θ and s/dF affect the geometrical and dilution characteristics of flows. According to the experiments conducted by Abessi and Roberts on 60° multiple jets in the presence of a lower boundary, the flow characteristics can be obtained by the empirical equations (Abessi & Roberts, 2014)

$$\frac{x_i}{\mathrm{dF}} = 2(\frac{\mathrm{s}}{\mathrm{dF}})^{1/2} \quad (4\text{-}8)$$

$$\frac{y_t}{\mathrm{dF}} = 1.9(\frac{\mathrm{s}}{\mathrm{dF}})^{1/2} \quad (4\text{-}9)$$

$$\frac{S_i}{\mathrm{F}} = 0.9(\frac{\mathrm{s}}{\mathrm{dF}}) \quad (4\text{-}10)$$

Along with θ and s/dF, the present study hypothesizes that the angle difference, φ, between adjacent jets on a multiport diffuser may also play a significant role in the flow behavior; see Figure 4-2. Considering the angle difference, the flow characteristics can be expressed as:

$$\frac{x_r}{\mathrm{dF}} = f_4\left(\theta, \frac{s}{dF}, \varphi\right) \quad (4\text{-}11)$$

$$\frac{y_t}{\mathrm{dF}} = f_5\left(\theta, \frac{s}{dF}, \varphi\right) \quad (4\text{-}12)$$

$$\frac{S_r}{\mathrm{F}} = f_6\left(\theta, \frac{s}{dF}, \varphi\right) \quad (4\text{-}13)$$

In previous studies on multiport diffusers, the jets were released at the same angle to the horizontal (θ=60°) (B. M. Miller et al., 2006) (Abessi & Roberts, 2014) and therefore (φ=0). This study aims to provide insight into the effect of φ on the mixing behavior by considering φ=0° and φ=20°.

(a) (b)

Figure 4-2 Side-view of multiport diffusers with (a) uniform and (b) non-uniform port orientation; demonstrating main angle (θ) and angle difference (φ).

4.3 Experimental Procedure

A schematic depiction and real photograph of the experimental setup are shown in Figure 4-3(a) and Figure 4-3 (b), respectively. The experiments were performed in a 2.04 m long, 1 m wide, and 1 m high tank located at the Hydraulics laboratory at the University of Cagliari.

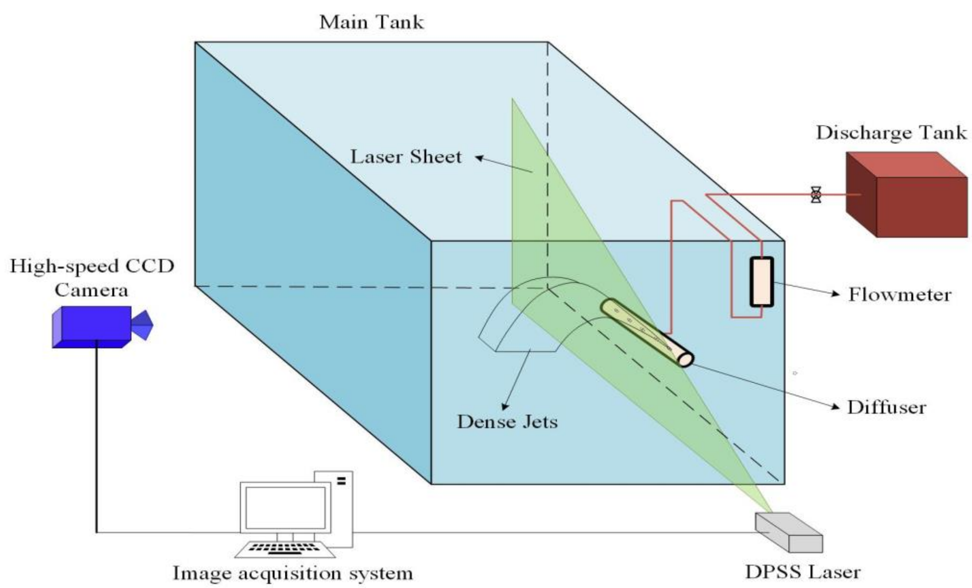

(a)

(b)

Figure 4-3 (a) Schematic depiction and (b) photograph of the laser-induced fluorescence (LIF) experimental setup.

The effluent was discharged through diffusers each incorporating five round nozzles with a diameter (d) of 3.25 mm spaced 8 cm apart. Different s/dF values were considered for the experiments by changing the Froude number such that s/dF<1.32, resulting in significant merging effects in all experiments (Abessi & Roberts, 2014). To investigate the effect of non-uniform port orientation, four diffusers, two with uniform angles (θ=50^o and θ=60^o) and two with non-uniform angles (φ=20^o) were constructed. The diffusers were designated as Type I, II, III, and IV in Table 4-1. Figure 4-4 shows real photographs of the diffuser types III and IV. The port angles were chosen to cover the range over which the highest dilution rates had been reported for single dense discharges (Jirka, 2008) (Papakonstantis et al., 2011) (Oliver et al., 2013a) (Abessi & Roberts, 2015). The Froude and Reynolds numbers of discharges were higher than 19 and 2200, respectively, to ensure fully turbulent flows. The water depth above the nozzles (H) was about 45 cm and deep enough, dF/H<0.24, for all experiments to avoid surface influence; Abessi and Roberts (Abessi & Roberts, 2016) showed that for dF/H<0.44, the deep-water condition exists and there is no surface effect on the jets' behavior. For the real case of the Perth Seawater Desalination

Plant outfall working under its full-flow capacity, dF/H was about 0.31 (Marti et al., 2011). The height of nozzles above the tank floor were about 50 cm, preventing bottom boundary effects.

Table 4-1 Experimental conditions for uniform and non-uniform diffusers.

Diffuser Type	Configuration	Ports Angle	Number of Experiments	Jet Velocity (m/s)	Brine Density (kg/m^3)	Froude Number	s/dF
I	Uniform	60º	7	0.746	1016-1049	19-33.1	0.76-1.32
II	Non-uniform	70º/50º	7	0.746	1016-1049	19-33.1	0.76-1.32
III	Uniform	50º	5	0.746	1020-1044	20-29.6	0.84-1.25
IV	Non-uniform	60º/40º	5	0.746	1020-1044	20-29.6	0.84-1.25

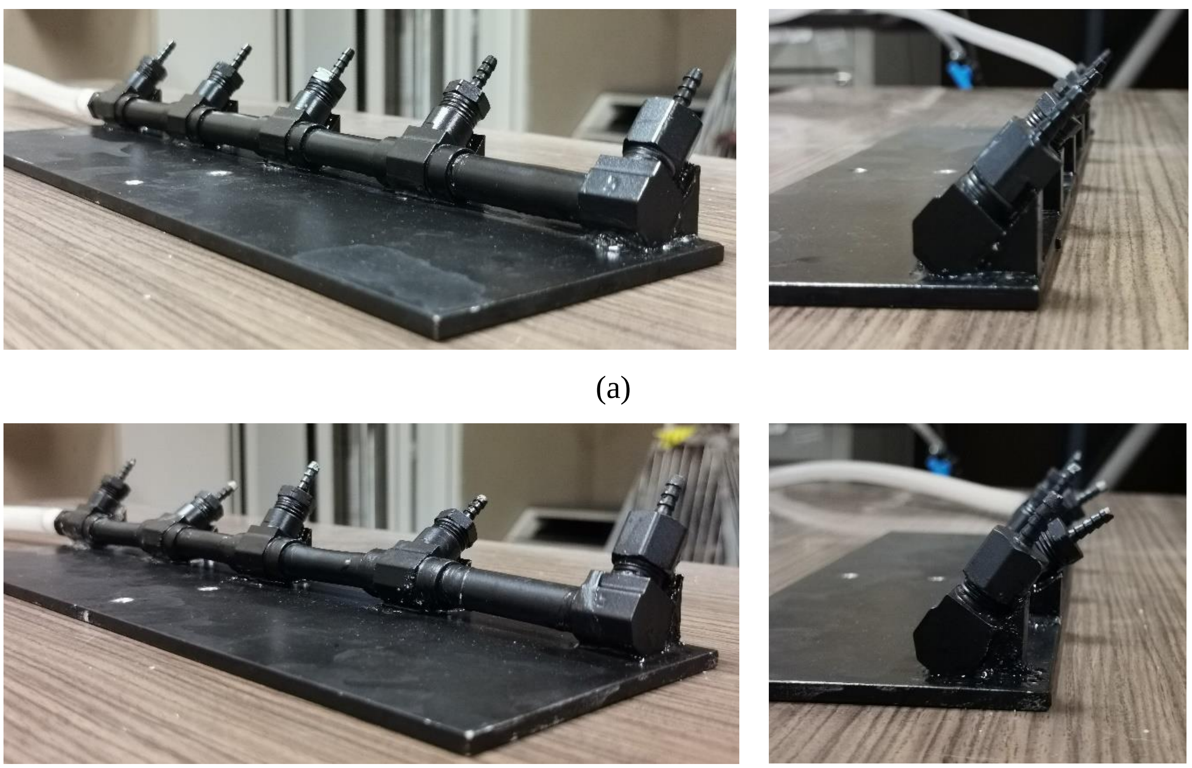

(a)

(b)

Figure 4-4 Photographs of the (a) uniform diffuser type III and (b) non-uniform diffuser type IIII

Concentration fields were obtained using the LIF system. The tank was filled with fresh water, simulating the receiving environment. The discharge tank was filled with effluent consisting of water, a pre-determined amount of salt (NaCl) as a density controller, and a small amount of Titanium dioxide as a tracer. The flow field was visualized using eight vertical laser sheets parallel to the diffuser axes, which were generated by moving one sheet sequentially across the flow, such that there was less space between the sheets closer to the diffusers; they were located at x/d=0, 3, 7, 12, 18, 25, 33, and 41, such that x/d=0 represents the location of nozzles' tip. The sheets created by a 5 W diode-pumped solid-state (DPSS) continuous green laser caused the tracer to fluoresce, and the emitted light was captured by a digital charge-coupled device (CCD) camera, Mikrotron EoSens 4CXP CoaXPress, at 50 frames per second (to ensure that the flow fields on two consecutive frames were uncorrelated) over 1 minute, resulting in about 24,000 images for each test. The concentration fields were obtained from the greyscale images using a calibration process in which each pixel was assigned a digital number between 0 to 255 based on the captured light intensity, where 0 and 255 represent pure black and white, respectively. Then color-coded time-averaged images of concentration fields were generated using a non-commercial MATLAB code, designed for the specific purposes of the present experiment, assuming a linear relationship between the light intensity and concentration (Tian, 2002).

4.4 Results

4.4.1 General Flow Behaviour

Figure 4-5 demonstrates time-averaged concentration profiles at different cross-sections close to and far from the diffusers. Images are shown for uniform diffuser Type I and non-uniform diffuser Type II with the same Froude number of 29.6. The evolution of the discharges and jet merging with distance from the diffusers are evident in these images. Close to the diffusers, e.g., Figure 4-5 (a and e), the jets for both configurations are separate with high concentrations at their centers. At x/dF=0.41 (b and f), the maximum concentrations are significantly reduced, and the discharges are more diffused, resulting from entrainment of clear ambient water into the jets. In both cases, the jets are not still wide enough to have significant interaction with their adjacent discharges. However, there is more space between the jets on the non-uniform diffuser than the uniform one. At farther distances, e.g., Figure 4-5 (c and g), the jets on the uniform diffuser merge such that there is almost no trace of low-concentrated water between the jets. However, the jets on the non-uniform diffuser are not completely merged and are distinctly identifiable. At x/dF=1.15 (d and h), the jets on both diffusers are fully merged, and there is no evidence of the individual jets. As evident from this section, the non-uniform diffuser results in lower concentrations of brine relative to the uniform one.

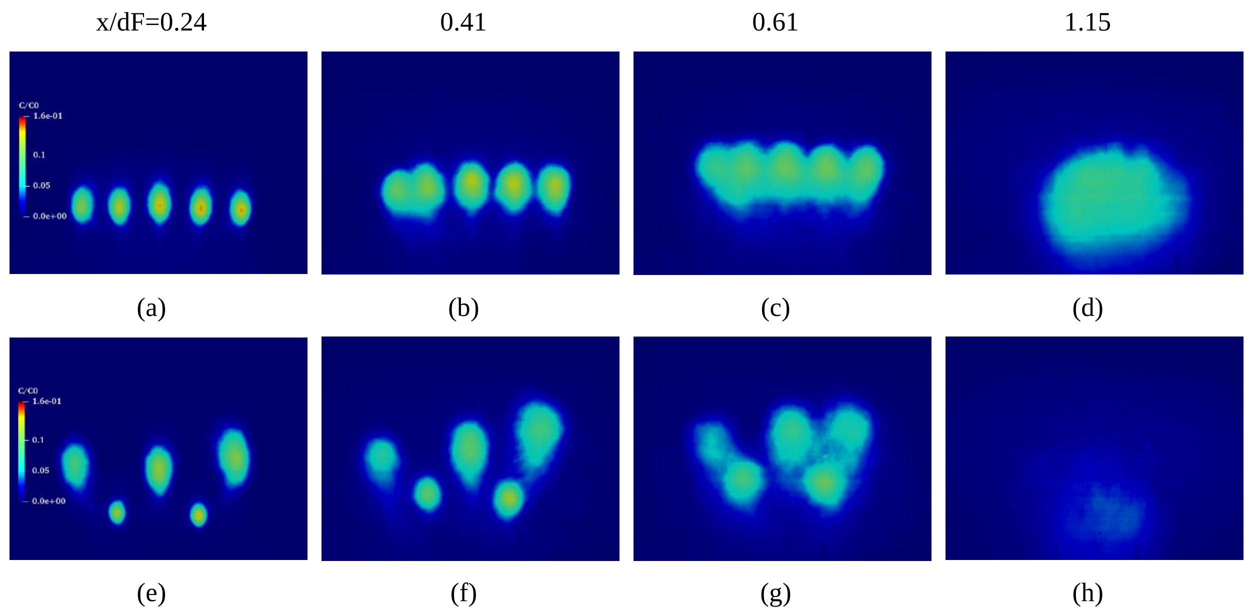

Figure 4-5 Lateral concentration profiles for the uniform diffuser Type I (a-d) and non-uniform diffuser Type II (e-h) at different cross-sections, F=29.6.

Figure 4-6 shows a snapshot of the concentration profiles at x/dF=0.61, where the jets on both diffusers interact with their neighboring jets. The image shows both the physical mechanisms impairing and contributing to the dilution of the jets. The concentration fields for both diffusers are very patchy, and the fluid motion is chaotic; locally steep concentration gradients and obvious gaps in the flow fields are evident in the images. The lower edges of the jets, under the jet centerline, are more expanded compared to their upper sides, due to buoyancy induced instabilities. At the inner side, the eddies entrain clean water into the jets and continuously dilute the jets. The mixed fluid close to the inner edge is subsequently detrained from the primary flow due to the unstable density gradient. It is evident that this detrainment or separation is more pronounced for 70^o inclined jets on the non-uniform diffuser than it is for 60^o inclined jets in the uniform case.

The jets get diluted and expand not only due to the vertical entrainment from the upper and lower sides but also by lateral entrainment. Eddies transporting clear ambient water deeply penetrate the 70^o inclined jets on the non-uniform diffuser and some even reach the jet centerlines; see the white arrows in Figure 4-6(b). This deep penetration of clear water into the jets makes a significant contribution to mixing and, consequently, to dilution. These kinds of eddies can also be seen on the 50^o inclined jets, but they entrain low concentrated brine and do not deeply penetrate them; see the yellow arrows in Figure 4-6(b). On the other hand, entrainment for the jets on the uniform diffuser is laterally restricted. The eddies trying to entrain water into one jet are affected by the motion of neighboring jets. There is a lateral re-entrainment, and eddies transport concentrated brines from one jet to its neighboring jets and the other way around, as seen in the zones shown in Figure 4-6(a).

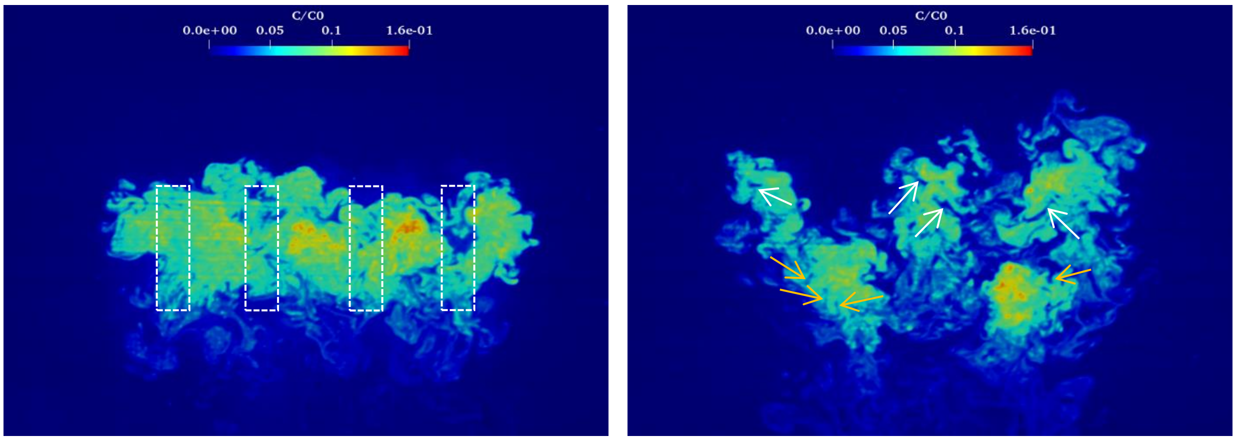

(a) (b)

Figure 4-6 Snapshot of concentration fields for the (a) uniform diffuser Type I and (b) non-uniform diffuser Type II, F=29.6, x/dF=0.61.

4.4.2 Major Flow Parameters

The major flow parameters of design interest, including the return point distance (x_r), terminal rise height (y_t), and return point dilution (S_r), were extracted from the concentration fields. To achieve this, we identified the flow parameters of each jet and then presented the mean parameter value over all jets. For uniform diffusers, the mean value of each parameter closely matched the flow parameter value of each jet. However, for non-uniform diffusers, the varying angle of jets led to distinct trajectories and flow parameters.

We explored the maximum concentration of each jet on every vertical plane. In cases where the maximum concentration of jets was not independently distinguishable on the last vertical sheets, we sought that on the line intersection of that y-z (vertical) plane and a plane passing through the nozzle. Utilizing cure fitting techniques with peak concentration points, we obtained the trajectory of each one. The return point was defined as the location where the jet trajectory returned to the average level of nozzles. x_r characterizes the horizontal distance between the nozzle tip and the mentioned return point. The definitions of y_t and S_r can be found in Section 4.2. To determine S_r, we focused on the dilution levels at points corresponding to the peak concentrations for each jet and plotted them against the trajectory. By fitting a curve to the data, we analyzed the variation of dilution along the trajectory, enabling us to identify the dilution at the return point. A summary of the experiments and values for the normalized flow parameters is presented in Table 4-2.

Table 4-2 Summary of experiments and flow parameters.

Experiment ID	Froude number	s/dF	Configuration	x_r/dF	y_t/dF	S_r/F
Exp1	19	1.32	I	1.7	2.04	---[1]
Exp2	20	1.25	I	1.45	1.99	1.05
Exp3	22.1	1.13	I	1.72	1.95	1.09
Exp4	23.5	1.06	I	1.51	2.05	0.78
Exp5	26	0.96	I	1.77	2.00	1.12
Exp6	29.6	0.84	I	1.62	2.09	0.92
Exp7	33.1	0.76	I	1.55	1.93	1.01
Exp8	19	1.32	II	1.38	2.08	---[1]
Exp9	20	1.25	II	1.40	2.05	1.35
Exp10	22.1	1.13	II	1.31	1.98	1.36
Exp11	23.5	1.06	II	1.45	2.09	1.04
Exp12	26	0.96	II	1.43	2.06	1.13
Exp13	29.6	0.84	II	1.42	2.09	1.27
Exp14	33.1	0.76	II	1.32	2.06	1.30
Exp15	20	1.25	III	1.72	1.71	0.97
Exp16	21.6	1.16	III	1.72	1.73	0.94
Exp17	23.5	1.06	III	1.63	1.75	0.78
Exp18	26	0.96	III	1.71	1.72	0.63
Exp19	29.6	0.84	III	1.72	---[1]	---[1]
Exp20	20	1.25	IV	1.52	1.82	1.31
Exp21	21.6	1.16	IV	1.71	1.81	0.95
Exp22	23.5	1.06	IV	1.51	1.78	1.02
Exp23	26	0.96	IV	1.60	1.77	0.78
Exp24	29.6	0.84	IV	1.64	---[1]	---[1]

[1] Not identified.

The normalized parameters of the return point distance (x_r/dF), terminal rise height (y_t/dF), and return point dilution (S_r/F) are presented versus the normalized port spacing (s/dF) in Figure 4-7,

Figure 4-8, and Figure 4-9, respectively. Previously reported values for uniform diffusers with 60^o inclined jets (B. M. Miller et al., 2006) (Abessi & Roberts, 2014), non-uniform diffusers with 60^o and 45^o inclined jets (Saeidi Hosseini et al., 2022), and single 60^o inclined jets (P. J. W. Roberts et al., 1997) are also shown. It is worth mentioning that, unlike the present study, all mentioned studies were conducted in the presence of a bottom boundary. Therefore, in Figure 4-7 and Figure 4-9, the values for prior research exhibit the normalized impact point distance (x_i/dF) and dilution (S_i/F) while the results of this study present the normalized return point distance (x_r/dF) and dilution (S_r/F).

To show the effect of non-uniform port orientation on the physical and mixing properties of multiport diffusers, the average of flow parameter values over all experiments for each diffuser type was obtained and then the mean values for diffuser Type I (θ=60^o and φ=0) were compared to those for II (θ=60^o and φ=20^o), and Type III (θ=50^o and φ=0) to IV (θ=50^o and φ=20^o). The non-uniform diffusers Type II (circle symbol) and IV (square symbol) resulted in on average 14.2% and 6% shorter return point distances than the uniform Types I (triangle symbol) and III (diamond symbol) respectively, see Figure 4-7. At some distances from the non-uniform diffusers, the rising part of shallower-angle jets interacted with the falling part of steeper-angle jets, impairing the flow movement in the x-direction. Figure 4-8 shows that the terminal rise height for the non-uniform diffusers Type II and IV were on average 2.6% and 4.1% higher than those for Types I and III, respectively.

The most important parameter in this study that demonstrates the overall performance of uniform and non-uniform diffusers is the return point dilution. The superiority of non-uniform diffusers in terms of dilution is evident in Figure 4-9, as the circle symbols are generally located above the triangle symbols and the square ones above the diamonds. The non-uniform diffusers II and IV lead to, on average, 25% and 22.1% higher dilution rates compared to Types I and III, respectively. This significant difference between dilution rates has its roots in different merging processes of jets for uniform and non-uniform diffusers.

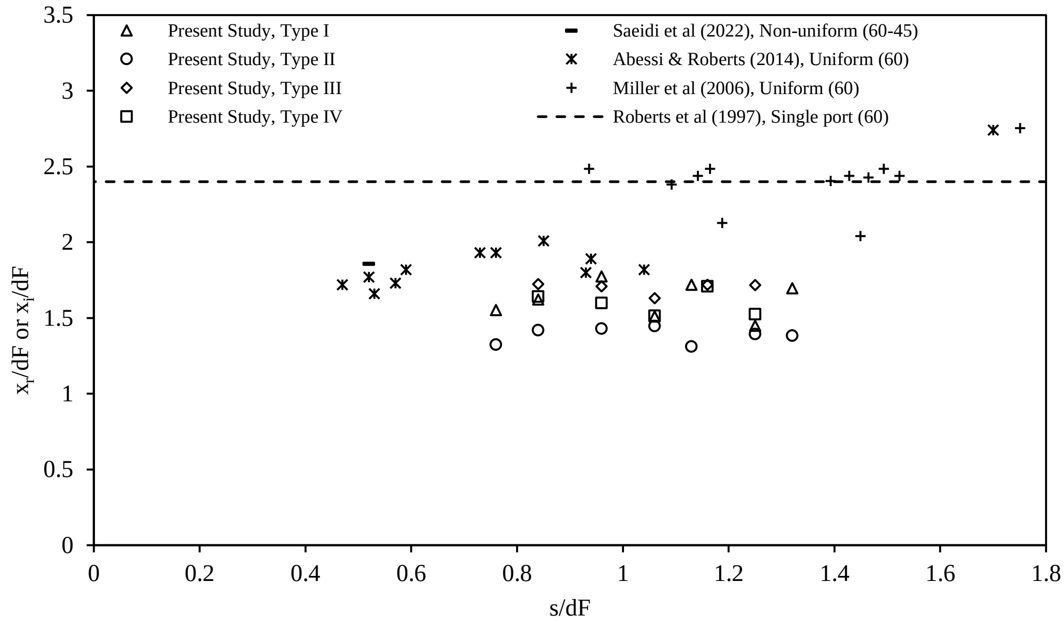

Figure 4-7 Return or impact point distance versus port spacing for various diffuser configurations.

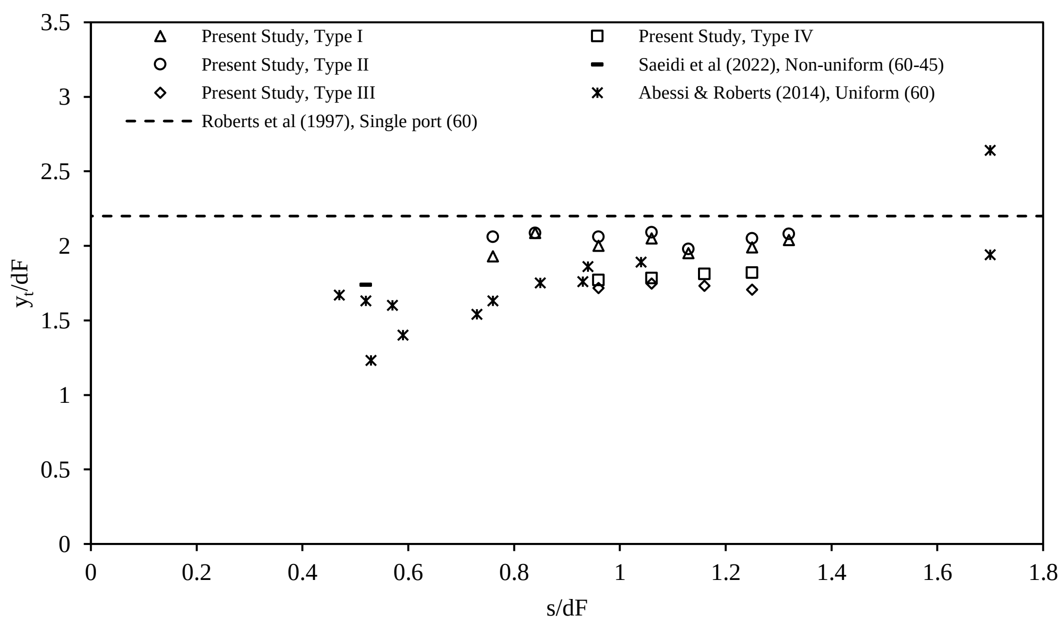

Figure 4-8 Terminal rise height versus port spacing for various diffuser configurations.

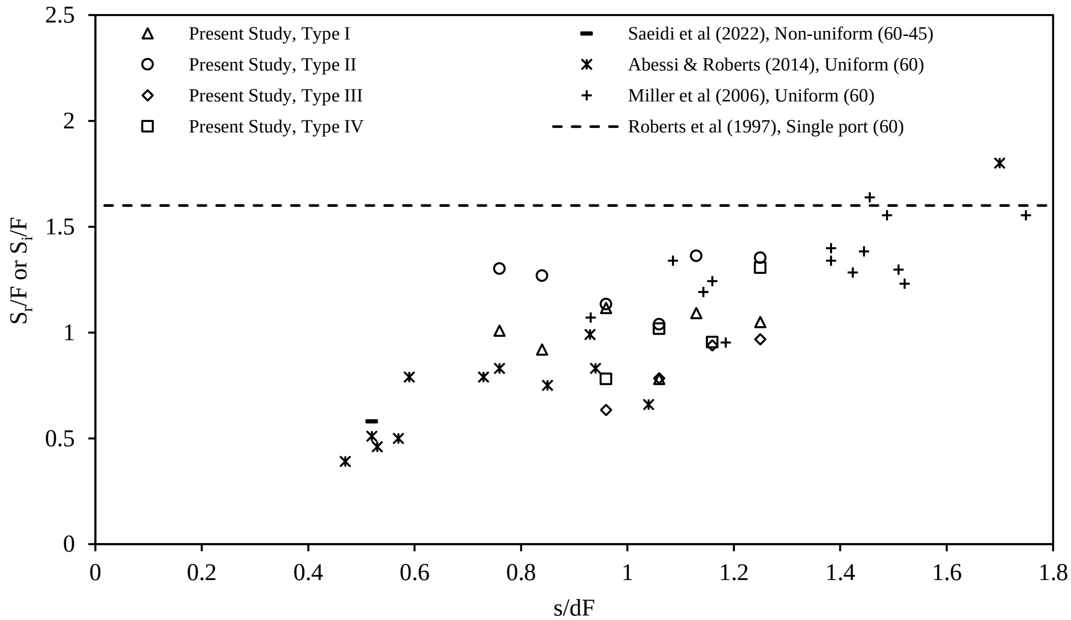

Figure 4-9 Return or impact point dilution versus port spacing for various diffuser configurations.

Although previous studies have been conducted in the presence of a bottom boundary, the results of the present study can still be compared. Prior research has mainly focused on 60^o jets, and the outcomes for the 60^o jets of this study are the most applicable for comparison. The return point distances of 60^o jets are somewhat lower than the impact point distances presented by Miller et al. (B. M. Miller et al., 2006) and Abessi and Roberts (Abessi & Roberts, 2014). The main source of this difference comes from the comparison of return with impact point distance, as impact point distance is higher than return point distance for 60^o jets. Moreover, the return point distance is extended due to the boundary's presence, resulting from a complex transition from a predominantly vertical flow orientation to a horizontal gravity current (Ramakanth et al., 2022). As shown in Figure 4-8 and Figure 4-9, measurements for the terminal rise height and return point dilution of 60^o jets are consistent with the previous studies. The better performance of non-uniform relative to uniform diffusers, concluded in this study, aligns with a recent computational study (Saeidi Hosseini et al., 2022) that showed a 14% increase in impact point dilution when applying a non-uniform diffuser with closely spaced 60^o and 45^o ports, as opposed to uniform diffusers with 60^o jets. The comparison of measurements for multiple jets in this study and single ones in prior research (P. J. W. Roberts et al., 1997) confirms the shorter trajectory and lower dilution rates for multiple INBJs compared to single jets, resulting from the Coanda interaction and jet merging effects.

4.4.3 Merging Process

To investigate the interaction of neighboring jets, normalized concentration profiles (C/C_0) over lines between the central jets and their neighbors were studied. Figure 4-10 shows the lines and concentration profiles for different cross-sections close to and far from the diffusers, x/dF=0.13, 0.3, 0.51, 0.77, and 1.06. The peak concentration for the central jet was always centered on the chart origin, r/d=0. Along the trajectory, the jets on both diffusers become more dilute due to the entrainment of surrounding water, due to shear induced entrainment at the jets' edges. The maximum concentrations gradually decrease, the jets become more diffused, and the gap between the jets is gradually filled with brine at farther distances.

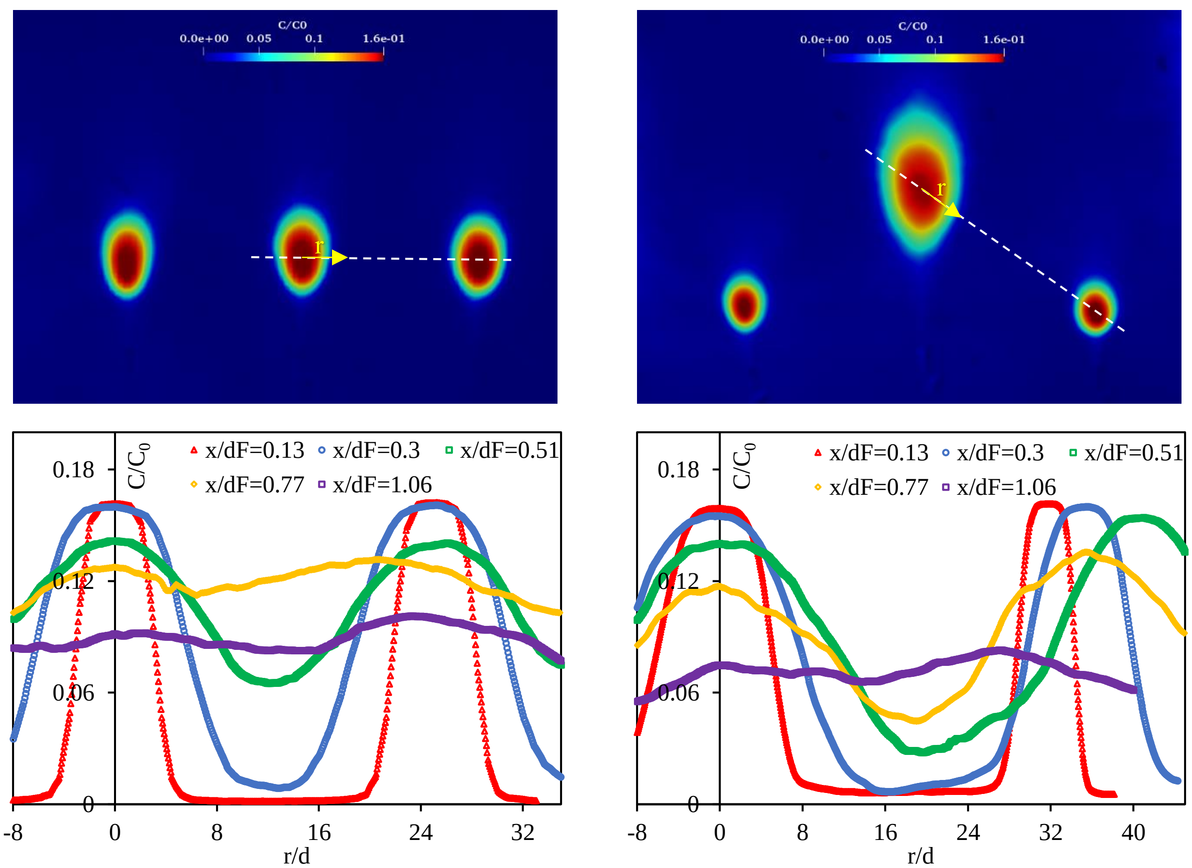

(a) (b)

Figure 4-10 Cross-sectional concentration profiles along the lines between the central jets and their neighbouring jets for the (a) uniform diffuser Type I and (b) non-uniform diffuser Type II, F=23.5.

The merging processes were analyzed by comparing concentration profiles for non-uniform and uniform diffusers at each cross-section. Close to the diffusers, e.g., x/dF=0.13, the central jets for both diffusers exhibited almost no interaction with their neighbors, and therefore there was almost no re-entrainment due to the neighboring jets. At x/dF=0.3, the jets were more diffused, but there was still a small region with almost no jet fluid between the jets for both cases. At x/dF=0.51, the central jets on both diffusers interacted with their adjacent discharges. However, the concentration in the region of interaction was much lower for the non-uniform case compared to the uniform one. In other words, there was less exchange of tracer in that region for the non-uniform diffuser. A jet on the uniform case re-entrained more concentrated brine into itself, which significantly hindered mixing. At x/dF=0.77, the uniform jets were almost fully merged, but the non-uniform jets were not yet fully merged. Entrainment for the uniform case was mainly from above and below the cloud since the gap was almost filled with tracer. However, there was still re-entrainment of low concentrated brine into the jets from the jets' gap for the non-uniform case. The lower levels of tracer exchange for the non-uniform case at different sections resulted in lower concentrations, or higher dilutions, where the jets for both cases are completely merged, e.g., x/dF=1.06.

Investigation of the concentration fluctuations reveals the different nature of mixing in the interaction zone of uniform and non-uniform diffusers. The non-dimensional variance of concentrations (σ^2/C_{Max}^2) at each section is shown in Figure 4-11, where σ is the concentration standard deviation. Close to diffusers, e.g., x/dF= 0.13 and x/dF=0.3, the variance profiles depict a low peak at the center of the jets and two high peaks beside it. These high peaks show that the jets entrain ambient water and feed themselves from the gap, while the low peaks, with almost zero variance, indicate that the centers of the jets are not yet involved in the mixing process. The presence of two well defined, separate peak profiles between two adjacent jets shows that the jets do not re-entrain their neighbouring jets. At some distances from diffusers, e.g., x/dF= 0.51, the difference between the mixing in interaction zones is evident, where there is one peak, point 3, between neighbouring jets for the uniform diffuser and two, points 1 and 2, for the non-uniform case. The presence of one variance peak between the jets means separate jets are still identifiable, but they significantly re-entrain adjacent jets into themselves instead of ambient water. At farther locations, the variance profiles are smoother. The concentration variance exhibits low variation at x/dF=0.77 and x/dF=1.06 for the uniform case, indicating that the jets behave as plane or 2D jets. Notably, as depicted in Figure 4-11(a), the trend of concentration variance against distance from the diffuser remains consistently ascending for both individual jets before complete merging (at x/dF=0.13, 0.3, and 0.51) and the formed line plume after merging (at x/dF=0.77 and 1.06). The only instance of a drop in the variance value is observed when comparing x/dF=0.51 and x/dF=0.77, which corresponds to the point when the jets coalesce into a line plume.

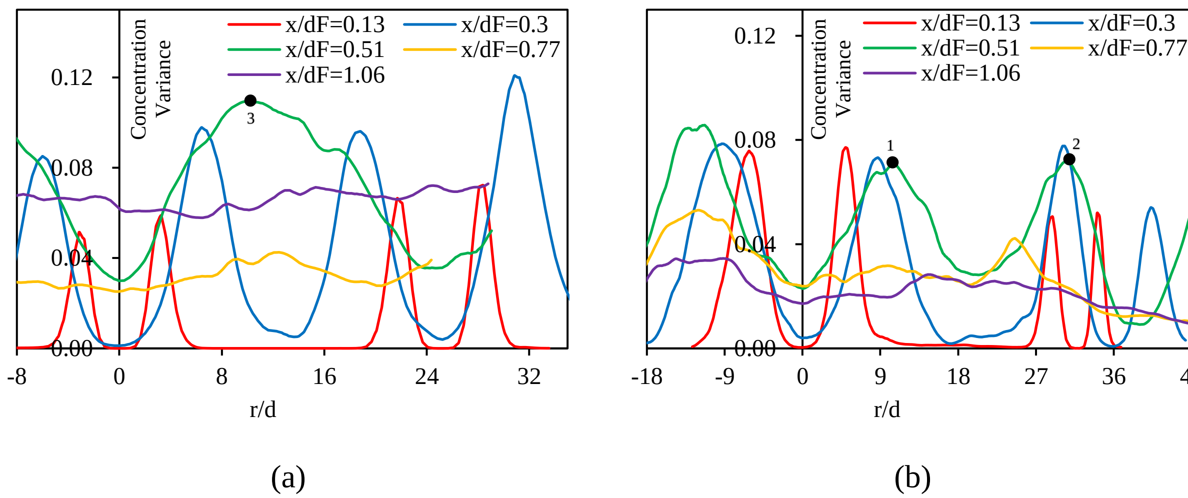

Figure 4-11 Variance of concentration (σ^2/C_{Max}^2) profiles over the lines presented in Figure 9 for the (a) uniform diffuser Type I and (b) non-uniform diffuser Type II, F=23.5.

The interaction of neighboring jets is significantly affected by the gap between the jets. Previous studies showed that jet merging impaired dilution in multiport diffusers and recommended providing more space between the ports to increase dilution (Abessi & Roberts, 2014). The present study finds that a reduction in this negative impact on dilution may not be solely achieved by increasing port spacing (s). For a uniform diffuser, the distance between the jets' centerline (d_j) at different distances from the diffuser is almost the same as port spacing. However, d_j changes at different distances from a non-uniform diffuser. Uniform and non-uniform diffusers may have the same port spacing, but different d_j at different locations, resulting in different merging processes. Figure 4-12 indicates how the normalized jet spacing (d_j/d) changes at different distances from diffusers Type I and II. The jet spacing for diffuser Type I gradually decreases as a result of the

Coanda effect while that for Type II increases up to a point and then decreases. The reduction in jet spacing originates at the onset of the descending part of the 70^{o} inclined jet. Generally, there is more space between the jets' centerline for diffuser Type II compared to Type I, as the dashed line is located above the solid line. Non-uniform port orientation can be an alternative for port spacing since it provides more space for the jets to expand before interacting with their adjacent jets, the same as the role of port spacing but with a potential lower building cost. It is expected that jet spacing, or non-uniformity, positively affect the mixing process in the angle range over which the highest dilution rates have been reported for single jets but not for very steep or gentle angles. Although non-uniformity provides more gap between discharges, the presence of gentle-angled ports on a diffuser may adversely affect the overall performance since they result in very short trajectories. The steep-angled jets also fall back on themselves, which may reduce the overall dilution.

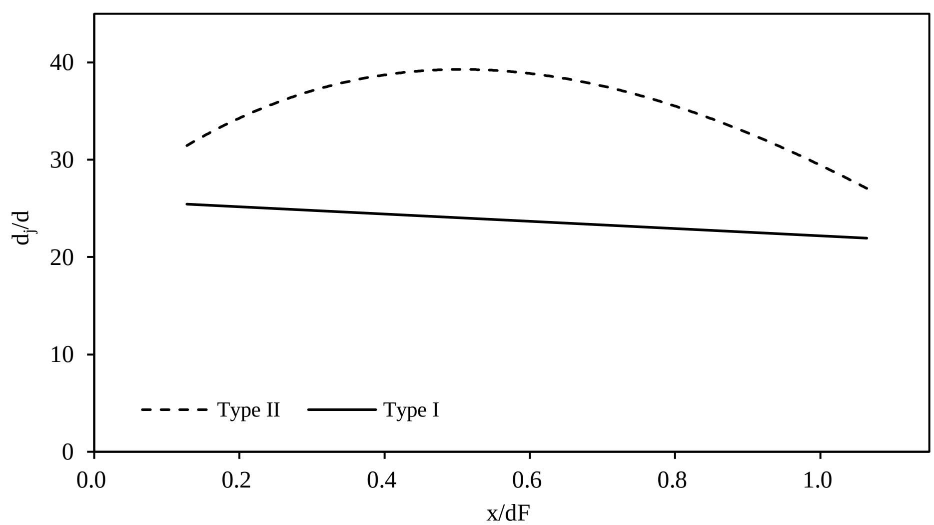

Figure 4-12 The distance between the jets' centerline versus distance to diffusers for the (a) uniform diffuser Type I and (b) non-uniform diffuser Type II, F=23.5.

4.5 Conclusions

An issue with multiport diffusers for brine disposal is jet interaction, which can significantly impair the mixing process. This study proposed multiport diffusers with non-uniform port orientations as a means for increasing dilution. A series of experiments adopting the LIF method were conducted for four types of diffusers consisting of two with uniform and two with non-uniform port orientations. The port angles were varied in the range over which the highest dilution rates had been reported for single discharges (40^o to 70^o). Flow behavior resulting from non-uniform diffusers was quantified using geometric and dilution measurements obtained from LIF and were compared to that of uniform diffusers.

The results revealed better performances of multiport diffusers with non-uniform port orientation over those with uniform port orientation. The non-uniform diffusers resulted in, on average, 6% to 14% shorter return point distance, 3% to 4% higher terminal rise height, and 22% to 25% higher return point dilution relative to the uniform diffusers. This improvement was attributed to different mixing behavior in the interaction zones. The investigations demonstrated that jet merging occurred closer to diffusers for uniform cases compared to non-uniform cases. At some distance from the diffusers, where the jets on non-uniform diffusers had little interaction with their adjacent jets and entrained almost clear water into themselves, there was high exchange of tracer between the jets on uniform diffusers, mixing was restricted in the lateral direction, and significant re-entrainment was evident. At the locations where separately identifiable jets on the non-uniform diffusers interacted, there was no trace of separate jets for the uniform cases, demonstrating limited lateral entrainment for the uniform cases and 2D-like (two-dimensional) behavior. Different mixing behavior in the interaction zones and consequently better performance of non-uniform diffusers was due to more space between the jets' centerline at different distances from diffusers for the non-uniform diffusers, compared to the uniform diffusers. Non-uniform port orientation provided more space between the jets to expand before interacting with their neighboring jets, resulting in higher dilution rates. Hence, the application of non-uniform diffusers can result in shorter port spacing and therefore diffuser length while resulting in the same dilution as an equivalent uniform diffuser.

This study questioned the application of formulae obtained from single jet experiments for multiport diffuser designs and showed that the source characteristics specific to multiport diffusers such as angle difference should be considered for efficient design of desalination outfalls. The new data and analysis provided in this study can benefit the design of desalination outfall systems with considerable potential cost savings, especially for tunneled outfalls. Moreover, the measured higher dilution can help in preventing environmental damages. The present study assumed two port angles, 50^o and 60^o and an angle difference of 20^o between adjacent jets on a multiport diffuser. The assumption of more port angles and angle differences may shed light on the combined effect of port angles and angle differences on mixing efficiency. However, it is not expected that significantly higher or lower port orientations than the investigated angle range would result in greater dilution rates. The combined effect of non-uniform port orientation and flowing current on the mixing behavior of desalination discharges may be also of interest. It is suggested to perform optimization studies considering the angle difference as a decision variable, alongside other decision variables previously defined in the literature, such as the number of ports, port and outfall diameters, and outfall and diffuser lengths.

Acknowledgement

This research was funded by Natural Sciences and Engineering Research Council of Canada (NSERC).

References

Abessi, O., & Roberts, P. J. W. (2014). Multiport Diffusers for Dense Discharges. Journal of Hydraulic Engineering, 140(8), 04014032. https://doi.org/10.1061/(ASCE)HY.1943-7900.0000882

Abessi, O., & Roberts, P. J. W. (2015). Effect of nozzle orientation on dense jets in stagnant environments. Journal of Hydraulic Engineering, 141(8), 06015009. https://doi.org/10.1061/(ASCE)HY.1943-7900.0001032

Abessi, O., & Roberts, P. J. W. (2016). Dense Jet Discharges in Shallow Water. Journal of Hydraulic Engineering, 142(1). https://doi.org/10.1061/(ASCE)HY.1943-7900.0001057

Abessi, O., Roberts, P. J. W., & Gandhi, V. (2017). Rosette Diffusers for Dense Effluents. Journal of Hydraulic Engineering, 143(4). https://doi.org/10.1061/(ASCE)HY.1943-7900.0001268

Baum, M. (2019). Dense jet behaviour in dynamic receiving environments, Ph.D. thesis, University of Queensland Brisbane.

Bleninger, T. (2006). Coupled 3D hydrodynamic models for submarine outfalls: Environmental hydraulic design and control of multiport diffusers, Doctoral Dissertation, Karlsruhe, Zugl.

Caldera, U., & Breyer, C. (2017). Learning curve for seawater reverse osmosis desalination plants: capital cost trend of the past, present, and future. Water Resources Research, 53(12), 10523–10538. https://doi.org/10.1002/2017WR021402

Chang, N. Bin, Yeh, S. C., & Chang, C. H. (2011). Optimal expansion of a coastal wastewater treatment and ocean outfall system under uncertainty (II): Optimisation analysis. Civil Engineering and Environmental Systems, 28(1), 39–59. https://doi.org/10.1080/10286600903243138

Ferrari, S., & Querzoli, G. (2010). Mixing and re-entrainment in a negatively buoyant jet. Journal of Hydraulic Research, 48(5), 632–640. https://doi.org/10.1080/00221686.2010.512778

Fischer, H.B., List, E.J., Koh, R.C.Y., Imberger, J., Brooks, N.H. (1979) Mixing in Inland and Coastal Waters; Academic Press: Amsterdam, The Netherlands.

Jiang, B., & Law, A. W.-K. (2013). Non-interfering multiport brine diffusers in shallow coastal waters. Journal of Applied Water Engineering and Research, 1(2), 148–157.

Jirka, G. H. (2008). Improved discharge configurations for brine effluents from desalination plants. Journal of Hydraulic Engineering, 134(1), 116–120. https://doi.org/10.1061/(ASCE)0733-9429(2008)134:1(116)

Kikkert, G. A., Davidson, M. J., & Nokes, R. I. (2007). Inclined Negatively Buoyant Discharges. Journal of Hydraulic Engineering, 133(5), 545–554. https://doi.org/10.1061/(ASCE)0733-9429(2007)133:5(545)

Kucera, J. (2019). Desalination: water from water, 2nd edition, John Wiley & Sons.

Lattemann, S., Kennedy, M. D., Schippers, J. C., & Amy, G. (2010). Global desalination situation. Sustainability Science and Engineering, 2, 7–39.

Loya-Fernández, Á., Ferrero-Vicente, L. M., Marco-Méndez, C., Martínez-García, E., Zubcoff Vallejo, J. J., & Sánchez-Lizaso, J. L. (2018). Quantifying the efficiency of a mono-port diffuser in the dispersion of brine discharges. Desalination, 431(October 2017), 27–34. https://doi.org/10.1016/j.desal.2017.11.014

Lyu, S. W. (2003). Behavior of merging buoyant jets discharged from uni-directional diffuser, Ph.D. Thesis, Seoul National Univ, Seoul.

Maalouf, S., Rosso, D., & Yeh, W. W. G. (2014). Optimal planning and design of seawater RO brine outfalls under environmental uncertainty. Desalination, 333(1), 134–145. https://doi.org/10.1016/j.desal.2013.11.015

Marti, C. L., Antenucci, J. P., David Luketina, ;, Okely, P., Imberger, J., & Asce, M. (2011). Near-Field Dilution Characteristics of a Negatively Buoyant Hypersaline Jet Generated by a Desalination Plant. Journal of Hydraulic Engineering, 137(1), 57–65. https://doi.org/10.1061/(ASCE)HY.1943-7900.0000275

Miller, B. (2011). Design of large desalination discharges with multiple jets, in: International Symposium on Outfall Systems, Mar del Plata.

Miller, B. M., Glamore, W. C., Timms, W. A., & Pells, S. E. (2006). Physical modeling of desalination brine outlet, Perth (stage2), WRL Techn, Rep 4.

Miller, B. M., & Tarrade, L. (2010). Design considerations of outlet discharges for large seawater desalination projects in Australia, in: 6th Int. Conf. on Marine Wastewater Discharges, Sharjah.

Missimer, T. M., Jones, B., & Maliva, R. G. (2015). Intakes and Outfalls for Seawater Reverse-Osmosis Desalination Facilities: Innovations and Environmental Impacts. Springer, New York, NY, USA.

Missimer, T. M., & Maliva, R. G. (2018). Environmental issues in seawater reverse osmosis desalination: Intakes and outfalls. Desalination, 434, 198–215.

Oliver, C. J., Davidson, M. J., & Nokes, R. I. (2013a). Behavior of dense discharges beyond the return point. Journal of Hydraulic Engineering, 139(12), 1304–1308. https://doi.org/10.1061/(ASCE)HY.1943-7900.0000781

Oliver, C. J., Davidson, M. J., & Nokes, R. I. (2013b). Removing the boundary influence on negatively buoyant jets. Environmental Fluid Mechanics, 13(6), 625–648. https://doi.org/10.1007/S10652-013-9278-3

Palomar, P., & Losada, I. J. (2010). Desalination in Spain: Recent developments and recommendations. Desalination, 255(1–3), 97–106.

Papakonstantis, I. G., Christodoulou, G. C., & Papanicolaou, P. N. (2011). Inclined negatively buoyant jets 2: Concentration measurements. Journal of Hydraulic Research, 49(1), 13–22. https://doi.org/10.1080/00221686.2010.542617

Ramakanth, A., Davidson, M. J., & Nokes, R. I. (2022). Laboratory study to quantify lower boundary influences on desalination discharges. Desalination, 529, 115641.

Ridoutt, B. G., & Pfister, S. (2010). A revised approach to water footprinting to make transparent the impacts of consumption and production on global freshwater scarcity. Global Environmental Change, 20(1), 113–120.

Roberts, P. J., Salas, H. J., Reiff, F. M., Libhaber, M., Labbe, A., & Thomson, J. C. (2010). Marine wastewater outfalls and treatment systems. IWA publishing.

Roberts, P. J. W., Ferrier, A., & Daviero, G. (1997). Mixing in inclined dense jets. Journal of Hydraulic Engineering, 123(8), 693–699. https://doi.org/10.1061/(ASCE)0733-9429(1997)123:8(693)

Saeidi Hosseini, S. A. R., Mohammadian, A., Roberts, P. J. W., & Abessi, O. (2022). Numerical Study on the Effect of Port Orientation on Multiple Inclined Dense Jets. Journal of Marine Science and Engineering, 10(5), 590. https://doi.org/10.3390/jmse10050590

Seawater Desalination Costs: White Paper. (2012).

Taherian, M., & Mohammadian, A. (2021). Buoyant Jets in Cross-Flows: Review, Developments, and Applications. Journal of Marine Science and Engineering, 9(1), 61. https://doi.org/10.3390/jmse9010061

Taherian, M., Saeidi Hosseini, S. A. R., & Mohammadian, A. (2022). Overview of outfall discharge modeling with a focus on turbulence modeling approaches. In Advances in Fluid Mechanics: Modeling and Simulation. Springer.

Tarrade, L., & Miller, B. M. (2010). Physical modeling of the Victorian desalination plant outfall, Sydney.

Tarrade, L., Rayner, D. S., & Miller, B. M. (2009). Physical modeling of brine diffuser, Sydney.

Tian, X. (2002). 3DLIF and its applications to studies of the near field mixing in wastewater discharges, Ph.D. Thesis, Georgia Institute of Technology.

Yan, X., & Mohammadian, A. (2019). Numerical modeling of multiple inclined dense jets discharged from moderately spaced ports. Water (Switzerland), 11(10), 14–16. https://doi.org/10.3390/w11102077

5 Summary, Concluding Remarks, and Recommendations

5.1 Summary and Concluding Remarks

The objective of this study was to improve the understanding of the mixing behavior of multiport diffusers and to propose design modifications for their optimization. Through a comprehensive review of the literature, this study identified the challenges associated with multiport diffusers that hinder the mixing process and limit dilution. The investigation revealed two main issues arising from the interaction of jets in a multiport diffuser. First, the accuracy of flow field hydrodynamic predictions using commercial mixing tools might be compromised because of their limitations in resolving certain aspects related to jet merging. Second, jet merging was identified as an undesirable phenomenon that could potentially increase environmental risks by impairing the mixing process. This study addressed these issues by conducting a comprehensive literature review, numerical analysis, and experimental investigation, all of which are explained below.

In chapter 2 of this thesis:

- A thorough explanation of the fundamental concepts related to outfall discharge modeling and a critical review of the current state of the art in this domain were provided.
- In-depth explanations and comparisons of RANS and LES models were provided. Also, prominent numerical studies on the simulation of single and multiple jets and their remarks were presented.
- A literature review revealed that CFD modeling has mainly been employed for simulating jet mixing behavior over the past two decades. Moreover, its usage is expected to expand significantly in engineering designs as computational resources continue to increase.
- Both RANS and LES provided reasonably good predictions of the jet mixing behavior and were recognized as promising tools for the simulation of outfall discharges.
- Among the different RANS turbulence models applied in previous studies, the realizable and RNG $k-\varepsilon$ models consistently exhibited superior performances in the simulation of single and multiple jets, respectively.
- In the literature, the main use of RANS models centered on EVMs, especially in the context of multiple jets, and the prediction capabilities of RSMs and LES for multiport diffusers have rarely been reported.

- Turbulence models have been predominantly validated for single discharges, and less attention has been paid to multiple jets.
- The literature shows a scarcity of applications of mesh-free CFD methods, such as smoothed particle hydrodynamics (SPH), in the context of outfall discharge modeling.

In chapter 3 of this thesis:

- The prediction capabilities of RSMs for multiple INBJs were evaluated for the first time. Specifically, 60º multiple dense jets were three-dimensionally simulated using the LRR turbulence model, and the predictions were compared to existing experimental data in the literature (Abessi & Roberts, 2014) for validation.
- The LRR turbulence model was further utilized for additional research on the effect of non-uniform port orientation on the merging process of multiple INBJs. In particular, this study examined diffusers with uniform (60°–60°–60°) and non-uniform (45°–60°–45°) port orientations, mainly assessing the impact of adjacent ports on the central ports.
- It was found that the LRR turbulence model could accurately predict the geometrical characteristics and impact dilution of multiple jets with mean absolute percentage errors of less than 5% and 7%, respectively, introducing the LRR model as a reliable tool for studying multiple INBJs. Furthermore, a comparison with previous studies revealed that the LRR model showed superior predictive accuracy compared to EVMs, including the standard and RNG k–ε turbulence models.
- A comparison of uniform and non-uniform diffusers showed that the jet merging process was significantly affected by the orientation of the ports. The middle discharge had a longer trajectory and therefore a higher dilution rate when its adjacent jets were disposed of at a different angle compared with that of uniform discharges. The terminal rise height, impact distance, and impact dilution of the central jet on a diffuser with non-uniform port inclination were 7%, 5%, and 14% higher than those of the uniform case, respectively.
- It was concluded that the behavior of the middle jet on the nonuniform diffuser was similar to that of a single jet, distinguishing it from uniform diffusers. When the nozzles were non-uniform, the negative effects of jet merging on the individual jet behavior, such as inward bending and reduced geometric features, became less noticeable.

In chapter 4 of this thesis:

- A novel concept for modifying multiport desalination outfalls was proposed to limit the negative effect of jet merging on the mixing of brine with ambient water, therefore decreasing the environmental risks.
- A series of experiments using the Laser Induced Fluorescence (LIF) technique were carried out, involving four distinct diffuser types: two with uniform port orientations and two with non-uniform port orientations. The port angles were adjusted to within the range where the highest dilution rates had previously been reported for single discharges (40°–70°). The flow characteristics resulting from nonuniform diffusers were quantified by geometric and dilution measurements via LIF and subsequently compared with those from uniform diffusers. Subsequently, an investigation was conducted to identify the root causes of the divergent behavior observed between uniform and non-uniform diffusers, with a focus on the interaction zone.
- The investigations showed that non-uniform diffusers exhibited, on average, return point distances 6–14% shorter, terminal rise heights 3–4% higher, and return point dilutions 22–25% higher than their equivalent uniform diffusers.
- It was found that the superior performance of non-uniform diffusers had roots in distinct mixing behaviors in the interaction zones. The jets on non-uniform diffusers merged at farther distances from the diffusers and experienced less re-entrainment of brine in the interaction zone because of the increased space between the jets.
- The use of formulas obtained from single-jet experiments in the design of multiport diffusers has been challenged. Instead, this study suggests incorporating source characteristics specific to multiport diffusers, such as angle difference, to enhance the design of desalination outfalls.
- The application of non-uniform diffusers for brine disposal can result in either shorter diffusers, decreased total outfall costs, or higher dilution rates, thus reducing environmental risks.

5.2 Recommendations for Future Studies

The following recommendations are proposed for future studies on multiport diffusers with non-uniform port orientations:

- This study concluded that the angle difference between adjacent jets (φ) on a multiport diffuser could increase dilution. Two main angles (θ=50^o and θ=60^o) and two angle differences (φ=0^o and φ=20^o) were considered. Considering a wider range of port angles and angle differences can provide valuable insights into how the combination of these factors affects mixing performance.
- The performances of uniform and non-uniform diffusers were compared in stationary ambient water. The superior performance of nonuniform diffusers, as indicated in this study, may not necessarily hold under different ambient conditions. Therefore, it is recommended that experiments be conducted with flowing ambient water to evaluate and compare the performance of both uniform and non-uniform diffusers.
- In this study, it was concluded that a non-uniform port orientation could serve as an alternative to port spacing because it could provide more space for the jets to expand before interacting with their neighboring jets, similar to the role of port spacing. This presents a potential for cost savings. However, it is impossible to estimate the exact amount of cost savings because of the limited range of port spacing considered in this study. A more comprehensive study incorporating a wider range of port spacing options would provide valuable insights into the potential cost savings.
- Although this study mainly focused on analyzing the mixing behavior up to the impact point, it would be valuable to extend the investigation to compare the performance of uniform and non-uniform diffusers at the end of the near field or even into the far field.
- Evaluating the prediction capabilities of integral models and hybrid numerical models, such as detached-eddy simulations (DES), for multiple INBJs and comparing their predictions with the LRR model would be valuable and interesting.
- The results showed that the jets on a non-uniform diffuser merged at farther locations than those on a uniform diffuser, resulting in enhanced dilution. However, the dynamics of jet merging can be significantly affected by shallow water conditions and ambient water stratification. Therefore, it would be interesting to evaluate the merging processes of both

uniform and nonuniform diffusers in scenarios involving surface interactions and ambient stratification.

- The angle difference should be included as a variable for optimization studies, in addition to the decision variables previously established in the literature, such as the number of ports, port and outfall diameters, and outfall and diffuser lengths.
- The experimental data presented in this study can be used to validate the numerical models. Therefore, different turbulence models can be applied, and their prediction capabilities can be evaluated against the outputs presented in this study.

References

Abessi, O., & Roberts, P. J. W. (2014). Multiport Diffusers for Dense Discharges. Journal of Hydraulic Engineering, 140(8), 04014032. https://doi.org/10.1061/(ASCE)HY.1943-7900.0000882

Appendix A: Large Eddy Simulation of Multiple Inclined Brine Discharges[4]

Abstract

Brine effluents are commonly discharged into water bodies through diffusers and may cause almost permanent adverse effects on marine habitats. Since the extension of such negative effects closely depends on the features of the outfall diffusers, it is essential to predict the mixing behavior of the jets for different types of diffusers. Although single-port discharges are theoretically superior in terms of mixing efficiency, currently, multiport diffusers are frequently applied due to the limitations in practical projects. The mixing behavior of multiport discharges compared to single-port ones is much more complicated because of the complex mechanisms resulting from jet interaction and the Coanda effect. Most of the numerical studies on discharges have focused on single-port discharges, and less attention has been given to the multiple jets. Also, the limited available numerical studies on the multiport diffusers have applied the Reynolds-averaged Navier-Stokes (RANS) turbulence models. In this study, the dilution and geometrical characteristics of the multiple 60^{o} inclined dense jets were numerically investigated in detail using the large eddy simulation (LES) approach with the Smagorinsky subgrid-scale (SGS) model. The LES predictions for the impact point location, impact point dilution, and terminal rise height were compared to the existing measurements in the literature. The results showed that the LES outcomes were in good agreement with the experimental data, and the LES approach was found to be a reliable tool for the investigation of multiport diffusers. The merging process of discharges was also studied based on the presented model.

Keywords: Large eddy simulations; Negatively buoyant jets; Multiple diffusers; Turbulence models; Mixing characteristics

[4] This chapter has been published as: Hosseini, S. A. R. S., Taherian, M., & Mohammadian, A. (2022, June). Large Eddy Simulation of Multiple Inclined Brine Discharges. In Proceedings of the 39th IAHR World Congress (Vol. 19, p. 24).

A.1 Introduction

Improper release of dense wastewaters into water bodies causes adverse environmental effects. Dense effluents are commonly discharged into water bodies through outfall diffusers as highly turbulent jets. Outfall discharges are mainly employed to provide rapid mixing, thereby protecting marine habitat. The mixing process of the discharges is significantly affected by the features of the diffusers (Yan and Mohammadian, 2019; Lai et al., 2015). Therefore, the study of the mixing process of the discharges for different types of diffusers can be of interest, as it can provide useful insights for outfall design purposes.

Wastewaters may be discharged into the seas and oceans as single-port or multi-port diffusers considering different factors in practical projects such as effluent flow rate, budget limit, and environmental regulatory demands. Although a free mix of single jets with the surrounding water causes them to be superior in terms of the mixing behavior, high wastewater flow rates may require multiple-port diffusers (Lyu et al., 2013; Wang and Davidson, 2003), as applied in Perth, Boston, Sydney, and Melbourne. As multiple jets are discharged, jet interaction and the Coanda effect lead to an intricate mechanism, which significantly affects the geometrical and mixing characteristics of the jets. Therefore, the study of the mixing process of multiple jets may be more complicated and differs from the single ones, highlighting the importance of a separate study on multiport diffusers. Unlike single dense discharges, the mixing behavior of multiple dense discharges has attracted less attention in prior research.

Most of the previous studies on multiple jets have been conducted experimentally (Xu et al., 2019; Shrivastava et al., 2019; Abessi et al., 2017; Abessi and Roberts, 2014; Marti et al., 2011; Adams, 1972), which have significantly shed light on the mixing process of multiple jets. However, experimental measurements are expensive and time-consuming options for the study of multiple jets. Integral entrainment models have always been an alternative method for the study of the mixing characteristics of jets. Many commercial tools, e.g. UM3 (Frick, 2004), CoreJet (Jirka, 2004), and JetLag (Lee and Chu, 2003; Lee et al., 1990), for the assessment of jet mixing process have been designed based on these models. The integral models are formed based on simplified mass and momentum equations (Taherian and Mohammadian, 2021), and they cannot resolve the Coanda effect and re-entrainment (Taherian and Mohammadian, 2021; Baum and Gibbes, 2020). The incapability of capturing the Coanda effect may be an important deficiency of these models when they are employed for the investigation of multiple jets since jet merging combined with the Coanda effect diminish terminal rise height and dilution of discharges (Roberts, 2015; Abessi and Roberts, 2014). In previous studies, major discrepancies for the estimation of dense jets' terminal rise height and dilution were found, where CoreJet, JetLag, and UM3 tools were employed for the simulations (Palomar et al., 2012).

Computational fluid dynamics (CFD) modeling considers fewer simplifying assumptions compared to the entrainment integral models (Baum and Gibbes, 2020), and its application in the prediction of the jet mixing process has increased in the last two decades (Taherian et al., 2022). However, CFD modeling has been limitedly employed for the prediction of multiport diffusers. Its application for multiple jets may be limited to some studies conducted in recent years, which have mainly applied the Reynolds-averaged Navier-Stokes (RANS) turbulence models. One study investigated the mixing behavior of multiple buoyant jets using two different models including an eddy viscosity model (EVM) and a CORMIX model and showed that the EVM was superior in terms of capturing the changes of plumes' depth along the trajectory (Tang et al., 2008). A recent study (Baum and Gibbes, 2020) applied k-ω shear stress transport (SST) model to investigate the dilution properties of multiple inclined dense jets in cross-flow and validated the performance of the model against field measurements. Another study (Yan and Mohammadian, 2019) evaluated the mixing characteristics of multiple inclined dense jets, employing the re-normalization group (RNG) and standard k-ε turbulence models. It was shown that the predictions of terminal rise height and impact point dilution were in good agreement with the experimental measurements obtained by Abessi and Roberts (2014). The RNG k-ε model could provide more accurate results, with less than 15% error, compared to the standard k-ε model, over 18% error. Moreover, multiple vertical jets were numerically modeled using different RANS models in another study (Yan et al., 2020), and it was concluded that the RNG k-ε model outperformed the standard k-ε, k-ω (SST), and standard k-ω turbulence models.

According to the presented review and the authors' knowledge, multiple dense discharges have not been yet simulated employing the large eddy simulation (LES) approach. The reason may be the high computational cost and convolution when it comes to the simulation of the complex geometry of multiple jets. However, as the large coherent eddies are directly resolved in the LES approach, it is expected that this model provides more accurate predictions, compared to the RANS models.

It can also provide more detailed information on the flow field and eddy structures. Therefore, the present study employs the Smagorisnky LES model for the prediction of the mixing behavior of multiple inclined dense jets and evaluates its prediction capabilities by comparing the results against the available experimental measurements. The validated model is further utilized for the study of the jet merging process.

A.2 Methodology

A.2.1 Multiple Jets Analysis

Figure A-1 illustrates the schematic plan and side views of multiple inclined dense discharges. The initial vertical momentum flux of the jets moves them upward to a maximum height, which is called the terminal rise height, y_t. Along the upward movement of jets, the entrainment and negative buoyancy continuously diminish the initial momentum, and there is almost no trace of the initial vertical momentum anymore at y_t. Beyond this point, the jets move downward and finally impact the bottom boundary at the impact point location, x_i. The dilution at this point is referred to as the impact point dilution, Si. These parameters are the most important ones while investigating the outfall systems as they are essential for design purposes. The values of these factors are numerically calculated using the LES approach and compared to the experiments on the 60^o multiple inclined dense jets conducted by Abessi et al. (2014) to evaluate the performance of the LES model.

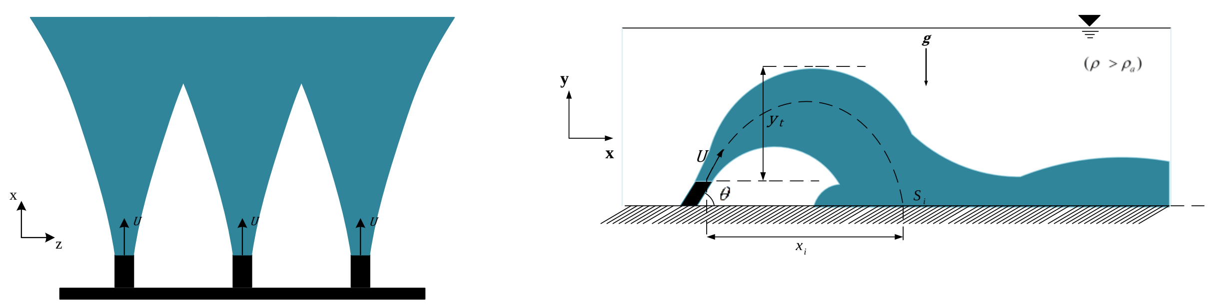

Figure A-1 Schematic plan and side views of multiple dense jets

A.2.2 Governing Equations

In the LES approach, large and small eddies are distinguished using a spatial filter; the unsteady nature of large eddies is directly computed, while the small eddies are modeled. The filtered

Navier-Stokes equations including continuity and momentum equations can be presented for an incompressible fluid as Equations A-1 and A-2, respectively.

$$\frac{\partial(\bar{u}_i)}{\partial x_i} = 0 \quad \text{(A-1)}$$

$$\frac{\partial(\bar{u}_i)}{\partial t} + \frac{\partial(\bar{u}_i\bar{u}_j)}{\partial x_j} = -\frac{1}{\rho}\frac{\partial \bar{p}}{\partial x_i} + \nu\frac{\partial^2 \bar{u}_i}{\partial x_j \partial x_j} - \frac{\partial \tau_{ij}}{\partial x_j} \quad \text{(A-2)}$$

where $\bar{u}_i$, t, ν, and $\bar{p}$ are the filtered velocity field, time, kinematic viscosity, and filtered pressure field, respectively. Also, τ_{ij} indicates the subgrid-scale (SGS) stresses which can be defined as follows:

$$\tau_{ij} = \overline{u_i u_j} - \bar{u}_i\bar{u}_j \quad \text{(A-3)}$$

In the present study, the Smagorinsky SGS model was adopted. The Smagorinsky model estimates the SGS stress tensor for an incompressible flow as below:

$$\tau_{ij}^{SGS} = -2\mu_t\tilde{S}_{ij} \quad \text{(A-4)}$$

where $\tilde{S}_{ij}$ is the rate of strain tensor for the resolved scale. The unknown term of SGS eddy viscosity, μ_t, can be determined using the following equations:

$$\mu_t = \rho(C_s\Delta)^2|\tilde{S}| \quad \text{(A-5)}$$

$$|\tilde{S}| = \sqrt{2\tilde{S}_{ij}\tilde{S}_{ij}} \quad \text{(A-6)}$$

where C_s is the Smagorinsky constant and Δ is the LES filter size.

A.2.3 Computational Setup

As the experiments were conducted based on the different numbers of ports, the computational domain was considered to include three ports. These ports could be the representatives of all possible jets on a diffuser since the side planes of the domain were considered as symmetry planes, which could mirror the flow field of the domain. Boundary conditions play a significant role in the stability and accuracy of fluid numerical calculations. The simulation domain was structured using seven planes including the inlet, back wall, outlet, atmosphere, lower wall, and two side planes (see Figure A-2). The boundary conditions at the back and lower walls were set to slip; the atmosphere and outlet planes to zero gradients; and side planes to the symmetry plane. Also, a fixed value of velocity was assigned to the inlets. The structured mesh, which was used for the discretization of the continuous domain, is shown in Figure A-2. The cell sizes were set to be much smaller at the locations close to the nozzles compared to other areas so that they could capture the velocity and pressure fields better. The detailed simulation parameters and domain characteristics are presented in Table A-1.

Table A-1 Simulation parameters

Nozzle diameter (cm)	Effluent density (Kg/m^3)	Ambient density (Kg/m^3)	Jet velocity (m/s)	F_d	Discharge angle (°)	Port spacing (cm)	Domain dimension (cm)	Number of cells (million)
0.193	1013.8	999.8	0.85	52	60	5.7	40x40x17.6	1.35

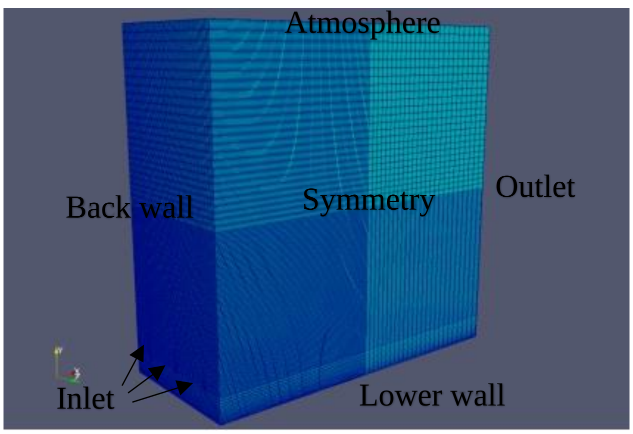

Figure A-2 Computational domain, mesh setup, and boundary conditions.

The finite volume method (FVM) was adopted for solving the presented equations, and an open-source code OpenFOAM was utilized to perform the simulations. The twoLiquidMixingFoam solver, which is a transient solver for multiphase fluids, in OpenFOAM software was used to solve the Navier-Stokes equations. This solver has been adopted for the simulation of various flow fields in previous studies (Yan et al., 2020; Jiang et al., 2019; Yan and Mohammadian, 2019; Li et al., 2016; Zhang et al., 2016; H Lai et al., 2015). The Euler scheme was utilized to discretize the temporal term; Gauss linear scheme was adopted for the discretization of the gradient and Laplacian terms; Gauss upwind, Gauss Vanleer, and Gauss linear schemes were applied to discretize the divergence terms. The time step was considered to be adjustable during the simulation based on the courant number, and the maximum courant number was set to 0.5 to provide small time steps. The outcomes were extracted based on time-averaging over the range of 70s to 130s since the results were found to be stable after 50s and the flow was fully developed. The simulation was performed in the advanced research computing (ARC) center of Compute Canada, and 16 processors were employed for parallel simulations.

A.3 Results and Discussion

The Smagorisky LES predictions were compared to the experimental measurements conducted by Abessi and Roberts (2014). Table A-2 demonstrates the model predictions and measurements for the impact point location (x_i), impact point dilution (S_i), and terminal rise height (y_t). Considering the errors, the LES predictions were in good agreement with the experimental data. The error for the geometrical characteristics of multiple dense jets was less than 10%, and it was less than 6% for the impact point dilution.

Table A-2 Comparison of experimental and numerical results

	Experimental results	Numerical predictions	Errors (%)
Impact point location (cm)	17.36	17.15	1.2
Impact point dilution	26	24.45	5.97
Terminal rise height (cm)	16.1	17.7	9.94

Concentration contours at the side view of the middle jet are shown in Figure A-3, where C0 denotes the initial concentration, C signifies the local concentration of the discharges, and C/C0 is the normalized concentration. In the ascending phase, the vertical component of the initial momentum resulted in the upward movement of the jets. As the discharges were dense jets, the negative buoyancy continuously hindered this momentum. At the end of this phase, there was no trace of it, and the jets started to turn downward. In the descending phase, the negative buoyancy was dominant, and this force moved the jets downward until they impinged to the bottom boundary. The contours show that the concentration continuously decreased along the trajectory, and the lower half of the jets expanded more widely compared to the upper half.

As discussed in Abessi and Roberts (2014), the multiple jets compared to the single ones have a reduced terminal rise height and impact point location, which have roots in the jet merging and Coanda effects. Figure A-3 visualizes the inward bending of multiple jets, subsequently resulting in a reduced impact point location.

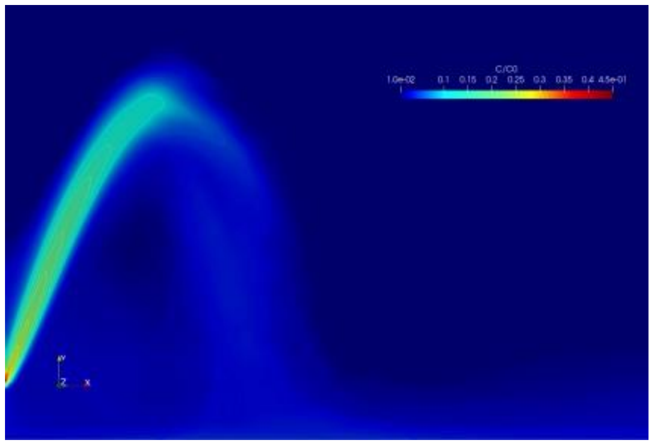

Figure A-3 Time-averaged concentration contours at the central plane.

Figure A-4 demonstrates the concentration fields at different cross-sections, covering the locations close to the ports and downstream areas. These cross-sections could provide an insight into the jet merging process. At the locations close to the nozzles, e.g., X/DF=0.23, the discharges were not expanded enough to merge, and they were almost like separate jets. The concentration at the center of the jets was very high. In farther areas from the ports, e.g., X/DF=0.5, shear stresses on the edges of the jets caused the entrainment of the ambient water. Subsequently, the concentration decreased, and the jets expanded. However, at this distance, the jets barely interacted with each other since they were not still diffused enough to merge. Farther away, e.g., X/DF=0.95, the jets were much more diffused and jet merging occurred. The concentrations at the jets' centers and the space between the jets were almost identical, and there was little freshwater between the jets. The jet merging leads to the formation of a virtually impenetrable wall that hinders the entrainment of surrounding water to inner surfaces and intensifies the Coanda effect, resulting in sharp inward bending of the jets (Abessi and Roberts, 2014). After the impact point, e.g., X/DF=1.92, the separate jets were indistinguishable.

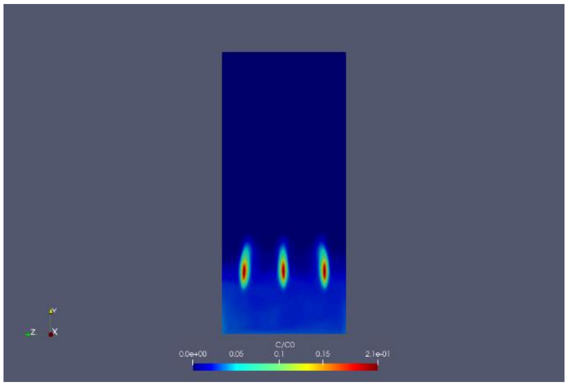

(X/DF=0.23)

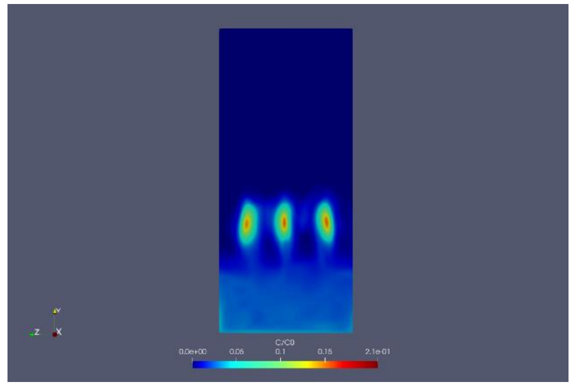

(X/DF=0.5)

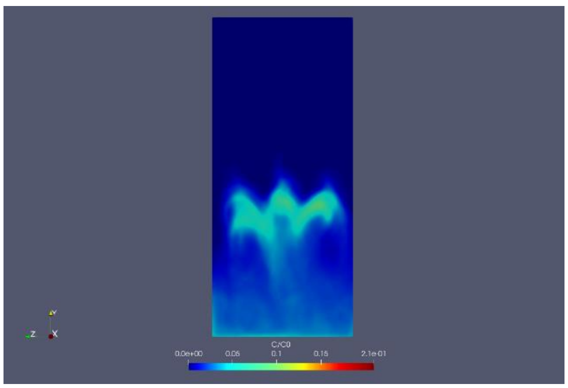

(X/DF=0.95)

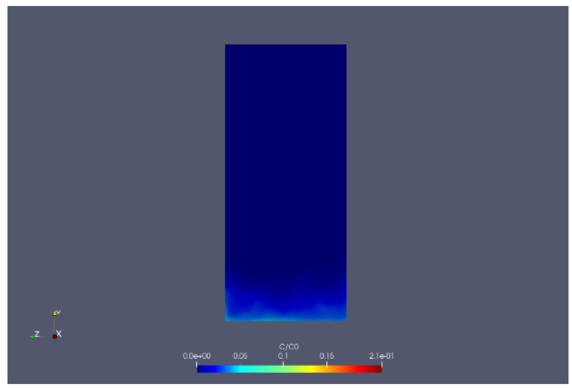

(X/DF=1.92)

Figure A-4 Concentration fields at various non-dimensional distances from the nozzles

A.4 Conclusions

The main objective of the current study was to evaluate the prediction capabilities of the LES approach for multiple dense jets. The multiple 60° inclined dense jets were numerically simulated employing LES with the Smagorisky SGS model, for the first time. The LES predictions for impact point location, impact point dilution, and terminal rise height were compared against the existing experimental data. The model was further employed to investigate the jet merging process, which is of significant importance in the study of multiport diffusers. The results showed that the LES model could predict geometrical and dilution properties of the multiple dense jets with errors less than 10% and 6%, respectively. Therefore, it can be concluded that the LES approach can be a reliable tool for the prediction of the mixing behavior of multiport diffusers. The merging process was discussed through the visualization of different cross-sections.

Acknowledgement

The authors would like to thank the advanced research computing (ARC) center of Compute Canada (a not-for-profit-organization) for providing the computational resources used in this study. The research of A.M. was supported by Natural Sciences and Engineering Research Council of Canada (NSERC).

References

Abessi, O., Roberts, P.J.W. (2017). Multiport diffusers for dense discharge in flowing ambient water. Journal of Hydraulic Engineering, American Society of Civil Engineers (ASCE), 143(6), 04017003.

Abessi, O., and Roberts, P.J.W. (2014). Multiport Diffusers for Dense Discharges. Journal of Hydraulic Engineering, American Society of Civil Engineers (ASCE), 140(8), 04014032.

Adams, E.E. (1972). Submerged multiport diffusers in shallow water with current (Doctoral dissertation, Massachusetts Institute of Technology).

Baum, M.J., and Gibbes, B. (2020). Field-Scale Numerical Modeling of a Dense Multiport Diffuser Outfall in Crossflow. Journal of Hydraulic Engineering, 146(1), 05019006.

Frick, W.E. (2004). Visual Plumes mixing zone modeling software. Environmental Modelling & Software, 19(7-8), 645-654.

Huai, W.X., Li, Z.W., Qian, Z.D., Zeng, Y.H., Han, J., & Peng, W.Q. (2010). Numerical simulation of horizontal buoyant wall jet. Journal of Hydrodynamics, 22(1), 58-65.

Jiang, M., Law, A.W.K., and Lai, A.C.H. (2019). Turbulence characteristics of 45° inclined dense jets. Environmental Fluid Mechanics, Springer Netherlands, 19(1), 27–54.

Jirka, G.H. (2004). Integral Model for Turbulent Buoyant Jets in Unbounded Stratified Flows. Part I: Single Round Jet. Environmental Fluid Mechanics, 4(1), 1–56.

Joseph W Lee, B.H., Member, A., and Cheung, V. (1990). Generalized Lagrangian Model for Buoyant Jets in Current. Journal of Environmental Engineering, American Society of Civil Engineers (ASCE), 116(6), 1085–1106.

Lai, A.C., Zhao, B., Law, A.W.K., & Adams, E.E. (2015). A numerical and analytical study of the effect of aspect ratio on the behavior of a round thermal. Environmental Fluid Mechanics, 15(1), 85-108.

Lee, J.H.W., Chu, V., & Chu, V.H. (2003). Turbulent jets and plumes: a Lagrangian approach (Vol. 1). Springer Science & Business Media.

Li, Y., Geng, X., Wang, H., Zhuang, X., and Ouyang, J. (2016). Simulating the frontal instability of lock-exchange density currents with dissipative particle dynamics. Modern Physics Letters B, 30(17), 1–9.

Lyu, S., Seo, I.W., & Kim, Y.D. (2013). Experimental investigation on behavior of multiple vertical buoyant jets discharged into a stagnant ambient. KSCE Journal of Civil Engineering, 17(7), 1820-1829.

Marti, C.L., Antenucci, J.P., David Luketina, Okely, P., Imberger, J., and Asce, M. (2011). Near-Field Dilution Characteristics of a Negatively Buoyant Hypersaline Jet Generated by a Desalination Plant. Journal of Hydraulic Engineering, American Society of Civil Engineers (ASCE), 137(1), 57–65.

Palomar, P., Lara, J., and Losada, I. (2012). Near field brine discharge modeling part 2: Validation of commercial tools. Desalination, 290, 28–42.

Roberts, P.J.W. (2015). Near field flow dynamics of concentrate discharges and diffuser design. Environmental Science and Engineering (Subseries: Environmental Science), Kluwer Academic Publishers, 369–396.

Shrivastava, I., & Adams, E.E. (2019). Mixing of tee diffusers in shallow water with crossflow: A new look. Journal of Hydraulic Engineering, 145(4), 04019006.

Taherian, M., and Mohammadian, A. (2021). Buoyant Jets in Cross-Flows: Review, Developments, and Applications. Journal of Marine Science and Engineering, Multidisciplinary Digital Publishing Institute, 9(1), 61.

Taherian, M., Saeidi Hosseini, S.A.R., and Mohammadian, A. (2022). Overview of outfall discharge modeling with a focus on turbulence modeling approaches. Advances in Fluid Mechanics: Modeling and Simulation, edited by Zeidan, D., Zhang, L., da Silva, E.G., and Merker., J. Singapore: Springer Nature, Accepted.

Tang, H.S., Paik, J., Sotiropoulos, F., and Khangaonkar, T. (2008). Three-Dimensional Numerical Modeling of Initial Mixing of Thermal Discharges at Real-Life Configurations. Journal of Hydraulic Engineering, 134(9), 1210–1224.

Wang, H.J., and Davidson, M.J. (2003). Jet Interaction in a Still Ambient Fluid. Journal of Hydraulic Engineering, American Society of Civil Engineers (ASCE), 129(5), 349–357.

Xu, Z., Otoo, E., Chen, Y., & Ding, H. (2019). 2D PIV Measurement of Twin Buoyant Jets in Wavy Cross-Flow Environment. Water, 11(2), 399.

Yan, X., Ghodoosipour, B., and Mohammadian, A. (2020). Three-Dimensional Numerical Study of Multiple Vertical Buoyant Jets in Stationary Ambient Water. Journal of Hydraulic Engineering, 146(7), 04020049.

Yan, X., and Mohammadian, A. (2019). Numerical modeling of multiple inclined dense jets discharged from moderately spaced ports. Water (Switzerland), 11(10), 14–16.

Zhang, S., Jiang, B., Law, A.W.K., and Zhao, B. (2016). Large eddy simulations of 45° inclined dense jets. Environmental Fluid Mechanics, Springer Netherlands, 16(1), 101–121.

Appendix B: Test setup and equipment employed in this research

Figure B-1 Hydraulics laboratory at the University of Cagliari, Italy, showing LIF setup.

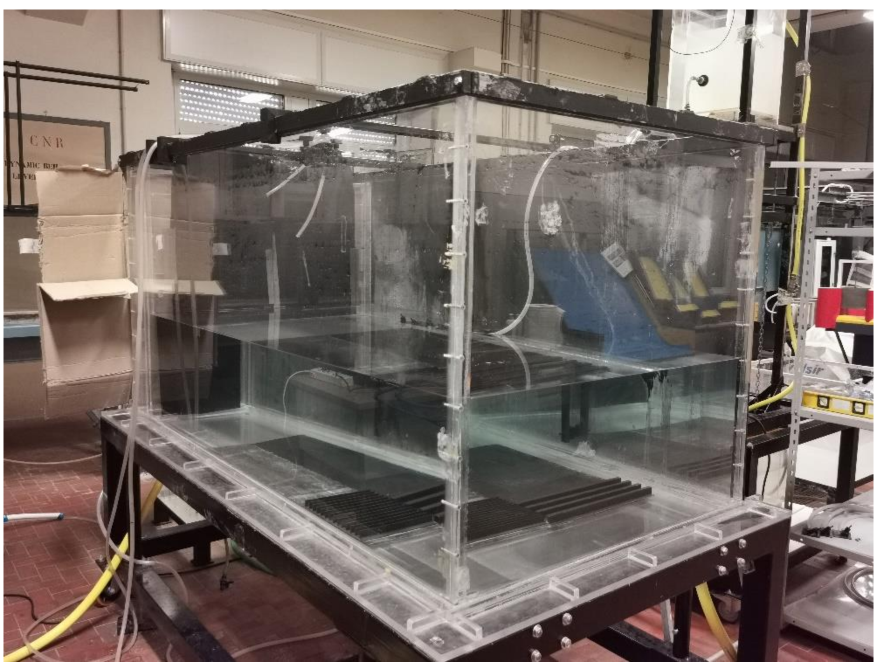

Figure B-2 Main tank used for the experiments.

Figure B-3 5-W diode-pumped solid-state (DPSS) continuous green laser.

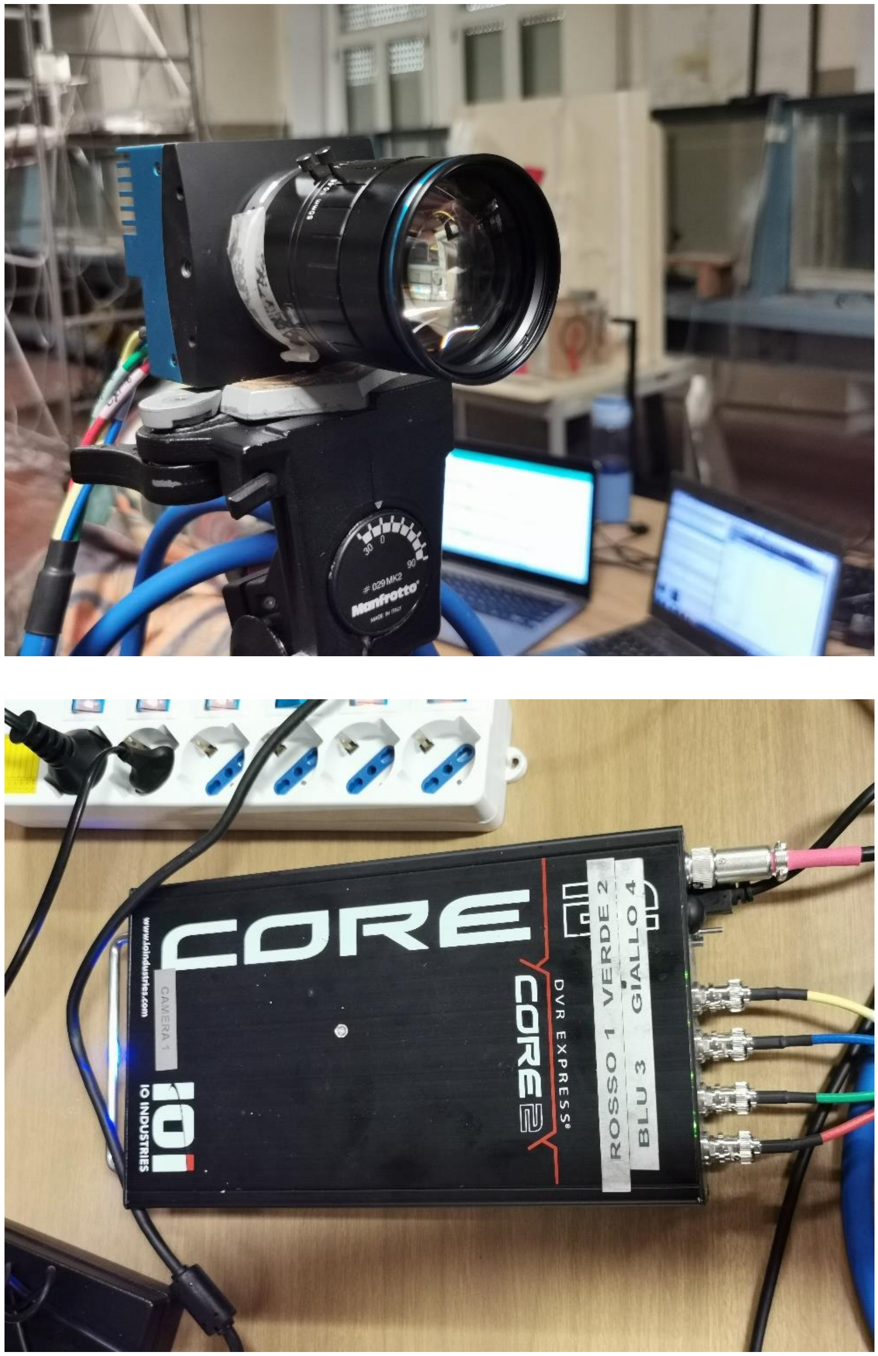

Figure B-4 Digital charge-coupled device (CCD) camera, Mikrotron EoSens 4CXP CoaXPress.

(a)

(b)

Figure B-5 Designed multiport diffusers with (a) uniform (50º) and (b) non-uniform (60º and 40º) port orientation.

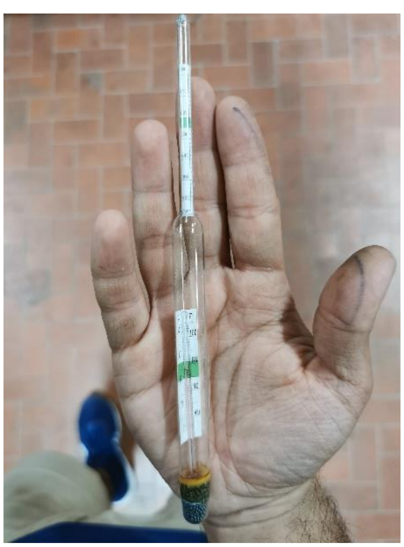

(a) (b)

Figure B-6 (a) Gravity hydrometer and (b) flow meter.

Figure B-7 Tool used to move the laser sheets, showing the laser setup.

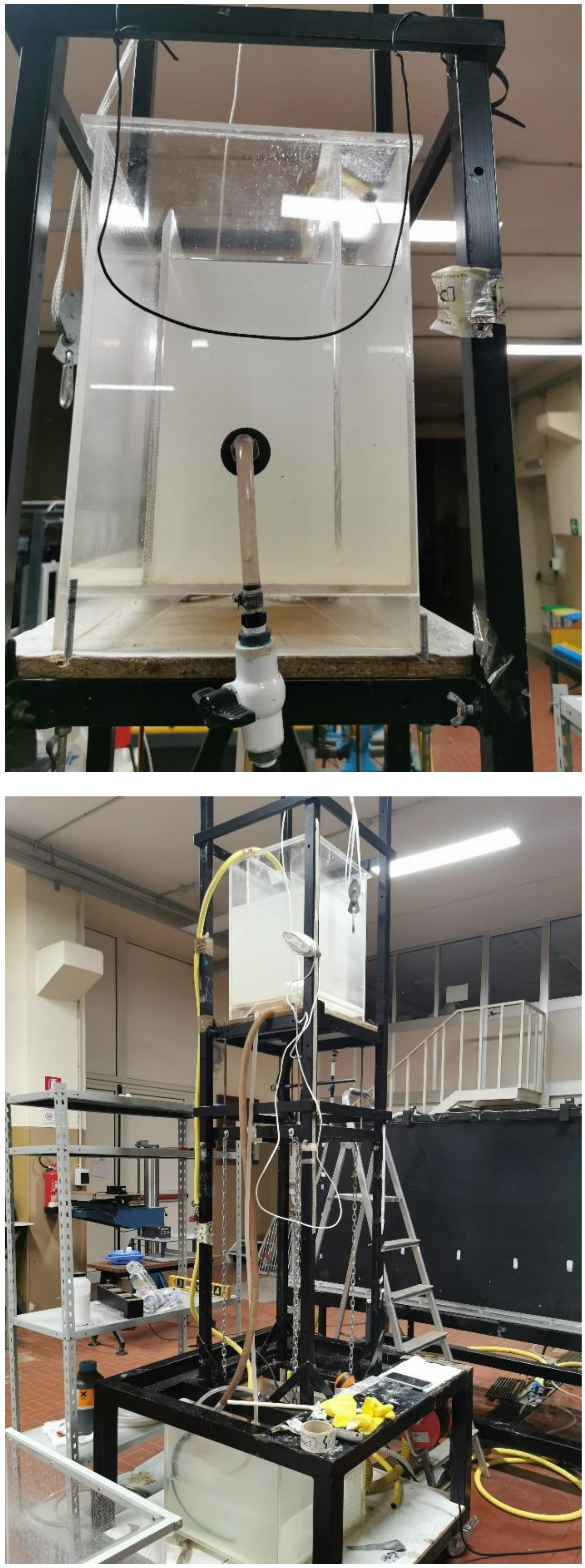

Figure B-8 Discharge tank and its setup.